Mechanistic insights into the mitotic checkpoint through biochemical characterisation and *in vivo* method development

Inaugural-Dissertation

zur
Erlangung des Doktorgrades

Dr. rer. nat.

Der Fakultät für Biologie

an der

Universität Duisburg-Essen

vorgelegt von

Amal Alex

aus Kerala, Indien

durchgeführt am

Max-Planck-Institut für molekulare Physiologie

Abteilung für mechanistische Zellbiologie

June 2021

Die der vorliegenden Arbeit zugrunde liegenden Experimente wurden am Max-Planck-Institut für molekulare Physiologie in der Abteilung für mechanistische Zellbiologie durchgeführt.

1. Gutachter: Prof. Dr. Andrea Musacchio

2. Gutachter: Prof. Dr. Michael Ehrmann

Vorsitzender des Prüfungsausschusses: Prof. Dr. Perihan Nalbant

Tag der mündlichen Prüfung: 20/09/2021

In the context of this doctoral work, the following articles were published:

- <u>Amal Alex</u>, Valentina Piano, Soumitra Polley, Marchel Stuiver, Stephanie Voss, Giuseppe Ciossani, Katharina Overlack, Beate Voss, Sabine Wohlgemuth, Arsen Petrovic, Yaowen Wu, Philipp Selenko, Andrea Musacchio, Stefano Maffini. 2019. Electroporated recombinant proteins as tools for in vivo functional complementation, imaging and chemical biology. eLife,8: e48287.

- Valentina Piano, <u>Amal Alex</u>, Patricia Stege, Stefano Maffini, Gerardo A. Stoppiello, Pim J. Huis in 't Veld, Ingrid R. Vetter, Andrea Musacchio. 2021. CDC20 assists its catalytic incorporation in the mitotic checkpoint complex. Science, 371: 67–71.

5. SUMMARY **95**

6. ZUSAMMENFASSUNG **96**

7. BIBLIOGRAPHY **97**

ACKNOWLEDGEMENTS 112

CURRICULUM VITAE 113

List of figures

List of tables

List of Abbrevations

Index

1. Introduction

The ability to proliferate is a fundamental feature of life on Earth. The continuation of every species depends on cell division, through which organisms grow and reproduce. In eukaryotes, cell division can be of two types: the mitotic cell division for the proliferation, growth and repair of individual organism and tissues; and the meiotic cell division for the production of gametes in sexually reproducing organisms. In this document, the term cell division will refer to mitotic cell division unless mentioned otherwise.

1. 1 The cell cycle

A cell reproduces by carrying out an orderly sequence of events in which it duplicates its contents and, then, divides in two daughter cells (Alberts et al., 2010). This cycle of duplication and division, known as the *cell cycle*, is the essential mechanism by which all living organisms reproduce. The eukaryotic cell cycle is organized in two phases. The most eventful part of the cell division is the M̲itotic (M) phase, where the genetic material gets equally divided into two new daughter cells. The period between one M phase and next is called *interphase*. Interphase can be further sub-divided into three different phases: G̲ap1̲ (G1), S̲ynthesis (S) and G̲ap2̲ (G2) phases (Figure 1-1). During S phase, the cell replicates its nuclear DNA. S phase is flanked by two phases in which the cell continues to grow. The G1 phase is the interval between the completion of M phase and the beginning of S phase. The G2 phase is the interval between the end of S phase and the beginning of M phase. The gap phases provide time for the cell to grow, double its cytoplasmic organelles and thereby increase the cellular mass before the next cell division.

To ensure the fidelity of the cell cycle, there are *checkpoints* along its course. Each checkpoint serves as a potential termination point to guarantee that the cell commits to next stage of the cell cycle only when favorable conditions are met (Hartwell et al., 1989). The first checkpoint in the late G1-phase, called *G1-S checkpoint*, allows the cell to secure that the environment is favorable for cell proliferation before committing to S phase. Suitable environment before genome duplication will be characterized by

adequate cell size, growth factors and cell nutrients (Pardee, 1974; Hartwell et al., 1974).
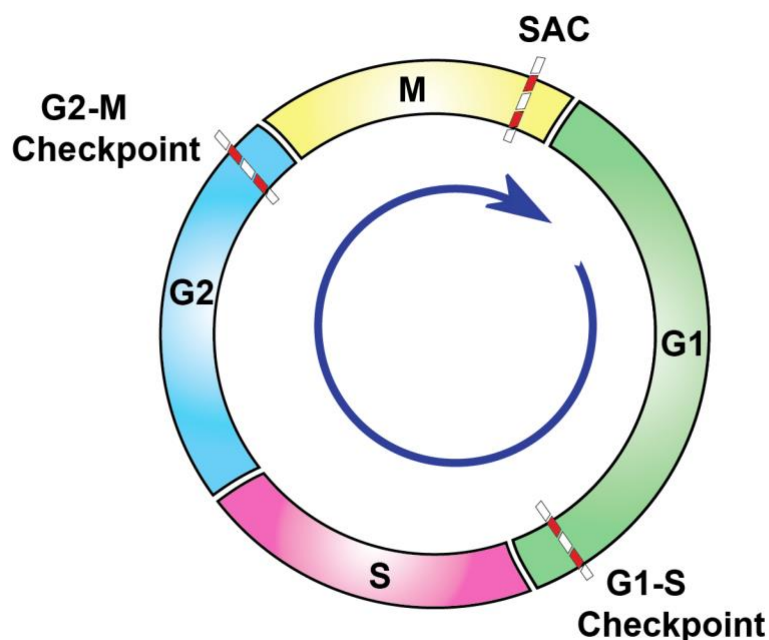
Figure 1-1 The eukaryotic cell cycle

The four phases of the eukaryotic cell cycle as well as the three main checkpoints are schematically shown. Details are described in the text.

The G2-M checkpoint, also called *DNA replication checkpoint*, is the second checkpoint, which ensures that all the chromosomes have been accurately replicated without any DNA damage. The third checkpoint, called *mitotic checkpoint* or *Spindle Assembly Checkpoint* (SAC) operates during mitosis. The SAC ensures that chromosomes are properly attached to spindle microtubules in a bi-oriented fashion before they are segregated to daughter cells (Musacchio & Salmon, 2007).

The cell cycle is an extensively regulated process. The cell-cycle control system governs the cell machineries by cyclically activating and inactivating the key proteins and protein complexes involved in each particular phase. The central players of the cell cycle control system are the so-called Cyclin-Dependent Kinases (CDKs), which belong to the serine-threonine kinase family. The activity of CDKs is regulated by proteins called *Cyclins,* whose levels vary in a cyclical fashion during the cell cycle. Cyclins have no enzymatic activity themselves, but they must bind to the CDKs for the kinases to become enzymatically active (Evans et al., 1983; Morgan, 1995). There are

several types of Cyclins and, in most eukaryotes, several types of CDKs involved in cell-cycle control. Different Cyclin–CDK complexes regulate different phases of the cell cycle (Coudreuse & Nurse, 2010; Loog & Morgan, 2005; Pines, 1991). Most Cyclins are present at low concentrations along the cell cycle, except for the specific cell cycle phase where they are needed. For example, human *CyclinB* peaks dramatically at G2-M transition and interacts with the kinase CDK1, constituting the main regulator of mitosis. In addition to the binding of Cyclins, the kinase activity of CDKs require an activating phosphorylation in the active site by a <u>C</u>DK-<u>A</u>ctivating <u>K</u>inase (CAK) (Jeffrey et al., 1995; Honda et al., 2005). This requirement for an upstream CAK is also well conserved across species (Saiz and Fischer, 2002).

1.1.1 Mitosis

Mitosis is the phase of the eukaryotic cell cycle where the parental mother cell divides into two genetically identical daughter cells. Mitosis involves a series of consecutive events that ensure the accuracy of chromosome segregation. Mitosis can be further subdivided in multiple stages called *prophase*, *prometaphase*, *metaphase*, *anaphase* and *telophase* (Figure 1-2) (Alberts et al., 2008). During prophase, the genetic material that has been duplicated in S phase is condensed into mitotic chromosomes. Each chromosome is composed by two identical sister chromatids that are separated along all the chromosome arms, except for the centromeric region, where they are held together by the Cohesin complexes. A multi-proteinaceous structure, called *kinetochore*, assembles at the centromeric region of each chromatid and attaches to the spindle microtubules emanating from the centrosomes. Centrosomes are microtubule nucleating centers and start assembling spindle microtubules from opposite poles of the cell. During prometaphase, phosphorylation of nuclear lamins result in disintegration of nuclear envelope (few exceptions like *Fungi* exist). During metaphase, the tension exerted by the depolymerizing microtubules attached to the kinetochores causes the alignment of chromosomes at the center of the spindle, forming the so-called *metaphase plate*. The sister chromatids of each chromosome must be attached to the spindle microtubules coming from opposite poles, in a fashion termed *bi-orientation*, in order to form and maintain the metaphase plate. Anaphase is initiated by mainly two events: 1) CyclinB degradation, that results in the inactivation of the mitotic kinase CDK1, and 2) the cleavage of Cohesin by the protease Separase, that results in sister chromatid separation. Once the cohesion is lost, sister chromatids

are pulled to the opposite spindle poles through the force exerted by depolymerizing spindle microtubules. Telophase is defined by the reverse events that happened in prophase and prometaphase. Indeed, the nuclear envelope reassembles around each set of sister chromatids and forms individual daughter nuclei, where the chromosomes start to decondense. M phase is completed by cytokinesis which is technically not a part of mitosis, but it is necessary for the completion of cell division in most eukaryotes. A contractile ring develops where the metaphase plate was, eventually pinching off the separated nuclei to form two new daughter cells.
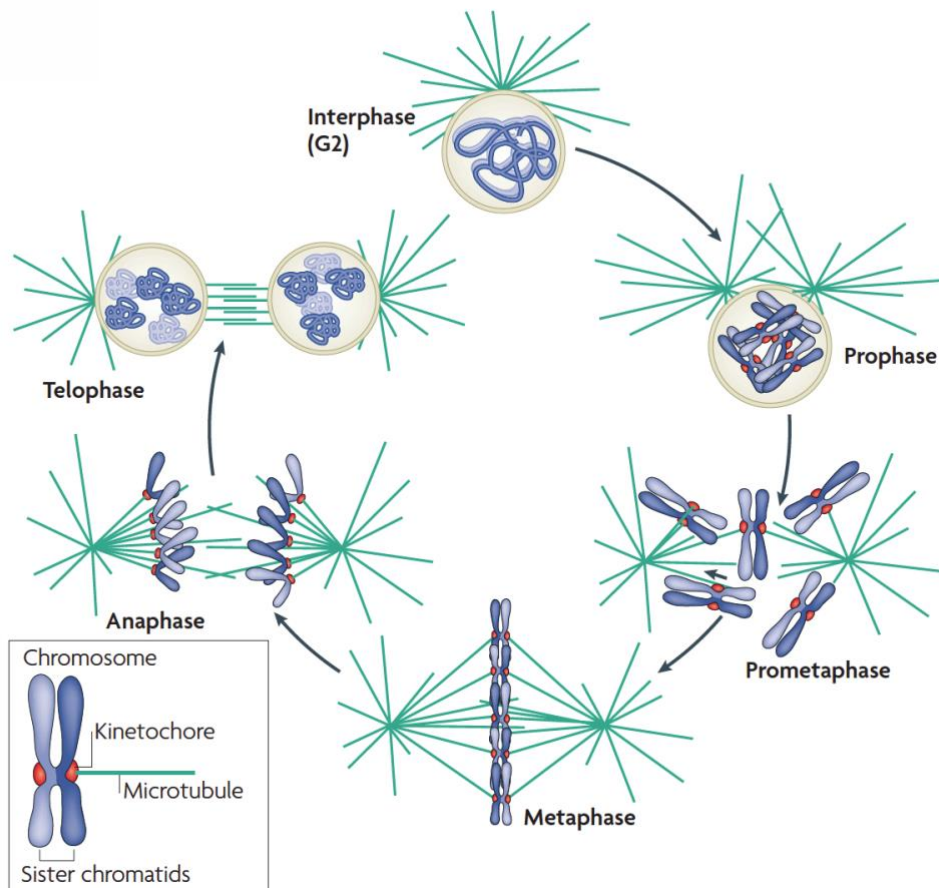
Figure 1-2 Schematic overview of mitotic cell division

During prophase, the replicated chromatin is condensed to form the mitotic chromosomes and the nuclear envelope breaks down. Microtubule-kinetochore interaction starts during prometaphase. In metaphase, chromosomes bi-orient at the center of the spindle. During anaphase, the separated sister chromatids are pulled toward opposite spindle poles. Following, during telophase, the two daughter nuclei formation occurs. M-phase is completed by cytokinesis (not shown here). Figure adapted from *Cheeseman & Desai, 2008*.

The errors occurring during mitosis are always detrimental to cells. Mitotic errors have been primarily identified as the main cause for aneuploidy, a condition in which cells end up having abnormal chromosome numbers. Furthermore, mitotic errors are also known to cause other deleterious defects to cells, such as DNA damage, genomic instability and tumorigenesis (Levine and Holland, 2018).

1.2 Kinetochore structure and function

Kinetochores are multi-subunit protein complexes whose overall architecture and functions are well conserved from yeast to mammals. The primary function of kinetochores is to act as platform for load bearing attachments between mitotic chromosomes and spindle microtubules. Kinetochores are fundamental for the regulation of the proteins involved in the correction of erroneous microtubule-kinetochore attachments and in the SAC, to ensure that mitotic chromosomes are properly bi-oriented (Musacchio and Desai, 2017). Early electron micrographs identified kinetochores as trilaminar structures with distinct electron dense inner and outer layers sandwiching an electron translucent middle layer (McEwen et al., 2007). A fourth fibrous layer, essential for the SAC function of the kinetochore, is visible only in absence of microtubules. This quadripartite structure can be correlated with the kinetochore composition and function (Musacchio and Desai, 2017). The distinct layers of the kinetochores are listed here and shown in *Figure 1-3*:

1) the *centromere* is the specialized chromatin region where the kinetochore assembles;

2) the *inner kinetochore* or Constitutive Centromere Associated Network (CCAN) consists of a 16-subunit protein complex that forms the physical link between centromere and the outer kinetochore. The CCAN subunits are involved in the recruitment of many outer kinetochore proteins and also in direct microtubule binding;

3) the *outer kinetochore* or KNL1-MIS12-NDC80 (KMN) network provides a physical linkage between kinetochores and spindle microtubules. The KMN network is essential for the recruitment of many SAC proteins that are necessary for proper checkpoint function;

4) A fibrous structure called *corona* is visible at unattached kinetochores and it contains many of the SAC proteins. The corona helps to increase the surface area of kinetochores and thereby improve the probability of stochastic microtubule binding.
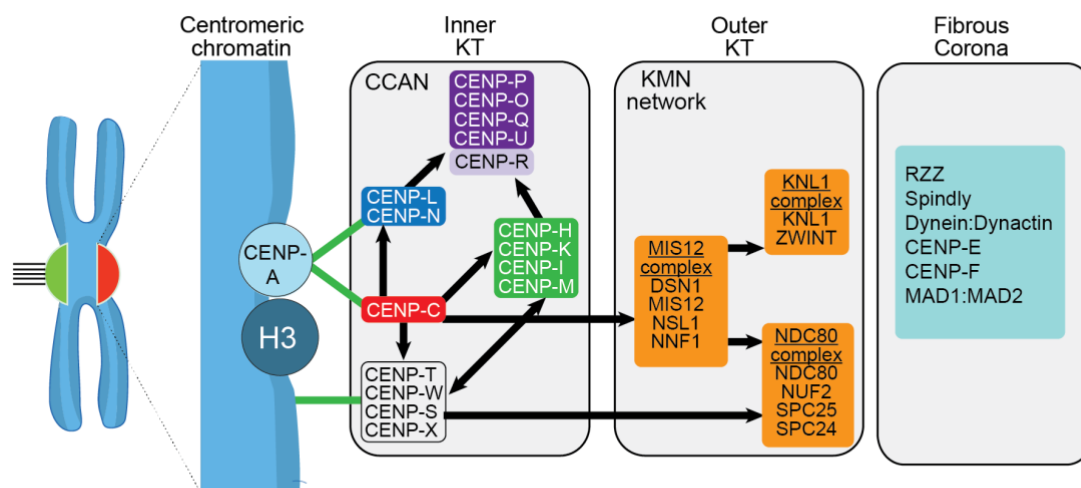
Figure 1-3 Organization of human kinetochore

In the cartoon of the mitotic chromosome, the left chromatid is unattached whereas the right chromatid is attached to microtubules. Different layers of vertebrate kinetochore, the centromere, the inner and outer kinetochore and fibrous corona with schematic depiction of subcomplexes is shown. Note that fibrous corona layer is assembled only at unattached kinetochores. Green lines indicate direct connection with centromeric DNA or chromatin. Black lines indicate recruitment dependencies (figure modified from Pesenti et al., 2018).

1.2.1 The centromere

Kinetochores are assembled at a specific chromatin *locus,* called centromere. There are two types of centromeres, depending on their overall size and factor specifying their identity. *Point centromeres* are small and a specific DNA sequence is necessary to define the centromere identity. For example, in budding yeasts the point centromere is specified by a small DNA sequence of approximately 125 base pairs (bps) (Malik and Henikoff et al., 2009). Most higher eukaryotes, on the other hand, have *regional centromeres*, that contain a large amount of repetitive DNA sequences (up to millions of bps) packed into heterochromatin. The DNA sequence contributes to centromere localization but it is not sufficient to specify the centromere identity. In all metazoans, the regional centromere identity is defined through epigenetic inheritance by the presence of the histone H3 variant Centromeric Protein A (CENP-A) (Black et al., 2007).

CENP-A was initially identified in the sera of patients suffering from Calcinosis, Raynaud's syndrome, Esophageal dysmotility, Sclerodactyly and Telangiectasia (CREST) syndrome (Earnshaw & Rothfield 1985). CENP-A is well conserved across

species, from yeast - where it is called Cse4 - to humans (Stoler et al., 1995; Sullivan et al., 1994). CENP-A is required for the kinetochore organization and its proper assembly, as it recruits other kinetochore components (Collins et al., 2005; Liu et al., 2006; Fachinetti et al., 2013). Depletion of CENP-A results in the mis-segregation of chromosomes during mitosis (Takahashi et al., 2000; Warburton et al., 1997), demonstrating its essential mitotic function. CENP-A deposition on to centromeric chromatin occurs during G1 phase and its deposition mechanism differs from the canonical nucleosomes, whose deposition is coupled to the DNA replication process (Black et al., 2007).

1.2.2 The inner kinetochore

Along with CENP-A, early studies from sera of patients diagnosed with autoimmune CREST syndrome, identified other kinetochore proteins associated to the centromeric chromatin (Earnshaw and Roth-field, 1985). Later studies using specific anti-centromere antibodies and proteomic analysis, identified 16 proteins associated with centromeres/kinetochores during the entire cell cycle, collectively called as the CCAN (Foltz et al., 2006; Okada et al., 2006, Izuta et al., 2006; Obuse et al., 2004). *In vitro* reconstitution and structural studies clarified that these 16 CCAN proteins are arranged into distinct sub-complexes: CENP-L and CENP-N form the CENP-LN complex (Carroll et al., 2009,2010); CENP-T, CENP-W, CENP-S, and CENP-X form the CENP-TWSX complex (Hori et al., 2008a; Nishino et al., 2012); CENP-H, CENP-I, CENP-K, and CENP-M form the CENP-HIKM complex (Basilico et al., 2014; Klare et al., 2015); CENP-O, CENP-P, CENP-Q, CENP-U, and CENP-R form the CENP-OPQUR complex (Hori et al., 2008b). The remaining CCAN protein, CENP-C, is the largest CCAN protein in humans. Sequence analysis predicts that most of the protein, except its C-terminal region containing a cupid domain, is intrinsically disordered.

The two CCAN subunits CENP-C and CENP-N have been identified to directly interact with CENP-A nucleosomes. CENP-C interacts with the C-terminal tail of CENP-A via two sequence-related motifs, the so-called *central region* and *CENP-C motif* sequences (Kato et al., 2013; Milks et al., 2009). CENP-C is recognized as the blueprint of the kinetochore as it binds MIS12 complex through its N-terminal region (Kwon et al., 2007; Przewloka et al., 2011), the downstream region binds to CENP-HIKM and CENP-LN (Klare et al., 2015; McKinley et al., 2015), the middle and the C-

terminal regions bind to CENP-A nucleosomes. Thus, CENP-C acts as structural link between nucleosomes and the outer kinetochore. CENP-N, on the other hand, interacts with the Centromere-Targeting Domain (CTD) of CENP-A (Caroll et al., 2009). The 7-subunit complex formed by the interactions of CENP-LN, CENP-HIKM and CENP-C, called the CENP-CHIKLMN complex, increases the binding affinity and specificity of both CENP-C and CENP-N for CENP-A nucleosome (Chittori et al., 2018; Falk et al., 2016; Guo et al., 2017; Pentakota et al., 2017; Weir et al., 2016).

The CENP-TW and CENP-SX subcomplexes associate to form the tetrameric CENP-TWSX complex. All four proteins of this complex contain histone fold domains. Direct interaction with the DNA has been described for the CENP-TWSX complex and it is dependent particularly on the histone fold domains of CENP-T and CENP-W (Takeuchi et al., 2014; Nishino et al., 2012). The interaction with CENP-HIKM is required for CENP-TW to be recruited at kinetochores (McKinley et al., 2015). CENP-TWSX complex contributes to the recruitment of additional MIS12, NDC80 and KNL1 copies, and thereby ensuring further microtubule binding sites in the kinetochore structure (independent of CENP-C recruitment pathway) (Nishino et al., 2012; Rago et al., 2015; Huis In 't Veld et al., 2016; Pesenti et al., 2016).

The CENP-OPQUR complex is recruited to kinetochores via its interaction with CENP-CHIKLMN (Foltz et al., 2006; Okada et al., 2006). This protein complex has been identified to be involved in multiple functions at kinetochores, such as the recruitment of Polo-like kinase 1 (PLK1) (Kang et al., 2006,2011; Singh et al., 2021), the recruitment of the microtubule motor protein CENP-E (Bancroft et al., 2015) and the cooperative binding to microtubules, along with NDC80 (Pesenti et al., 2018). In summary, the epigenetically marked human centromeric region is recognized by a series of interactions among the CCAN and the centromeric proteins, that are required to direct a stable outer kinetochore assembly.

1.2.3 The outer kinetochore

The outer kinetochore mainly performs two functions: 1) it serves as the binding platform for spindle microtubules, 2) it is the recruitment platform for SAC proteins to unattached kinetochore and, thereby, contributes to the checkpoint effector complex production. The KMN network constitutes the core of the outer-kinetochore, that

includes the two-subunit KNL1 complex, four-subunit MIS12 complex and four-subunit NDC80 complex (Foley and Kapoor, 2013). Unlike the inner kinetochore components, the KMN network is recruited upon mitotic entry and dissociates again during telophase from kinetochores (Cheeseman & Desai, 2008). An overview of the KMN organization is shown in *Figure 1-4*. I will briefly discuss the specific functions along with the known interactions at kinetochore of the KMN subcomplexes here.

KNL1C is composed of KNL1 and Zwint subunits. KNL1 is the largest outer-kinetochore protein - with 2316 residues - and is largely intrinsically disordered, except for the C-terminal 500 residues organized in RWD domains. The unstructured N-terminal portion of KNL1 contains the canonical binding site for the phosphatase PP1 (refer to section 1.3.5 for functional details) and is shown to bind microtubules (Espeut et al., 2012). The binding of PP1 and microtubules to KNL1 N-terminal region is mutually exclusive (Bajaj et al., 2018). KNL1 also contains multiple Met-Glu-Leu-Thr (MELT) motifs, whose phosphorylation by MPS1 at the threonine residues contributes to the recruitment of BUB1/BUB3 complex and downstream SAC components (Yamagishi et al., 2012; Primorac et al., 2013; refer to section 1.3.2 for more details). The KNL1 C-terminal region, consists of a predicted coiled-coil followed by tandem RWD domains. The C-terminal region is involved in the interaction with the NSL1 subunit of the MIS12 complex (Petrovic et al., 2010) and with Zwint (Kiyomitsu et al., 2007). Zwint is believed to further recruits ZW10, a member of the Rod-Zwilch-ZW10 (RZZ) complex, that is involved in SAC regulation during mitosis (Kops et al., 2005).

The MIS12C constitutes of four subunits MIS12, NNF1, DSN1 and NSL1. The crystal structure of the MIS12C revealed, that the four subunits are helical proteins which pairs in DSN1-NSL1 and MIS12-NNF1 subcomplexes and meet in a central stalk domain (Petrovic et al., 2016). MIS12C is the main linker between inner kinetochore and the outer kinetochore. The NNF1 subunit binds to the CENP-C of inner kinetochore and this interaction is important for the kinetochore localization of MIS12C (Screpanti et al., 2011). MIS12C is the crucial component of the KMN network with the DSN1:NSL1 sub-complex binding to both the NDC80C and KNL1 (Petrovic et al.,2010; Petrovic et al., 2016). As discussed in the last section, MIS12C is recruited to the kinetochore also via interaction with CENP-T. These two independent recruitment pathways are

hypothesized to be effective in maintaining kinetochore as a multi-valent microtubule binder (Walstein et al., 2021).
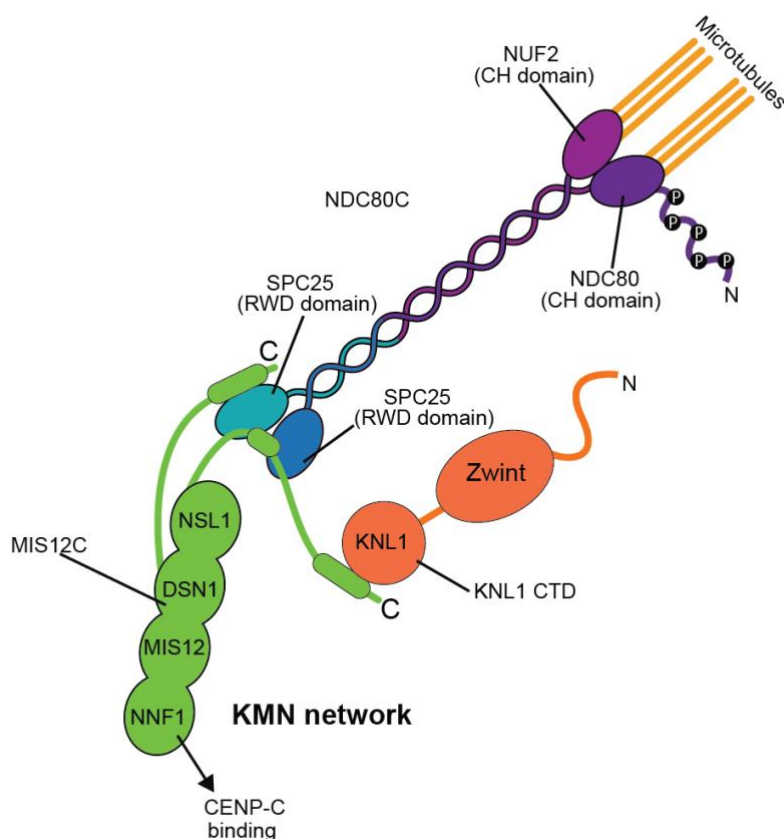
Figure 1-4 The KMN network

Schematic organization of the KMN network. The relevant interactions between the subcomplexes are discussed in the text. Figure modified from (Pesenti et al., 2016)

The NDC80C is the primary microtubule receptor at the kinetochore and it consists of the four subunits NDC80 (also called HEC1), NUF2, SPC24 and SPC25. It is an approximately 55 nm long dumbbell-shaped structure, with globular domains of each subunit at the two ends, connected by coiled-coil segments in the middle (Ciferri et al., 2005; Wei et al., 2006; Wei et al., 2007). The globular RWD domains of the SPC24-SPC25 pair is involved in the kinetochore localization of NDC80C, through its interaction with DSN1 and NSL1 subunits of the MIS12C (Ciferri et al., 2008; DeLuca et al., 2006; Petrovic et al., 2010). The N-terminal region of CENP-T is also shown to bind the SPC24-SPC25 in a CDK1 phosphorylation dependent manner (Huis In 't Veld et al., 2016; Nishino et al., 2013). At the opposite end of NDC80C, the globular heads of HEC1 and NUF2 fold into to a calponin-homology (CH) domain and bind to positive ends of depolymerising microtubules, forming load-bearing attachments. The CH

domain of HEC1 recognizes both α- and β-tubulin at the intra and inter-tubulin interfaces (Alushin et al., 2010). Additionally, the electrostatic interaction between positively charged disordered N-terminal HEC1 tail with the negatively charged C-terminal tails of tubulin monomers is shown to promote microtubule binding (Alushin et al., 2012). Phosphorylation by Aurora B kinase at residues in this HEC1 tail neutralizes the positive charge of the tail and thereby decreases the binding affinity for microtubules. Thus, Aurora B phosphorylation of HEC1 N-terminal region negatively regulates microtubule binding (Wei et al.,2007; Miller et al., 2008). The fibrous corona is assembled only at unattached kinetochores and is discussed briefly in section 1.3.2. To conclude this part, the outer kinetochore is the structural platform of the kinetochore that primarily binds microtubules and in the absence of microtubule binding, the KMN network recruits SAC proteins to promote checkpoint signalling.

1.3 The Spindle Assembly Checkpoint

The SAC is the signalling pathway that ensures the fidelity of chromosome segregation during mitosis in all eukaryotes. During prometaphase, the chromosomes must bind spindle microtubules in a conformation termed *bi-orientation*, where the kinetochores of sister chromatids are attached to microtubules emanating from opposite poles of the mitotic spindle. This attachment status is fundamental for metaphase plate formation and for even chromosome segregation at anaphase. The SAC monitors the status of kinetochore-microtubule attachment during prometaphase and, even if a single kinetochore is not correctly attached, the SAC signalling remains active. Lack of bi-orientation can occur if a kinetochore is either completely unattached or improperly attached to the mitotic spindle microtubules. The unattached or improperly attached kinetochore is the signalling hub for the SAC, and it recruits in a hierarchic manner the SAC proteins to the outer kinetochore to ultimately allow the assembly of the SAC effector, the Mitotic Checkpoint Complex (MCC).

MCC inhibits the Anaphase Promoting Complex or Cyclosome (APC/C). The APC/C, a 1.2 MDa protein complex, is an E3-ubiquitin ligase that targets the degradation of several proteins via the proteasome (Pines 2011). The activation of APC/C in mitosis requires the binding of its co-activator CDC20. The CDC20-activated APC/C, APC/C^{CDC20}, tags proteins with ubiquitin for proteasomal degradation. APC/C^{CDC20} targets proteins containing specific degron motifs, called destruction (D)-boxes and

KEN-boxes for ubiquitination (Kramer et al., 1998; Peters, 1998). Two important substrates of APC/C^{CDC20} are CyclinB and Securin. As discussed above, CDK1 is inactive without CyclinB and therefore once CyclinB is destroyed, the phosphorylation of substrates necessary to sustain mitosis fails, ultimately leading to mitotic exit. Securin binds to the protease Separase and keeps it inactive. Degradation of Securin results in active Separase, which then cleaves the Cohesin complexes still present between the sister chromatids. Loss of cohesion leads to sister chromatid separation and anaphase onset. To prevent mitotic exit in the presence of unattached or incorrectly attached kinetochores, the MCC docks onto the APC/C^{CDC20} active site as pseudo-substrate, and further inhibiting its activity through allosteric structural changes and competing with the binding of the E2-ubiquitin conjugate on the APC/C. The continuous assembly of the MCC ensures that as long as improperly attached chromosomes remain, the SAC halts cells in mitosis and provides time sufficient for the cells to overhaul the erroneous attachments (Figure 1-5).
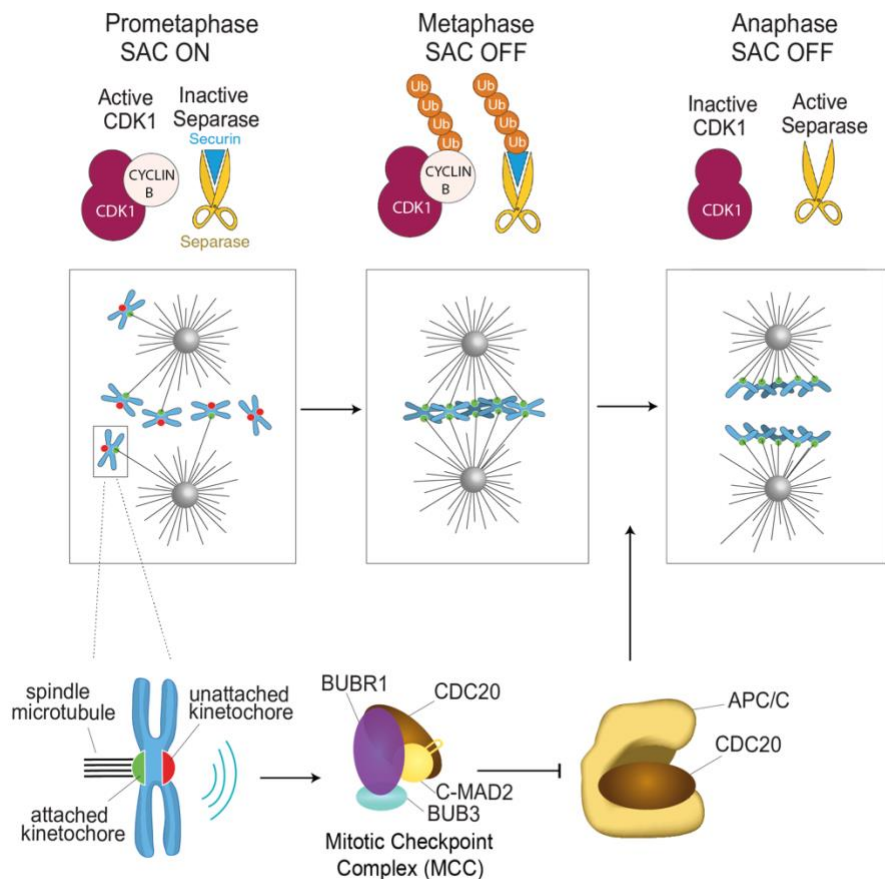
Figure 1-5 The spindle assembly checkpoint

Mitosis is initiated by activation of the CDK1-CyclinB complex. During prometaphase, if a chromosome is not bioriented, unattached or improperly attached kinetochores (red) emit the SAC signal. The signaling results in the assembly of an effector complex, MCC, which is a quaternary protein complex

as shown in the figure. MCC binds and inhibits APC/C^{CDC20}, which is required for the metaphase–anaphase transition, thus preventing entry into anaphase. When the last unattached kinetochore gets bound to microtubules, SAC signaling stops and APC/C^{CDC20} gets reactivated, resulting in CyclinB and Securin ubiquitination and proteolysis. Their destruction starts anaphase onset and cell exit mitosis (figure adapted from Musacchio, 2015).

The SAC is a signaling cascade controlled by the kinetochore-microtubule attachment status, which is sensed as a mechanical stimulus and, then, transduced to a diffusible chemical signal, the MCC. There are two distinct models that describe the possible stimuli sensed by the kinetochores and that determine the SAC activation and inactivation, the *attachment model* and the *tension model*. Over the last three decades, there have been many studies supporting and contradicting these two models. The *attachment model* claims that the attachment of the kinetochore proteins to the microtubules is sufficient to control the SAC signaling. This means that when the outer-kinetochore proteins are not interacting with microtubules, the SAC signaling is initiated and when the attachment to microtubules occurs, this is sufficient to satisfy the SAC and silence it (Reider et al., 1995, O'Connell et al., 2008). There have been two recent studies that support this model. They claim that stable end-on attachment of microtubules to kinetochores is sufficient to satisfy the SAC, even in the absence of detectable microtubule pulling forces or kinetochore tension (Tauchman et al., 2015; Etemad et al., 2015). Opposing this view, the *tension model* claims that the tension exerted on kinetochores by the bipolar microtubule attachment is required for SAC silencing (McIntosh, 1991; Li and Nicklas, 1995). The inter-dependency between the microtubule attachment status and the tension exerted on kinetochores makes it an extremely difficult task to distinguish their independent contributions to the activation/inactivation of the SAC response. Nonetheless, more recently, a general consensus has been achieved on the hypothesis that the SAC monitors the stretching happening within the kinetochore architecture (Uchida et al., 2009), and this intra-kinetochore stretching only occurs via end-on but not lateral microtubule attachments (Kuhn et al., JCB 2017). The intra-kinetochore distance (measured from CENP-A to the HEC1 subunit of NDC80) has been shown to increase from ~65 nm - without tension - to ~102 nm in the presence of microtubule-dependent tension (Joglekar et al., 2009; Maresca & Salmon, 2009; Wan et al., 2009).

1.3.1 Regulation of the phosphorylation status of kinetochore

Aurora B is a S/T kinase that is part of the chromosomal passenger complex (CPC), which also comprisees the Inner Centromeric Protein (INCENP), Survivin, and Borealin, that together form for the localization module of CPC (Tanaka et al., 2002; Carmena et al., 2012; Krenn and Musacchio, 2015). The CPC has been reported to be involved in the regulation of chromosome structure, kinetochore–microtubule attachment and SAC response during early mitosis (Carmena et al., 2012). The recruitment of the CPC to the centromere occurs via two distinct pathways mediated by different mitotic kinases phosphorylating components of the nucleosomes. In the first pathway, the histone protein H3 is phosphorylated at the Thr3 residue by Haspin kinase and the phosphorylation creates the binding site for the CPC component Survivin (Wang et al., 2010, 2012; Yamagishi et al., 2010). In the second pathway, the histone protein H2A is phosphorylated by BUB1 kinase at the Thr120 residue to recruit the mitotic protein Shugoshin1 (Sgo1), that, in turn, binds the CPC component Borealin (Kawashima et al., 2010; Yamagishi et al., 2010; Liu et al., 2015). A recent *in vivo* study showed that the described phosphorylation events on H3 and H2A are spatially distinct and individually capable of recruiting the CPC to centromeres. The study also showed that the Haspin-mediated pathway recruits Aurora B to the inner-centromeric region whereas the BUB1 mediated pathway results in a kinetochore-proximal outer centromeric pool of Aurora B (Broad et al., 2020).

Aurora B regulates the microtubule-kinetochore interaction, as it can de-stabilize the attachments through the phosphorylation of KMN network proteins. The so-called *spatial separation model* suggests that Aurora B activity on its outer kinetochore substrates – mainly NDC80C - depends on the distance of the substrates from the inner centromere, where Aurora B is localized (Liu et al., Science, 2009; Lampson and Cheeseman, 2010) (Figure 1-6). In other words, the intra-kinetochore stretching induced by microtubule pulling forces keeps Aurora B spatially separated from its substrates at the outer-kinetochore. Thus, once bi-orientation is established, further Aurora B phosphorylation of KMN network is prevented, allowing the mitotic phosphatases to reverse the Aurora B phosphorylation events and, thereby, stabilizing the kinetochore-microtubule attachments. This model also assures that, in the presence of kinetochore-microtubule attachments that fail to generate proper tension

(syntelic or monotelic), Aurora B substrates remain phosphorylated and attachments intrinsically unstable (Krenn and Musacchio, 2015; Liu et al., Science, 2009). It is understood that Aurora B phosphorylation of the KMN network components, primarily the HEC1 subunit of NDC80C, not only destabilizes the attachment to microtubules, but also initiates the SAC signaling cascade at kinetochores. Aurora B works together with HEC1 to recruit MPS1, another major mitotic kinase involved in the SAC response, to kinetochores (Saurin et al., 2011). Once at kinetochore, MPS1 phosphorylates many substrates required for the recruitment of other SAC proteins and the assembly of the effector complex, as discussed in detail in the next section.
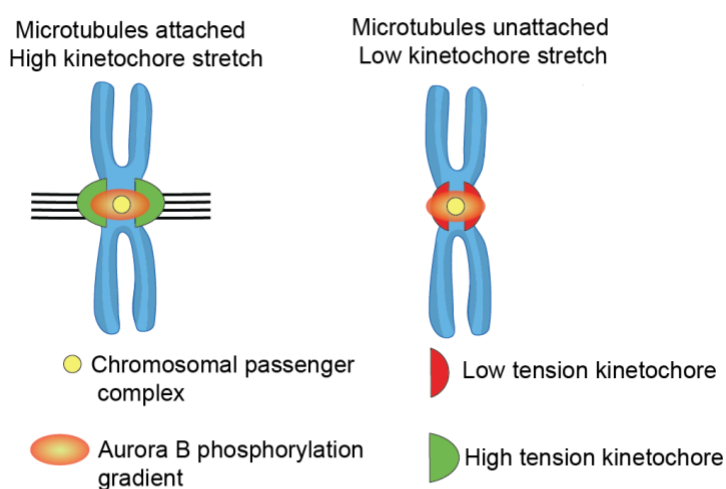
Figure 1-6 *Spatial separation model* of Aurora B activity regulation
A highly tuned Aurora B phosphorylation gradient extends from centromere, where the CPC localizes (light yellow), to the outer kinetochores. When microtubules are attached, kinetochores undergo stretching (green) and as a result, substrates (e.g., in the KMN network) are no longer in the vicinity of Aurora B localized at centromeres. The increased distance decreases the degree of kinetochore components phosphorylation and increases kinetochore affinity for microtubules. Contrarily, when the kinetochores are unattached (red), there is no intra-kinetochore stretching. Aurora B can still reach and phosphorylate the kinetochore substrates (represented in the figure by the phosphorylation gradient reaching till the end of the red kinetochores).

1.3.2 Kinetochore recruitment of SAC proteins

The kinetochore functions not only as a structural scaffold bridging mitotic chromosomes and microtubules, but also as SAC signaling hub by recruiting numerous SAC proteins when unattached (note that from here onwards *unattached kinetochore* refers to a kinetochore with any type of attachment error, including lack of attachment,

that can activate SAC). In this section, I will briefly discuss about the recruitment pathways and localization patterns of the SAC proteins at kinetochore during the mitotic checkpoint. Although the exact hierarchy of recruitment of SAC proteins to KMN network is not yet fully elucidated, it is now rather well understood that phosphorylation of KMN components by mitotic kinases Aurora B and MPS1 is an upstream process in these recruitment pathways that lead to SAC activation.
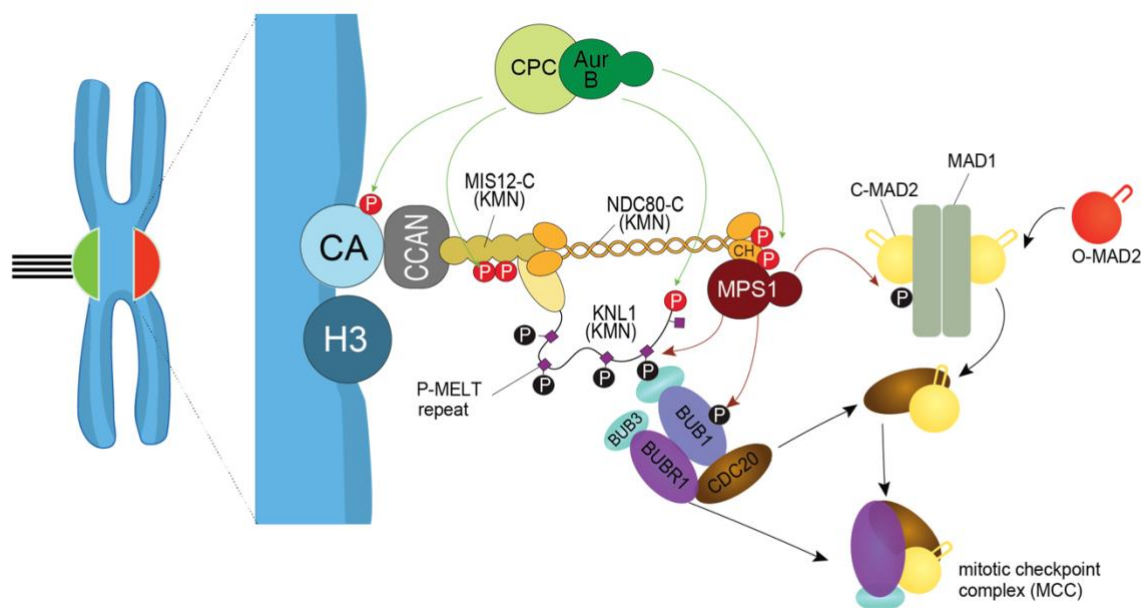
Figure 1-7 Kinetochore recruitment of SAC proteins and MCC assembly

The recruitment of SAC proteins at kinetochores depends primarily on the KMN network components Knl1 and NDC80. Aurora B and MPS1 kinases phosphorylate different sites on these complexes (in the figure the phosphorylation is shown as P) and promote the recruitment of the SAC proteins BUB1:BUB3, BUBR1:BUB3, CDC20, MAD1:C-MAD2, and O-MAD2. The phosphorylation-mediated interaction of SAC proteins and kinetochore components ultimately results in the formation of MCC. For more details see text. Many SAC proteins described in the text are not represented in the schematic both to avoid complexity and because for some of them the recruitment mechanism is still not fully understood. The figure is adapted from *Musacchio, 2015*. Green arrows show the phosphorylation by Aurora B, brown arrows show the phosphorylation by MPS1, black arrows show interaction dependencies for the formation of MCC.

Monopolar Spindle Protein 1 (MPS1) (Weiss & Winey, 1996) is a S/T protein kinase that lies at the pinnacle of SAC signaling. Its catalytic activity at the KMN network is imperative for the recruitment of the downstream SAC components (Pachis et al., 2018; Musacchio, 2015) (Figure 1-7). However, the exact molecular mechanism of MPS1 kinetochore recruitment remains elusive. Knocking down MPS1 or inhibiting its

kinase activity results in premature mitotic exit with chromosome segregation errors (Abrieu et al.,2001; Stucke et al., 2002; Lan et al., 2010). There is an ample number of studies claiming that MPS1 binds to the HEC1 subunit of NDC80 and this interaction is dependent on Aurora B activity (Hiruma et al., 2015; Ji et al., 2015; Dou et al.,2015; Nijenhuis et al.,2013; Saurin et al., 2011). The observation that MPS1 binds to Calponin Homology (CH) domain of HEC1, which is also the microtubule binding site of HEC1, suggests a competition between microtubules and MPS1 for the binding to HEC1 (Hiruma et al., 2015; Ji et al., 2015). There are contradicting results about whether MPS1 removal from kinetochores is sufficient for SAC satisfaction and mitotic exit (Maldonado et al., 2011; Jelluma et al., 2010). Also, a recent study reported that kinetochores can bind MPS1 and microtubules simultaneously (Koch et al., 2019). So further investigations are necessary to understand whether any additional recruitment pathways for MPS1 exist at kinetochores.

At kinetochores, MPS1 phosphorylates the MELT repeats present in the N-terminal region of KNL1 and, thus, creates the docking site for the binding of BUB1:BUB3 complex (London et al., 2012; Shepperd et al., 2012; Yamagishi et al., 2012). BUB3 (Budding Uninhibited by Benzimidazole 3) contains a WD40 domain and forms a constitutive complex with BUB1 and BUBR1 by interacting with their BUB3-binding motifs (also called GLEBS) (Taylor et al.,1998). Although BUB1 and BUBR1 are paralogs, there are major functional differences between the two proteins: 1) BUB1 is not embedded in the MCC, whereas BUBR1 is an essential component of MCC; 2) BUBR1 is a pseudo-kinase, while BUB1 is a catalytically active kinase; 3) in BUB1:BUB3 complex, a short loop of BUB1 located upstream the GLEBS enhances the binding of BUB3 with the phosphorylated KNL1, while in BUBR1 this loop is essential for the ability of BUB3 within the MCC to inhibit APC/C activity (Overlack et al., 2015). Therefore, the BUB3-BUBR1 complex cannot directly bind to the phosphorylated MELT motifs and, for this reason, the kinetochore recruitment of BUBR1 requires a direct and *pseudo-symmetric* interaction with BUB3-BUB1 (Zhang et al., 2015; Overlack et al., 2015). Kinetochore localization of CDC20 depends on the presence of both BUB1 and BUBR1 at kinetochore and the ABBA and KEN motives present in both proteins have a major role in the interaction with CDC20 (Li et al., 2010; Di Fiore et al., 2015).

The ROD–ZW10–Zwilch (RZZ) complex (Starr et al., 2000; Karess, 2015) forms oligomers at kinetochores and, along with other SAC proteins, forms the expandable corona structure. Spindly, a dynein adaptor, is one of the known interactors of the RZZ complex. Spindly needs to be farnesylated at its C-terminus for the successful recruitment at kinetochores and for its interaction with RZZ (Holland et al., 2015; Moudgil et al., 2015, Mosalaganti et al., 2017). The expanded corona structure increases the likelihood of microtubules to be captured by the kinetochores during early prometaphase and the structure disassembles once end-on attachment is established. Different studies demonstrated that RZZ components interact with outer kinetochore proteins, like NDC80C (Cheerambathur et al., 2013; Samejima et al., 2015) and KNL1 (Caldas et al., 2015).

Mitotic Arrest Deficient 1 (MAD1) is a 90 kD coiled-coil protein with a characteristic rod shape. The MAD1 C-terminal domain (CTD) contains an N-terminal coiled-coil and a RWD domain (Sironi et al., 2002; Kim et al., 2012). MAD1 forms a constitutive hetero-tetramer with the protein MAD2 and it is recruited to unattached kinetochore via two possible pathways, depending on BUB1:BUB3 and RZZ complexes. Phosphorylation of the middle region of BUB1 (CM motif) by MPS1 facilitates its interaction with MAD1 (London et al., 2014), making BUB1:BUB3 a structural scaffold at the kinetochore for MAD1 recruitment. In addition to this, evidences in human cells suggest that RZZ contributes to targeting MAD1:C-MAD2 to the corona, the expanded fibrous layer of proteins outside to KMN network (Caldas et al., 2015; Silio et al., 2015).

1.3.3 The Mitotic Checkpoint Complex: structural perspective

The MCC is formed by the association of the four SAC proteins MAD2, CDC20 and the constitutive complex BUBR1:BUB3. I will briefly discuss the important structural features of these proteins that are relevant for the SAC signaling.

BUBR1 is characterized by an N-terminal helix-loop-helix (HLH) region, containing the KEN1 motif, essential for the binding to CDC20 and the GLEBS motif which is the binding site of BUB3 (Larsen et al., 2007). Further domains and motifs of BUBR1 that are not relevant for the interaction with MCC components are depicted in the schematic representation for clarity (Figure 1- 8A). CDC20 contains a WD40 domain, surrounded by a long N-terminal disordered region and a short C-terminal extension required for

its interaction with the APC/C. CDC20 performs a dual and contrary role during mitosis. It functions both as a co-activator of the APC/C, promoting substrates ubiquitination, and as an inhibitor of the APC/C when it is embedded in the MCC to prevent anaphase onset. The C-box at the N-terminal extension is important for CDC20 to function as co-activator of APC/C. Conversely, the MAD2 Interacting Motif (MIM) is required for MAD2 binding. Finally, the C-terminal IR tail mediates CDC20 binding to the APC/C (Luo et al., 2002; Primorac et al., 2013).
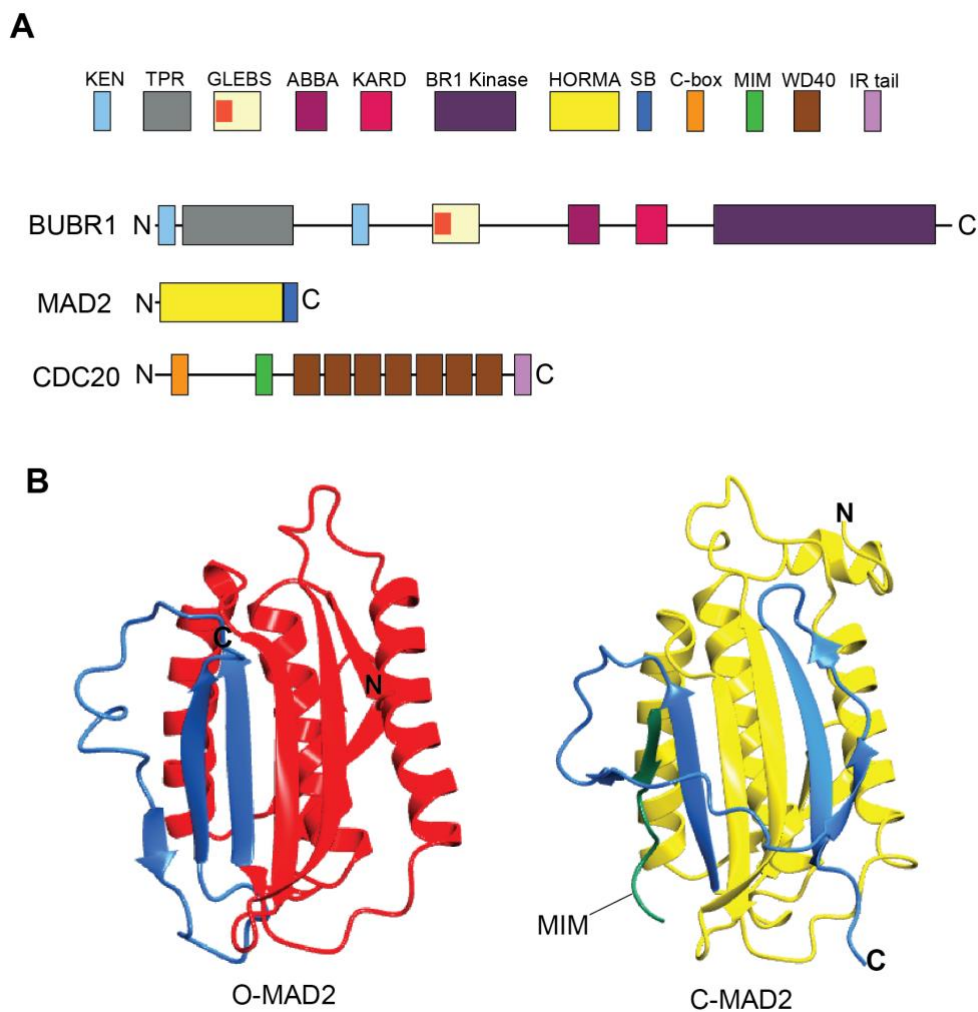
Figure 1-8 Domains of MCC components and MAD2 conformational change

A) Schematic of the domain organization of human BUBR1, MAD2 and CDC20.TPR, tetratricopeptide repeats; KEN, lysine (K)- glutamic acid (E)- asparagine (N) box; GLEBS, GLE2p-binding sequence; ABBA, Cyclin A, BUB1, BUBR1, Acm1-motif; KARD, kinetochore associated regulatory domain; WD, tryptophane (W)- aspartic acid (D) repeats; SB, safety belt region; MIM, MAD2 interacting motif, IR tail, Isoleucine (I)- Arginine (R) tail. B) Crystal structures of O-MAD2 and C-MAD2 (PDB ID 2V64), with the C-terminal safety belt region shown in blue. The MIM[CDC20] (residues 111-138 of CDC20) has been embraced by the 'safety belt' in the C-MAD2 structure. MIM[CDC20] is shown in green.

MAD2 is a HORMA (Hop1, Rev7, MAD2) domain protein that exists in two different conformations in the cell, named *open* and *closed* MAD2 (O-MAD2 and C-MAD2) respectively. MAD2 adopts the closed conformation when it binds to the MIM of MAD1 or CDC20 to form a stable complex (Luo et al 2002; Luo et al., 2004; Sironi et al., 2002). O-MAD2 is the conformation adopted by MAD2 when it is free of any binding partners. The transition from the O-MAD2 to the C-MAD2 requires a major topological rearrangement of the C-terminal tail of MAD2, the so-called *safety belt* region, which is reorganized to wrap around the MIM of the ligand (Figure 1-8 B). It has been also observed that purified O-MAD2 can spontaneously convert into unliganded C-MAD2 at very slow rates *in vitro* (Yang et al., 2008).

The determination of the crystal structure of the MCC from *Schizosaccharomyces pombe* (PDB ID 4AEZ) represented a significant advance in the field (Chao *et al.,* 2012). The authors showed that the MCC is a triangular heterotrimeric complex of MAD3 (yeast ortholog of BUBR1), MAD2 and CDC20. MAD2 and CDC20 interact primarily by the sequestration of CDC20 MIM by the MAD2 safety belt. The HLH motif, along with the nearby KEN box, and TPR domain of BUBR1 simultaneously make contacts with both MAD2 and CDC20, reinforcing the cooperative assembly of MCC. In this assembly, C-MAD2 is required to confer high-affinity binding of BUBR1 to CDC20, consistent with previous studies (Davenport et al., 2006; Burton & Solomon, 2007), and MAD2 and BUBR1 synergize to inhibit CDC20-mediated activation of APC/C^{CDC20}. Two highly conserved surfaces on the CDC20 WD40 domain are the receptor for the D-box and the KEN-box of the substrates of the APC/C (Chao et al., 2012). The MCC inhibits the APC/C by obstructing these receptor sites on CDC20 in the APC/C^{CDC20}.

The mechanism by which MCC inhibits APC/C has been characterized by a following study from Alfieri *et al.*, 2016, where the authors determined the structure of the human APC/C^{CDC20}–MCC complex (APC/C^{MCC}) with near-atomic resolution. Both CDC20 and BUBR1 within the MCC make inhibitory contacts with APC/C. BUBR1 contacts the CDC20$^{APC/C}$ through the N-terminal KEN2 motif and the TPR region, blocking the degron recognition sites of the CDC20$^{APC/C}$. BUBR1 also occludes the binding of the E2 enzyme UbcH10 to further repress APC/C ubiquitination activity. The authors observed two additional contacts of CDC20^{MCC} through its C-terminal IR tail and WD40

domainto APC8A and APC4 subunits of APC/C respectively. The conformational flexibility of the APC15 subunit generates structural variants of the APC/C^{MCC} structure, including variants capable of associating with UbcH10, leading to CDC20^{MCC} auto-ubiquitination. This leads to spontaneous reactivation of the APC/C^{CDC20} when the SAC is silenced (Pan et al., 2004; Reddy et al., 2007; Stegmeier. et al., 2007; Zhang and Chang et al., 2016; Alfieri et al., 2016).

1.3.4 The Mitotic Checkpoint Complex: its catalytic assembly

O-MAD2 binds the MIM of CDC20 to form the CDC20:C-MAD2 complex. This complex then binds the constitutive BUBR1:BUB3 sub-complex to form the MCC. The binding of MAD2 to CDC20 is the rate limiting step of MCC formation, because of the topological change of MAD2 that requires a large activation energy and is an extremely slow reaction in isolation (Simonetta et al., 2009; Musacchio, 2015). On the other hand, experiments in human cells have demonstrated that SAC activation happens abruptly in a few minutes (Hagting et al., 2002; Dick and Gelrich, 2013), suggesting that MCC assembly may be catalyzed in cells. Over the years, our laboratory has identified the catalytic components involved in this process along with describing the biochemical mechanisms relevant for catalysis.

The first identified catalyst of MCC assembly is the MAD1:C-MAD2 complex. Upon mitotic entry, MAD1:C-MAD2 is recruited to kinetochore through mechanisms described in section 1.3.2 and, once at kinetochores, the MAD1:C-MAD2 complex promotes the recruitment of the cytosolic O-MAD2 via the dimerization with C-MAD2. This so-called *MAD2 template model* (De Antoni et al., 2005) proposes that O-MAD2 and MAD1 bound C-MAD2 constitute two different pools of MAD2 and the transient *conformational* dimerization of O-MAD2 with the C-MAD2 *template* of the MAD1:C-MAD2 complex facilitates the binding of O-MAD2 to CDC20 (Figure 1- 9). Many *in vivo* observations later verified the MAD2 template model indirectly. For instance, the removal of MAD1:C-MAD2 from kinetochores upon microtubule attachment is required for SAC silencing (Howell et al., 2001; Chan et al., 2009) and artificial tethering of MAD1:C-MAD2 at kinetochores prevents SAC silencing (Maldonado et al., 2011; Kuijt et al., 2014).

In vitro observations showed that MAD1:C-MAD2 could accelerate binding of O-MAD2 to CDC20 by a factor of 4, further supporting the MAD2 template model (Simonetta et al., 2009). However, this acceleration is not sufficient to explain the rapid SAC response reported in cells, suggesting additional players or mechanisms involved in MCC catalysis. Almost a decade later, in 2017, a study from our laboratory described the construction of FRET sensors to monitor MCC assembly in real-time, thus allowing the measurement of assembly kinetics *in vitro* (Faesen et al., 2017). The two FRET sensors designed in this study have a CFP and TAMRA fluorophore pair coupled with BUBR1/CDC20 and MAD2 respectively, both of which resulted in increased FRET signaling upon MCC assembly. The results showed that BUB1:BUB3 and MAD1:C-MAD2, both necessarily phosphorylated by MPS1, function as catalysts responsible for MAD2 conformational change and MCC assembly. MPS1 phosphorylates MAD1^{RWD} domain and is essential for the catalysis. Also, the binding of BUB1 and MAD1 was observed *in vitro* and MPS1 activity is indispensable for this interaction to happen. The contribution of BUB1 to catalysis is attributed to its ability to bind CDC20 through the KEN1-ABBA motif (Di Fiore et al., 2015; Diaz-Martinez et al., 2015; Faesen et al., 2017). Further mechanistic details of the spatial interaction between the catalytic components and the importance of kinetochore in MCC catalysis needs to be investigated.
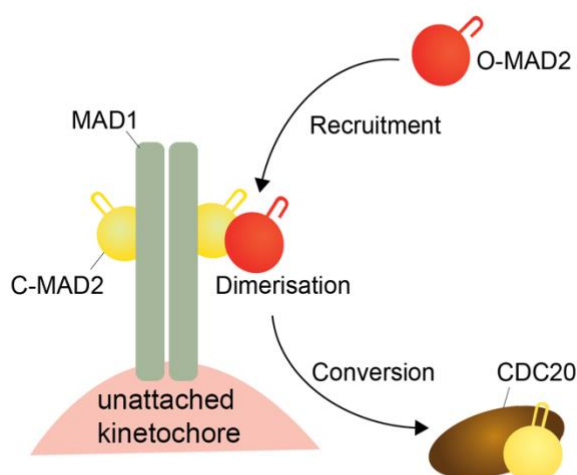
Figure 1-9 Schematic of MAD2 template model

Unattached kinetochore recruits MAD1:C-MAD2 complex to the kinetochore. Once at the kinetochore, this complex recruit O-MAD2 from the cytosol by forming C-MAD2: O-MAD2 homodimers. The dimerization induces a conformational change in the recruited O-MAD2 allowing it to bind CDC20 present at kinetochores to form CDC20:C-MAD2 complex.

1.3.5 SAC silencing

As soon as the last unattached kinetochore is correctly attached to microtubules, the APC/C has to be quickly reactivated to silence the SAC and promote mitotic exit. The SAC silencing involves mainly two processes: sensing the microtubule attachment/tension to silence the signaling at kinetochores and rapid MCC disassembly to relieve APC/C of inhibition.

Silencing of kinetochore SAC signaling happens by the active removal of SAC proteins from the attached kinetochore, and through the activity of phosphatases that counteract mitotic kinases (Lischetti and Nilsson, 2015). The active removal of checkpoint proteins mainly occurs through the minus-end directed motor protein *dynein* upon stable kinetochore-microtubule attachment (Howell et al., 2001). The checkpoint proteins MAD1, MAD2, BUB1, and BUBR1 have been identified as dynein cargoes and are redistributed from attached kinetochores to spindle poles, in a dynein-dependent manner (Silva et al., 2014). It has been shown that tethering of MAD1 to bi-oriented kinetochores, by fusing MAD1 to MIS12, delays anaphase onset (Maldonado & Kapoor, 2011) and it is a clear indication that dynein mediated removal of MAD1 is imperative for SAC silencing. The RZZ complex, along with its adaptor protein Spindly, has been implicated in the kinetochore recruitment of dynein. Spindly N-terminal coiled-coil uses distinct motifs to bind the dynein light intermediate chain and the pointed-end complex of dynactin (Gama et al., 2017). This Spindly-mediated targeting of dynein/dynactinto kinetochores is required for the poleward transport of checkpoint proteins (Chan et al., 2009; Gassmann et al., 2008; Gassmann et al., 2010).

The primary phosphatase that has been identified to promote SAC silencing at kinetochores is the Protein Phosphatase 1 (PP1). KNL1 has a PP1-binding motif in its N-terminal region, and SAC silencing has been shown to be dependent on PP1 recruitment by KNL1 (Liu et al., 2010; Rosenberg et al., 2011). Once at kinetochores, PP1 dephosphorylates the MELT motifs on KNL1 and promotes the removal of BUB1/BUBR1:BUB3 proteins from kinetochores (Espert et al., 2014; Nijenhuis et al., 2014). In agreement with these observations, increased kinetochore levels of BUB1 and BUBR1 are observed when the PP1 binding site on KNL1 is removed (Zhang et al., 2014). PP1 also dephosphorylates the Aurora B substrates at kinetochores to

promote SAC silencing. The PP1 binding site on KNL1 contains a consensus site for Aurora B phosphorylation, which when phosphorylated, prevents PP1 binding (Liu et al., 2010). Thus, PP1 and Aurora B activities antagonize each other at the outer kinetochore.

Additionally, Protein phosphatase 2A (PP2A), is a ubiquitous S/T phosphatase that has structurally similar catalytic domainto that of PP1 (Ingebritsen et al.,1983). PP2A-B56 holoenzyme (B56 is a regulatory subunit) can bind LxxIxE motif on proteins and thereby localize to specific regions in cells (Hertz et al., 2016). By similar interactions, BUBR1 recruits PP2A-B56 to kinetochores (Xu et al., 2013). BUBR1-associated PP2A-B56 has been identified as a key phosphatase for the removal of the MPS1-mediated KNL1 phosphorylation (Espert et al., 2014). SAC silencing is thus promoted by a negative feedback loop involving the MPS1 dependent recruitment of BUBR1:BUB3 via BUB1:BUB3, which in turn mediates the recruitment of PP2A-B56. Further studies on the substrate specificity of the individual PP1 and PP2A phosphatases are necessary to clearly distinguish their functional roles in a cellular context.

1.4 The Mitotic Checkpoint Complex disassembly

SAC inactivation requires the disassembly of its effector complex, the MCC. In recent years, it has been shown that the tug of war between MCC assembly and disassembly occurs throughout mitosis, and both processes require timely regulation to determine the resultant MCC concentration in cells (Musacchio, 2015; Foley and Kapoor, 2013; Liu and Zhang, 2016). Since MCC is a stable complex, its dissociation does not occur spontaneously. Currently two major mechanisms for the disassembly of MCC have been described: APC/C mediated CDC20 ubiquitination (Alfieri et al., 2016; Yamaguchi et al., 2016) and TRIP13 mediated remodeling of MAD2 (Eytan et al., 2014; Ye et al., 2017; Alfieri et al., 2018). As described in section 1.3.3, the conformational flexibility of the APC/C^{MCC} complex enables UbcH10 association and, thereby, the ubiquitination of the CDC20 molecule inside the MCC (CDC20^{MCC}), a process that results in MCC disassembly and APC/C reactivation. The ubiquitination of CDC20 is mediated by the APC15 subunit (Foster et al., 2012; Mansfeld et al., 2011) and the depletion of APC15 leads to higher levels of CDC20^{MCC} associated to the APC/C^{CDC20} (Uzunova et al., 2012).

1.4.1 AAA+ ATPase TRIP13 mediated MCC disassembly

The AAA+ (ATPases associated with various cellular activities) ATPases are a functionally diverse group of proteins which can bind and hydrolyze ATP to generate conformational changes in a wide range of protein substrates (Hanson and Whiteheart 2005). The AAA+ ATPases are involved in a broad array of cellular processes, including protein degradation, DNA replication, cellular checkpoint functioning, and membrane fusion pathways. Examples of members of this protein family include 1) the NSF (N-ethylmaleimide-sensitive factor), a protein that associates to its adaptor α-SNAP and disassembles the SNARE complexes (Whiteheart et al., 2001); 2) Cdc48, also known as p97, which mediates protein degradation through ubiquitin fusion degradation (UFD) pathways (Xia et al, 2016; Olszewski et al, 2019); and 3) Vps4p, another AAA+ ATPase involved in membrane fusion pathways (Babst et al, 1998).

The AAA+ ATPases consist of an N-terminal domain (NTD) involved in cofactor binding and one or two ATPase domains. Each ATPase domain consists of Walker-A and Walker-B motifs essential for binding and hydrolyzing ATP, respectively. The Walker A motif has a consensus sequence of GXXXXGK[T/S], where X is any amino acid (Hanson and Whiteheart 2005) and the Walker-B motif is characterized by the sequence hhhhDE, where h represents any hydrophobic residue and the C-terminal residues are aspartate and glutamate (Hanson and Whiteheart 2005).The aspartate residue helps in binding Mg^{2+}, which is required for ATP hydrolysis, and the glutamate residue activates water for the hydrolysis reaction. Mutation of this Glu to Gln is commonly used as so-called Walker-B mutant for functional studies (WB^{EQ}). This mutant is still able to bind ATP, but it cannot hydrolyze it and, therefore, the ATPase is inactive and cannot impart conformational changes on substrates.

With the exceptions, most of the AAA+ ATPases are known to oligomerize into a closed barrel-like hexameric ring with an open central channel (Wang et al. 2001). The ATP binding sites are positioned at the interface between subunits, allowing for direct linkage between the nucleotide binding sites of adjacent subunits. All hexameric AAA+ ATPases have a central cavity or pore that is defined by residues belonging to each of the subunits. These residues facing the pores are of great importance for substrate binding and processivity, because most of the AAA+ ATPases thread their substrates

through the pore loops for imparting conformational changes. Depending on the state of nucleotide binding/hydrolysis, AAA+ ATPases undergo conformational changes and force conformational changes onto bound substrates. The subdomains of the ATPase domains undergo topological shifts when switching from ATP bound to ADP bound state. The reciprocal repositioning of the monomers in the hexamer is used by the ATPase to mechanically remodel the substrates (Wang et al., 2001; Rouiller et al., 2002; DeLabarre et al., 2005).
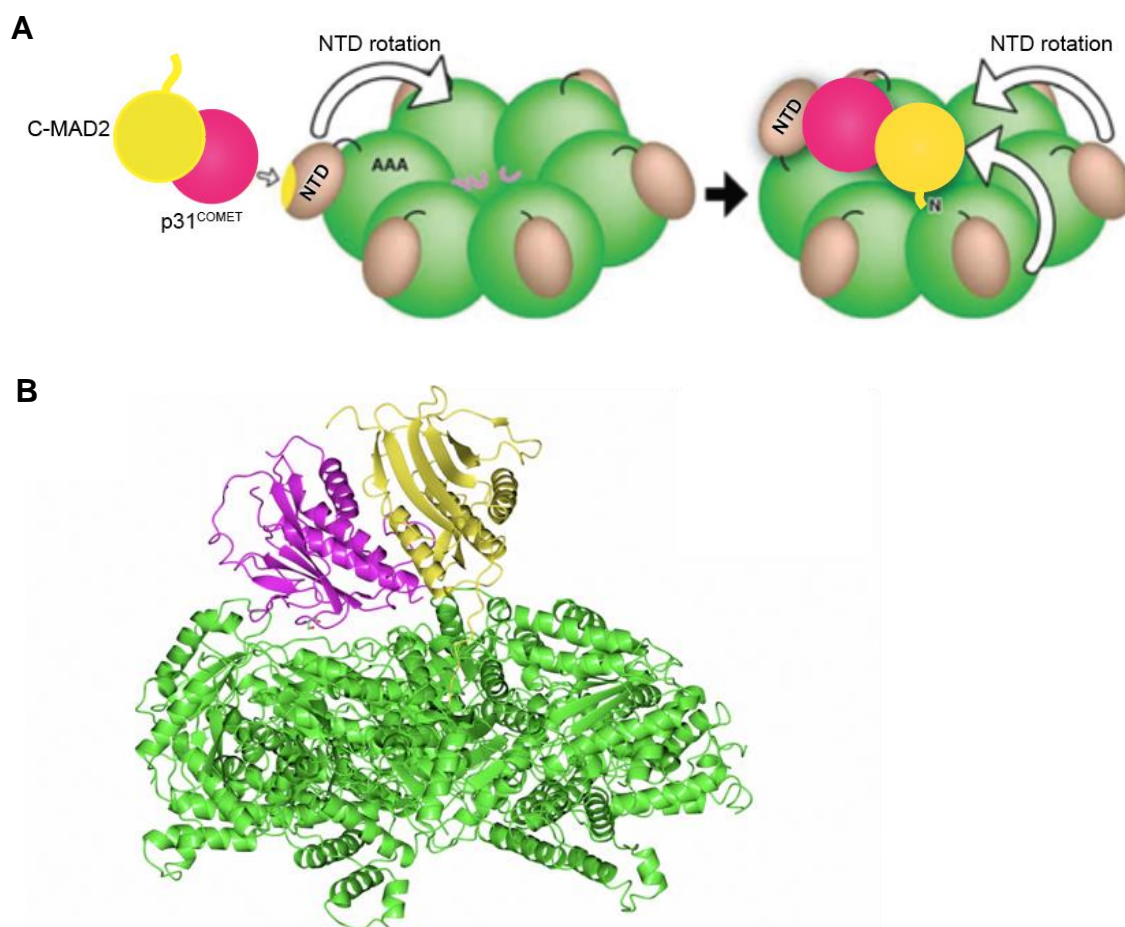
Figure 1-10 Interaction of TRIP13 with C-MAD2 substrate

A) Schematic of TRIP13 mediated conversion of MAD2. C-MAD2-p31[COMET] complex binds to the NTD of TRIP13 and undergoes a conformational switch by which the MAD2 N-terminus interacts with the pore residues of TRIP13. The details of the later ATPase mediated activity are discussed in the text (NTD, N-terminal domain; figure modified from Ye et al., 2017). B) Structure of C-MAD2: p31[COMET] complex where the N-terminus of MAD2 is directly interacting with TRIP13 pore (PDB: 6F0X).

TRIP13 is a AAA+ ATPase known to be a regulator of HORMA domain proteins (Joshi et. al, 2009; Roig et. al, 2010). The homolog of TRIP13 in yeast, the Pachytene checkpoint 2 (Pch2), is known to regulate processes like meiotic DNA recombination

and chromosomal axis formation (Vader, 2015). Homologs of TRIP13 have also been identified in worms, fruit flies, plants and mammals. p31^{COMET}, which acts as a TRIP13 co-factor in the remodeling of MAD2, is, like MAD2, a HORMA domain protein that forms heterodimers with C-MAD2, resembling the O-MAD2:C-MAD2 dimer formed at unattached kinetochores (Yang et al., 2008).

The molecular mechanism by which TRIP13 together with its cofactor p31^{COMET} converts C-MAD2 to O-MAD2 and disassembles MCC or MAD2:CDC20 complex (MC) is well understood. p31^{COMET} dimerizes with C-MAD2 within the MCC or MC and this cofactor-substrate complex later binds to TRIP13 via p31^{COMET} engagement to TRIP13 NTD. The cofactor binding to TRIP13 positions the disordered MAD2 N-terminus near the TRIP13 pore loop, which directly engages and unfolds MAD2 by using the energy obtained from ATP hydrolysis (Ye et al., 2017; Alfieri et al., 2018) (Figure 1-10). Structural data coupled with molecular modelling show that sequential ATP-driven translocation of TRIP13 subunits along the hexameric ring induces steric clashes with the globular domains of the p31^{COMET}:C-MAD2 complex. This steric clash leads to a rotation of p31^{COMET}:C-MAD2 complex globular domains with respect to TRIP13 axial pore loops. The tight binding of MAD2 N-terminus with TRIP13 pore loop residues induces the unwinding of the α-helix at the N-terminus of C-MAD2. The unwinding of the α-helix induces the conversion of C-MAD2 to O-MAD2, through the disruption of contacts between adjacent β8'-β8" hairpin that destabilize C-MAD2 conformation. Once MAD2 is converted back to the open conformation, it dissociates from p31^{COMET} and CDC20 to complete the MCC disassembly (Alfieri et al., 2018).

TRIP13:p31^{COMET} enzymatic machinery has been shown to disassemble C-MAD2 substrates in its various forms, such as C-MAD2:CDC20 (Eytan et al., 2104), MCC (Eytan et al., 2104), and MCC bound to APC/C (Alfieri et al., 2018; Kim et al., 2018). Whether MAD1:C-MAD2 is a substrate for TRIP13 still remains a fundamental unanswered question. It has been observed that p31^{COMET} can dimerize with C-MAD2 (Yang et al., 2007;2008) bound in the MAD1:C-MAD2 complex and be recruited to unattached kinetochores (Fava et al., 2011; Westhorpe et al., 2011). In *C. elegans*, TRIP13 orthologue is recruited to kinetochores via its interaction with p31^{COMET} and MAD1:C-MAD2 (Nelson et al., 2015). In this context, it is intriguing to investigate

whether MAD1:C-MAD2 is a TRIP13 substrate in humans and its possible implication on SAC function.

The MCC is also assembled during interphase as a safeguard measure to prevent premature mitotic exit prior to checkpoint activation (Liu and Zhang, 2016). TRIP13 mediated MCC disassembly occurs during interphase and TRIP13 catalytic activity is required to maintain a pool of O-MAD2 sufficient for MCC assembly, thereby supporting the mitotic checkpoint activation (Kim et al., 2018; Ma et al., 2018). The continuous TRIP13 mediated MCC disassembly is also required for maintaining O-MAD2 pool in the cytosol even when the SAC is already activated. The biochemical mechanisms by which MCC assembly is regulated both spatially and temporally is well understood. However, very little is known about the regulation of MCC disassembly during mitosis, especially through the TRIP13: p31^{COMET} pathway.

1.5 Electroporation of Recombinant Proteins for *in vivo* Functional Studies

So far, I have introduced many kinetochore and SAC proteins relevant for the biological questions discussed in the next section. While experimentally tackling these questions, we faced the problem of functionally characterizing the recombinant proteins that we use for our *in vitro* experiments inside live cells. To solve this experimental issue, we developed a method that employs *protein electroporation* (EP), to introduce recombinant proteins into sizable cell populations and subsequently perform functional studies. In this section I will introduce such methodology and its advantages for the purposes of cellular studies.

Cells are surrounded by plasma membranes, which constitute essential protective barriers for cellular integrity but impede the targeted delivery of biological macromolecules, such as proteins. Historically, introduction of protein variants into cells has been performed by transient transfection of DNA plasmids encoding these entities. Recipient cells, then, typically express the desired proteins within 1-2 days with levels that vary according to cell lines and among individual cells (Kim and Eberwine, 2010). Owing to the ease of transient transfection protocols, the method is widely used. Stable transfection of cultured mammalian cells offers more uniform protein expression, but the generation of stable clones is labor-intensive and time-consuming (Kim and Eberwine, 2010).

A significant fraction of cellular proteins exists within stable or dynamic multi-subunit assemblies (Vidal et al., 2011; Aloy et al., 2004). To study these protein complexes by endogenous expression methods becomes even more laborious, especially in terms of establishing similar expression levels for multiple subunits. As a rich collection of tools for the recombinant expression of protein complexes in heterologous systems, such as bacteria and insect cells, has been developed for structural studies (Perrakis et al., 2011), exploiting these tools for direct delivery of recombinant proteins in cells became highly attractive. Furthermore, recombinant proteins are amenable to various functional chemical modifications that would not be otherwise possible to achieve by genetic expression, thus, expanding the spectrum of applications for recombinant proteins in living cells. Microinjection is the most commonly used method for the introduction of recombinant proteins into mammalian cells (Komarova et al., 2007). This approach, even though it serves the purpose, has major limitations such as its low-throughput and the requirement of considerable handling skills. High-throughput approaches that enable protein delivery to a large number of cells are available, for instance the use of cell-penetrating peptide (CPP) tags (Inomata et al., 2009) or pore-forming bacterial toxins (Ogino et al., 2009; Teng et al., 2016), but present uncertainties with regard to protein uptake efficiencies and cytotoxicity.

Batch protein EP is an alternative method to directly deliver proteins into cultured mammalian cells (Lambert et al., 1990; Chakrabarti et al., 1989; Vienken et al., 1978; Shi et al., 2018; Furuhata et al., 2019). EP-mediated protein delivery has been used in recent years for many applications. For instance, protein EP has been used for cellular structural biology with isotopically labelled proteins (Theillet et al., 2016), introduction of immunoglobulins coupled with a *Trim-Away* approach for the targeting and degradation of endogenous proteins (Clift et al., 2017), and the delivery of ribonucleotide particles (RNPs) in CRISPR-Cas9-based approaches (Kim et al., 2014; Lin et al., 2014; Hashimoto and Takemoto, 2015). While these applications of EP are encouraging, acceptance of the methodology for routine applications of protein delivery requires strict evidences that the delivered proteins behave as expected, in terms of subcellular localization and functional replacement of the endogenous counterparts. With the intent of developing a robust method for the delivery of recombinant proteins into living cells, we rigorously investigated the use of EP to achieve such goals.

1.6 Objectives

During the time frame of my PhD, I was involved in investigating primarily two different scientific projects. For the convenience of the reader, these two consecutives, yet independent projects will be discussed separately starting from this section.

1.6.1 Establishing electroporation of recombinant proteins into mammalian cells as tool for functional studies

We often face the task of functional analysis of proteins in cells to endorse the biochemical characterization studies performed *in vitro*. Commonly used DNA transfection method for protein expression in mammalian cells have drawbacks including lack of homogenous expression and failure to study multi-subunit proteins. Direct delivery of recombinant proteins into mammalian cells is an alternative experimental approach that shows great potential for protein localization and function studies. Batch EP is a suitable method for the above-mentioned purposes, but its development and potential applications for cell biology studies has never been characterized in depth. In this context, I aimed to explore the potential of EP as a protein delivery method for phenotypic and protein interaction studies *in vivo*. I took advantage of structurally and biochemically well characterized kinetochore components and SAC proteins for this purpose. This study will help to expand the general understanding of EP as a technique for cell biology applications currently unexplored. In addition, this work formulates a series of experimental methods that are useful for studying mitotic checkpoint in cells using recombinant proteins.

1.6.2 Studying the regulation of MCC disassembly during mitosis

As described in the introduction section, the SAC is a signal transduction mechanism that ensures the fidelity of chromosome segregation during mitosis. The MCC is a stable and diffusible effector complex produced during the SAC response that inhibits APC/C and halts cell in mitosis. SAC proteins recruited to unattached kinetochores are involved in the catalysis of MCC assembly. On the other hand, a AAA+ ATPase TRIP13 and its cofactor p31^{COMET} are the main players involved in the energy dependent disassembly of MCC. p31^{COMET} is also known to bind MAD1:C-MAD2 complex at kinetochore and this interaction can likely curtail O-MAD2 recruitment.

Since the catalysis of both MCC assembly and disassembly occur during mitosis, it is the offset steady state MCC concentration at each time point that determines the outcome of SAC activation, maintenance and inactivation. Equivalent to MCC assembly, the disassembly of MCC by TRIP13 also needs to be a well-regulated process for ensuring SAC responsiveness towards kinetochore-microtubule occupancy and for the continuous replenishment of O-MAD2 pool in the cytosol.

I describe here two logical reasons for which we hypothesized that TRIP13 mediated MCC disassembly needs to be regulated proportionally to the number of kinetochores signaling for SAC. 1) A single unattached kinetochore is able to produce enough MCC to inhibit anaphase onset for a long time (Rieder et al.,1994; Dick and Gelrich, 2013), but the presence of many unattached kinetochores does not produce a proportionately stronger inhibition (Chen et al., 2019). This implies that to prevent an overactive SAC response, either the SAC signaling by individual kinetochore decreases when more kinetochores are signaling, or MCC disassembly increases proportionally. 2) Independently of whether there is only one or more kinetochores signaling for SAC, O-MAD2 and other SAC proteins get recruited to all unattached kinetochores (Aravamudhan et al., 2016). To ensure sufficient and continuous recruitment of O-MAD2, MCC disassembly needs to be regulated proportionally to the number of SAC signaling kinetochores.

With the overall objective of understanding the regulation of TRIP13:p31[COMET] enzymatic machinery during mitosis, I addressed the following questions: 1) What is the mechanism by which p31[COMET] is removed from MAD1:C-MAD2 at unattached kinetochores in order to favor MCC catalysis? 2) Is MAD1:C-MAD2 a substrate for TRIP13 enzymatic machinery? 3) Is the TRIP13 mediated MCC disassembly regulated during mitosis and how is it regulated?

To precisely address these questions, we biochemically reconstituted the MCC assembly and disassembly *in vitro* using different fluorescence-based sensors. This study will help to understand better the mechanisms by which mitotic cells modulate the SAC response, the fidelity of which is fundamental for genomic integrity.

2. Materials and Methods

2.1 Materials

2.1.1 Chemicals

Table 2-1 Chemicals

Chemical	Company
4-(2-hydroxyethyl)-1-piperazineethanesulfonic acid (HEPES)	Carl Roth
4′,6-diamidino-2-phenylindole (DAPI)	Serva Electrophoresis
Acetic Acid	AppliChem
Acrylamide solution 30 %	AppliChem GmbH
Agarose powder	Invitrogen
Ammonium persulfate (APS)	Serva Electrophoresis
Bradford solution (5x)	Carl Roth
Bromophenolblue	Sigma-Aldrich
Coomassie G250/R250	Serva Electrophoresis
Dimethyl sulfoxide (DMSO)	Serva Electrophoresis
Dithioerythritol (DTE)	Carl Roth
Ethylenediaminetetraacetic acid (EDTA)	Merck/Sigma-Aldrich
Glycerol	Gerbu Biotechnik
Glycine	Carl Roth
Isopropyl β-D-1-thiogalactopyranoside (IPTG)	Carl Roth

Magnesium chloride (MgCl$_2$)	AppliChem
Maltose monohydrate	Sigma-Aldrich
Milk powder	Carl Roth
Mowiol	Calbiochem
Nonidet P-40 (NP-40)	Fluka
Paraformaldehyde (PFA) 16 %	Alfa Aesar GmbH
Phenylmethylsulfonyl fluoride (PMSF)	Serva
Sodium dodecyl sulfate (SDS) pellets	Carl Roth
Tetramethylethylenediamine (TEMED)	Carl Roth
Tris	Carl Roth
Tris(2-carboxyethyl) phosphine (TCEP)	Biosynth AG
Triton X-100	Sigma-Aldrich
Tween-20	VWR Chemicals
WesternBright ECL Spray Detection Reagent	Advansta Inc.

2.1.2 Consumables

Table 2-2 Consumables

Consumable	Company
96- well Polystyrene flat bottom plates	Griener
Cell culture dishes (6 cm, 10 cm, 15 cm)	Sarstedt
Cell culture flasks (T-175)	Sarstedt
Cell culture plates (6 well, 12 well, 24 well)	Sarstedt

Nitrocellulose membrane	GE Healthcare
Polyvinylidenfluorid (PVDF) membrane	GE Healthcare
Test tubes (0.5 ml, 1.5 ml, 2 ml)	Sarstedt

2.1.3 Antibiotics

Table 2-3 Antibiotics for bacteria

Antibiotic	Concentration
Ampicillin	100 µg/ml
Kanamycin	50 µg/ml
Gentamycin	10 µg/ml
Tetracyclin	7 µg/ml

Table 2-4 Antibiotics for Mammalian cell culture

Antibiotic	Concentration
Blasticidin	5 µg/ml
Hygromycin	250 µg/ml
Penicillin	100 U/ml
Streptomycin	0.1 mg/ml

2.1.4 Bacterial strains and media

Plasmids were amplified in OmniMax E. coli cells (kindly provided by the Dortmund Protein Facility), bacmids for insect cell expression were recombined in E. coli DH10EmBacY cells. For bacterial expression of proteins, we used E. coli BL21-DE3cells made competent in-house. Bacteria were cultured in LB medium or in TB

supplemented with the appropriate antibiotics and grown at 37 °C. All bacterial culture media used in this work were produced in-house.

Table 2-5 Media for bacterial culture

Media	Formulation (per litre)
Terrific Broth (TB)	12 g tryptone, 24 g yeast extract, 4 ml glycerol, 100 ml phosphate buffer
Lysogeny Broth (LB)	10 g tryptone, 5 g yeast extract, 10 g sodium chloride

2.1.5 Enzymes

Table 2-6 Enzymes

Enzyme	Company
Benzonase nuclease	Sigma-Aldrich
DNase I	Roche
Fast Digest Restriction Enzymes	Thermo Fisher Scientific
Gibson Assembly Master Mis	New England BioLabs
Pfu Turbo Polymerase	Agilent Technologies
preScission protease	produced in-house
Q5 polymerase 2 x Master Mix	New England BioLabs
T4 Ligase	New England BioLabs

2.1.6 Antibodies

All primary and secondary antibodies that were used for Western blot (WB) and Immunofluorescence (IF) studies are listed in the following tables.

Table 2-7 Primary antibodies

Antibody	Origin	Dilution	Company
anti-BUB1	Rabbit	1:1000	abcam
anti-CENP-A	Rabbit	1:1000	Cell Signaling
anti-CDC20	Mouse	1:100 (IF) 1:500 (WB)	Santa cruz biotech.
anti-GFP	Rabbit	1:1000	produced in-house
anti-MAD2	Mouse	1:1000	produced in-house
anti-mCherry	Mouse	1:2000	Novus Biologicals
anti-MIS12	Rabbit	1:2500	abcam
anti-p31^{COMET}	Mouse	1:100	produced in-house
anti-PMF1	Mouse	1:1000	produced in-house
anti-Tubulin	Mouse	1:10,000	Sigma Aldrich Corp.
anti-Vinculin	Mouse	1:15,000	Sigma Aldrich Corp.
CREST sera	Human	1:200	Antibodies Inc.

Table 2-8 Secondary antibodies

Against	Coupled	Origin	Dilution	Company
Human	Alexa Fluor 647	Goat	1:200	Jackson ImmunoResearch
Mouse	Alexa Fluor 488	Goat	1:200	Invitrogen
Mouse	Rhodamine Red	Goat	1:200	Jackson ImmunoResearch
Mouse	HRP	Sheep	1:10,000	GE Healthcare
Rabbit	Alexa Fluor 488	Donkey	1:200	Invitrogen

| Rabbit | HRP | | Donkey | 1:10,000 | GE Healthcare |

2.1.7 Oligonucleotides

Oligonucleotides that were used for the polymerase chain reaction (PCR), cloning and site-specific mutagenesis were synthesized by Sigma-aldrich and are listed in the following table.

Table 2-9 Oligonucleotides

Name	Sequence (5' to 3')
P31comet_S102A	AGCACTTTTACCGAAAACCTGCTCCCCAGGCAGAGGAGATGCT
P31comet_S102D	AGCACTTTTACCGAAAACCTGATCCCCAGGCAGAGGAGATGCT
P31comet_S160A	TCCTTGGGGGCAATGCCCTAGCCCCCAAGGAGTTCTATGAACT
P31comet_S160D	TCCTTGGGGGCAATGCCCTAGACCCCAAGGAGTTCTATGAACT
His_Mad2_TEV	ATGCATCACCATCACCATCACGAAAACCTGTACTTCCAGGGTGCGCTGCAGCTCTCCCGG
Myc_petp31_mutagenesis	ATGGGTCGCGGATCCATGGAACAAAAACTCATCTCAGAAGAGGATCTGGCGGCGCCGGAGGCGGAGGT
P31resistant_oligo1	GGCAATGCCCTAAGCCCCAAAGAATTTTACGAGCTGGATTTGTCTCTGCTGGCCCCC
P31resistant_oligo2	CAGCCGCAGTCCCTGATTTAGAATGGTACGAAAAATCTGAGGAGACTCACGCCTCCCAGATA

p31_insert _forward	TTGGTACCGAGCTCGGATCCATGGAACAAAAACTCATCTCAG
p31_insert _reverse	TTCCACCACACTGGACTAGTTCACTCGAGTGCGGCCGCAAGCTT
PCDNA5_p31_forward	AAGCTTGCGGCCGCACTCGAGTGAACTAGTCCAGTGTGGTGGAA
PCDNA5_p31_reverse	CTGAGATGAGTTTTGTTCCATGGATCCGAGCTCGGTACCAAGC
3Xmyc_PFL_cdc20_forward	GTACCGAGCTCGGATCCATGGAGCAAAAACTAATATCAGA
3Xmyc_PFL_cdc20_reverse	TGAGTTTTTGTTCCATGGATCCTAAGTCTTCTTCCGAAATTAAT
GFP_NDC80_forward	ATTAAGTCTTCTGAAGAAATGGCACACCATCACCAC
GFP_NDC80_reverse	CCTCTAGTACTTCTCGACTCAGGGACCCTGAAACAGAAC

2.1.8 Mammalian cell lines

Table 2-10 Cell lines

Cell line	Source/reference
HeLa	Imaging Facility, FOM-IEO Campus, Milan
mCherry-H2B HeLa	Imaging Facility, FOM-IEO Campus, Milan
HEK293	Provided by the laboratory of Dr. Alex Bird
A2780	Selenko Lab, Theillet et al.,2016
RCSN3	Selenko Lab, Theillet et al.,2016

| B65 | Selenko Lab, Theillet et al.,2016 |
| Flp-In T-REx HeLa | Thermofischer |

2.1.9 Mammalian tissue culture reagents

Table 2-11 Tissue culture reagents

Reagent	Company
Doxycycline	Sigma-Aldrich
Dulbecco's modified eagle medium (DMEM)	Thermo Fisher Scientific
Fetal bovine serum (FBS, Tetracycline-free)	Thermo Fisher Scientific
Lipofectamine RNAiMAX	Thermo Fisher Scientific
MG132	Merck
Opti-MEM	Thermo Fisher Scientific
Poly-L-Lysine	Sigma-Aldrich
Protease Inhibitor mix (500x)	Serva
Reversine	Cayman Chemical
RO3306	Merck
Trypsin	Pan Biotech

2.1.10 Instruments used in this study

Table 2-12 Instruments

Instrument	Company
Agarose gel electrophoresis system	Carl Roth Chemie GmbH, Germany

AKTA Purifier, AKTA micro	GE Healthcare, UK
Centrifuges	Thermo Fisher scientific,USA Beckman Coulter, USA
DNA Trans illuminator	Thermo Fisher scientific,USA
Gel documentation system	BioRad systems
Mariana 3i -confocal microscope	Intelligent Imaging Innovations, Zeiss
NEON Transfection System	Thermo Fisher
Olympus FV1000 confocal microscope	Olympus
PCR Thermocycler	Analytik, Germany
Purificationcoloumns; Superdex (S200 10/300, S200 16/600) Resource Q, HisTrap	GE Healthcare, UK
Tryptan blue cell counting chamber	Invitrogen
ITC200 micro calorimeter	GE Healthcare, UK

2.1.11 Software's used in this study

Table 2-12 Softwares

Software	Version	Company
Adobe Illustrator CS5.1	15.1.0	Adobe Inc.
CCP4MG	2.9.0	Diamond light source, UK
Excel	16.30	Microsoft Corp.
FIJI	2.0.0-rc-69	National Institutes of Health
GraphPad Prism	7.0	GraphPad Software Inc.

ImageLab	5.1	Bio-Rad Laboratories GmbH
Imaris	7.3.4	Bitplane
JediFLIM	---	MPI Dortmund
Matlab	R2014b	Mathworks
Word	16.30	Microsoft Corp.

2.2 Methods

2.2.1 Molecular biology methods

2.2.1.1 Polymerase chain reaction

Polymerase Chain Reaction (PCR) is used to amplify fragments of DNA. This technique relies on the thermostable polymerase and requires DNA primers for the amplification of the region of interest. In this work, the Q5 high-fidelity polymerase (New England BioLabs) was used to amplify the DNA fragments which were subsequently digested by restriction enzymes and ligated with a plasmid backbone using T4 ligase. The temperature for primer annealing and time for elongation steps were adjusted according to the primer composition and template length, respectively. PCR reactions were set up thermocycler machine according to the manufacturer's protocol for Q5 polymerase reaction.

2.2.1.2 Restriction digestion and DNA ligation

Restriction digestions were performed using FastDigest restriction enzymes (Thermo Fisher Scientific). The PCR products purified using the PureLink PCR purification kit (Invitrogen) or 1 µg of plasmid DNA were digested using 0.5 µl of each restriction enzyme in a total volume of 30 µl for 2-4 hours at 37 °C. After successful restriction digestions of insert and the vector, both were purified by gel extraction with the Monarch DNA gel extraction kit (New England BioLabs) according to the protocol provided by the manufacturer. To ligate the restriction digested plasmid DNA with the insert DNA, 10-20 ng of plasmid backbone and a threefold molar excess of insert DNA were mixed with 1 µl of 5 x Rapid Ligation buffer (Thermo Fisher Scientific) and 1 U T4

DNA ligase (New England BioLabs) in a total volume of 5 µl. The reaction mixture was incubated for 15 min at 22 °C. Reactions were subsequently transformed into competent E. coli OmniMax cells as detailed in section 2.2.1.6.

2.2.1.3 Gibson Assembly

We used Gibson assembly reaction (Gibson et al., 2009) for the cloning of some constructs used in this study. In this approach, the DNA fragments to be joined contain a 25-base pair overlap, that was added by PCR to both ends of the insert DNA fragments. 10-20 ng of linearized plasmid backbone was mixed with a threefold molar excess of insert DNA fragments into the Gibson Assembly Master Mix (New England BioLabs) and incubated in a thermocycler for 1 h at 50 °C. The Master Mix contains a DNA exonuclease, a DNA and a DNA ligase in it. The reaction mixture was later transformed into competent OmniMax cells.

2.2.1.4 Agarose gel electrophoresis

Agarose gel electrophoresis was used to separate DNA molecules by size. The agarose was dissolved in Tris-acetate-Ethylenediaminetetraacetic acid (EDTA) buffer to reach a final concentration of 1% agarose. To detect the separated DNA by UV-light, Midori green advance was added in a 1:25,000 dilution to the liquid agarose. The electrophoresis was usually performed at 140 V for 20-30 min. The molecular-weight marker GeneRuler 1 kb Plus DNA ladder (Thermo Fisher Scientific) was loaded along with the samples to compare the size of DNA fragments.

2.2.1.5 Site directed mutagenesis

Site directed mutagenesis protocol uses custom designed primers in order to confer a desired mutation at a specific site within the gene of interest. Usually, the primers are designed in a way that the mutant codon is flanked by the overlapping oligonucleotides. Site-specific mutations were introduced by using a quick-change protocol from Stratagene. Briefly, the *PfuTurbo* DNA polymerase in the reaction mixture amplifies the plasmid using the mutated primer with overlapping oligonucleotides. After PCR reaction, 1 µl of DpnI enzyme was added that will only digest the methylated template

DNA, but not the synthesized DNA strand. This PCR product was then transformed into chemically competent OmniMax cells.

2.2.1.6 Transformation of competent bacterial cells

Chemically competent E. coli OmniMax cells were thawed on ice. Afterwards, 50 µl of bacterial cells were mixed with 0.5-1 µg of plasmid DNA and kept on ice for 15 minutes. The mixture was given a heat-shock at 42 $^\circ$C for 45seconds and later put back on ice for 2 minutes. Next, LB-medium was added and cells were incubated at 37 °C for 1 hr shaking at 300 rpm, giving time for recovery. 50 µl cell suspension was plated on a LB agar plate containing the required antibiotics for selection and incubated overnight at 37 °C.

2.2.1.7 Plasmid isolation from bacterial cells

Single colonies were picked from the LB-agar plate and transferred into 4 mL LB medium containing necessary antibiotics for screening. The inoculated culture was incubated overnight at 37 °C with shaking at 150rpm. Subsequently, the bacterial culture was centrifuged at 18,000 g for 1 min and the cell pellet was processed for alkaline lysis-based plasmid isolation using Plasmid-Miniprep kit (Thermo Fisher Scientific) following the manufacturer's protocol.

2.2.2 Biochemical methods

2.2.2.1 Tricine-sodium dodecyl sulfate polyacrylamide gel electrophoresis

Sodium dodecyl sulfate polyacrylamide gel electrophoresis (SDS-PAGE) was performed using a TRIS-Tricine buffer system (Schagger and von Jagow, 1987). The SDS-PAGE separates proteins by their molecular masses in an electric field. The negatively charged detergent SDS denatures protein structure and evenly covers the polypeptide chain with portions of negative charge. Once an electric field is applied to the protein samples loaded on to the polyacrylamide gel, they start moving towards the anode. Smaller proteins move through the acrylamide network faster than the larger proteins and as a result protein can be separated based on their size. In this work, Tricine polyacrylamide gels with an acrylamide concentration of 10-12% was used. Before running the SDS-PAGE, protein samples were mixed with SDS-PAGE

sample loading buffer and boiled at 95 °C for 5 min. To estimate the molecular weight of the separated proteins, the Precision Plus Protein marker (Bio-Rad) was loaded on the gel.

2.2.2.2 Coomassie blue staining

Coomassie blue staining was performed to visualize the proteins separated by size in SDS-PAGE gels. Gels were stained in buffer A and subsequently de-stained in buffer B for several hours on a shaker.

Table 2-13 Buffers for Coomassie blue staining

Buffer A	25 % (v/v) isopropanol, 10 % (v/v) acetic acid, 0.05 %(w/v) Coomassie R250
Buffer B	10 % (v/v) acetic acid

2.2.2.3 Western blotting

Immunodetection of proteins by Western blotting was performed as follows. The negatively charged proteins from SDS-polyacrylamide gel are transferred to a positively charged nitrocellulose membrane by the application of an electric current across the western blot transfer apparatus (Mini-PROTEAN II Cell, BioRad). The wet transfer was performed at 400mA at 4 °C for 90 minutes in western transfer buffer. The nitrocellulose membrane was then blocked in 5 % milk powder/TBST for 45 minutes at room temperature on a rocking platform. Blocking of the membrane was followed with an incubation using the appropriate dilution of the primary antibody in 2.5%(w/v) milk powder/TBST overnight at 4^0C. The membrane was then subjected to 3 washes of 15 minutes each. This was followed by incubation of the membrane with the appropriate dilution of the horseradish peroxidase (HRP)-conjugated secondary antibody in 2.5%(w/v) milk powder/TBST. The membrane was again washed for 20 minutes with TBST for 3 times. Chemiluminescence with ECL Prime or ECL Select Western Blotting Detection Reagent (GE Healthcare) was used according to manufacturer's instructions to detect the protein signal on the membrane. Images were acquired using ChemiDoc MP Imaging System (BioRad). Composition of buffers used for western blotting procedure is shown in Table 2-14.

Table 2-14 Buffers for Western blotting

Transfer buffer (1x)	25 mM Tris, 200 mM Glycine, 20 % (v/v) Methanol
TBST	50 mM Tris-HCl, 150 mM NaCl, 0.1 % Tween 20

2.2.2.4 Amylose resin pulldown assay

The amylose-resin pull-down assay were performed to check the binding of p31^{COMET}, TRIP13, and other SAC components to MBP-tagged MAD1:C-MAD2 complex. The proteins were diluted with 'binding buffer A' in a total volume of 50 µl. The concentration of the protein in the mixture varied depending on the particular experiment but the bait MBP/MBP-MAD1:C-MAD2 was diluted to 4 µM concentration always. After mixing the proteins and the beads, 5 µl was taken as input. The rest of the solution was mixed with 15 µl amylose beads (New England BioLabs) and for each condition is pipetted into a separate Pierce^{TM} micro-spin column (Thermofischer) and was incubated at 4 °C for 1 h. To separate the proteins bound to the amylose beads from the unbound proteins, the samples were centrifuged at 800 g for 2 min at 4 °C. Then, the beads were washed four times with 500 µl 'binding buffer A'. After the last washing step, 25 µl of elution buffer (binding buffer A +10 mM Maltose) was added to the column and were centrifuged at 800 g for 2 min at 4 °C. The eluted protein solution is collected from the bottom Eppendorf and added 6 µl of 5x SDS-PAGE sample loading buffer before analyzing by SDS-PAGE and CBB staining. Binding buffer A= 20 mM Hepes pH 7.5, 150 mM NaCl, 5% Glycerol (20 mM MgCl$_2$ is also added to pulldown assays checking the activity of TRIP13^{WT}).

2.2.2.5 Glutathione resin pulldown assay

The glutathione-resin pull-down assay were performed to check the ability of TRIP13 and p31^{COMET} to disassemble GST-MIM^{CDC20}:MAD2 substrate bound to beads. The protocol is similar to the amylose-resin pulldown described above except for the buffers used. Binding buffer A= 20 mM Hepes pH 8.0, 50 mM NaCl, 5% Glycerol, 20 mM MgCl$_2$; Elution buffer= buffer A+ 10 mM reduced glutathione.

2.2.2.6 MCC FRET assay

The FRET sensors used in this study were previously described in Faesen et al., 2017 and Piano et al., 2021. We used this sensor to study both MCC assembly and MCC disassembly under various conditions in this study. All measurements were performed on a Clariostar plate-reader (BMG Labtech), using UV clear 96-well-plate flat-bottomed (Greiner) and the software Prism 6 for analysis and visualization. In short, to monitor MCC assembly, the sensor components along with MCC assembly catalysts (BUB1:BUB3, MAD1:C-MAD2 pre-phosphorylated by MPS1 as described in Faesen et al., 2017) were added in a final reaction volume of 100µl and start the reading. For the experiments to monitor MCC disassembly, we pre-assembled MCC with the FRET sensor components and add the disassembly catalysts (TRIP13 and p31^{COMET}) just before the start of the reading to the final reaction volume. Unless stated otherwise, assays were performed using 100 nM final concentration of the FRET pair components (BUBR1^{CFP}& MAD2^{TMARA} for the sensor1; CDC20^{CFP} & MAD2^{TMARA} for the sensor2). The final concentration of catalysts changed depending on the experiment which will be reported in the respective sections. Mixtures were excited using the filter 430-10 nm and the dichroic filter LP 504 nm, and the emissions were scanned from 450 to 650 nm. Buffer used= 10 mM Hepes (pH 8.0), 50 mM NaCl, 2.5% glycerol, 10 mM β-mercaptoenthanol and 20 mM MgCl$_2$.

2.2.2.7 Fluorescence polarization-based assay

Fluorescence polarization (FP) measurements were performed on the Clariostar plate-reader (BMG Labtech) using UV clear 96-well-plate flat-bottomed (Greiner) at 25 °C. The software MARS (BMG Labtech) was used to calculate the FP values and the software Prism6 (Graphpad Software, Inc.) was used for analysis and visualization. We incubate O-MAD2 protein with FAM-labelled CDC20 -MIM peptide (MIM^{FAM}) overnight at 4 °C to form the C-MAD2: MIM^{FAM} substrate complex and add the disassembly catalysts (TRIP13 and p31^{COMET}) to the final reaction mixture. The final volume of the reactions is 100 µl, in assay buffer containing 10 mM Hepes (pH 8.0), 50 mM NaCl, 2.5% glycerol, 10 mM β-mercaptoenthanol and 20 mM MgCl$_2$. The final concentration of the substrate complex was always 100 nM, the catalyst concentration changed depending on the experiment. TRIP13 was incubated at 20x concentration with ATP 30 mins at 4°C before starting the assay. Measurements were acquired

every 90s for 60 minutes, shaking 60s at 500 rpm before the first cycle; focal height 5.5 mm, 200 flashes, excitation filter 482-16 nm, dichroic filter LP 504 nm, emission filter 530-40 nm.

2.2.2.8 NADH coupled ATP consumption assay

The ATP consumption by the ATPase in the reaction is measured by a coupled reaction to NADH reduction. The details of the coupled reaction are explained later in section 3.2.7. The absorbance of NADH at 340 nm is measured on the Clariostar plate-reader (BMG Labtech) at 25 °C. Assay conditions: 1 mM ATP, 3 mM PEP, 20 U/ml PK, 20 U/ml LDH, ~ 300 μM NADH. Different substrates such as preassembled C-MAD2:MIM^{CDC20} substrate, MCC and MAD2:CDC20^{FL} are used in the assay to characterize TRIP13 ATPase activity. TRIP13 is incubated with ATP prior to the assay for 30 min before adding to the final reaction mixture. Measurements were acquired every 90s for 2h, shaking 60s at 500 rpm before the first cycle. The velocity of the reaction, expressed in ATP min^{-1}enz^{-1} is corrected for the ATP consumption in absence of the ATPase. The concentration of NADH is calculated interpolating the measured absorbance with a standard curve that we made.

2.2.2.9 Protein expression in insect cells

In this study, we expressed BUBR1, NDC80C-GFP, CFP-MIS12C and mCherry-Spindly in insect cells. The genes for the constructs to be expressed in the baculovirus/insect cell system was cloned into the pBIG MultiBac vector (Bieniossek et al., 2012) (for NDC80C and MIS12C constructs) or pLIB vector (for BUBR1 and Spindly constructs) and verified by sequencing. Those plasmids were transformed into DH10EMBacY cells following the standard transfection protocol, with the exception of extending the recovery time to 5 h at 37 °C. EMBacY cells contain the baculovirus genome as a bacterial artificial chromosome into which the gene of interest is integrated by homologous recombination. Transformed cells were plated in different dilutions onto LB-agar plates containing 50 μg/ml Kanamycin, 10 μg/ml Gentamycin, 7 μg/ml Tetracyclin, 40 μg/ml IPTG and 100 μg/ml X-Gal. Positive colonies were selected by blue (negative)-white (positive) screening. Single white colonies were grown over

night at 37 °C in LB medium supplemented with 50 µg/ml Kanamycin, 10 µg/ml Gentamycin and 7 µg/ml Tetracyclin. From these cultures the Bacmid-DNA was

isolated using the QIAprep Miniprep Kit (Qiagen). For virus production, the Bacmid-DNA was transfected using Fugene (Promega) into Sf9 (Spodoptera frugiperda) cells. Baculovirus was amplified through three rounds of amplification and used to infect Tnao38 cells for protein expression. Cells infected with virus were cultured for 72 hr before harvesting.

2.2.2.10 Protein expression in bacteria

Proteins used in this study such as MAD2, CDC20, p31[COMET] and TRIP13 were expressed in bacterial cells and use the same protocol is used for expression. E. coli BL21(DE3) codon cells were transformed with plasmids containing the respective protein and the bacterial culture was grown in LB supplemented with antibiotics. Isopropyl-β-D-thiogalactopyranoside (IPTG) at 0.2 mM concentration was added after OD_{600} reached 0.6 and the culture was incubated at 20 °C for further 16 h. Subsequently, the culture was centrifuged for 20 min at 5000 g and the pellets were lysed and proceed for purification steps.

2.2.2.11 NDC80C-GFP purification

Cell pellets from expression in insect cells were resuspended in buffer A (50 mM HEPES pH 8, 200 mM NaCl, 20 mM Imidazole, 5% glycerol, 2 mM TCEP) supplemented with protease-inhibitor mix (Serva) and 0.2% Triton, lysed by sonication and cleared by centrifugation. NDC80C[9A]-GFP was then eluted in buffer B (50 mM HEPES pH 8, 200 mM NaCl, 300 mM Imidazole, 5% glycerol, 2 mM TCEP) and the eluate was diluted six times in volume using ion exchange buffer C (50 mM HEPES pH 8, 25 mM NaCl, 5% glycerol, 2 mM TCEP, 1 mM EDTA) and applied to a 6 mL Resource Q anion-exchange column pre-equilibrated in the same buffer. Elution of bound protein was achieved by a linear gradient (25–400 mM NaCl in 25 column volumes). Relevant fractions were concentrated in 10 kDa molecular mass cut-off Amicon concentrators and applied to a Superose 6 16/70 column equilibrated in size-exclusion chromatography buffer D (50 mM HEPES pH 8, 250 mM NaCl, 5% glycerol, 2 mM TCEP). Peak fractions containing the NDC80C[9A]-GFP complex were collected

and further concentrated in a 10 kDa cut-off Amicon concentrator before being flash frozen in liquid N$_2$ and stored at −80 °C.

2.2.2.12 CFP-MIS12C purification

CFP-Mis12C was purified by a three-step protocol, as described previously for the non-fluorescent version (Petrovic et al., 2016); i) affinity purification of filtered supernatant with 5 ml HisTrap FF column (GE Healthcare) and step elution with 300 mM imidazole; ii) anion-exchange of the dialyzed eluate with 6 ml Resource Q column, elution with linear NaCl gradient; and iii) final polishing step via size-exclusion on a Superdex 200 10/300 column (GE Healthcare) equilibrated in 20 mM Tris-HCl (pH 8.0), 0.15 M NaCl, and 1 mM TCEP.

2.2.2.12 BUBR1 purification

Expression cell pellets from insect cells were lysed in buffer A (25 mM HEPES (pH 7.5), 300 mM NaCl, 10% glycerol, 2 mM TCEP, 1 mM PMSF). Soluble lysates were passed over a 5 ml Ni-NTA column and, after washing with 20 column volumes buffer A, the proteins were eluted by adding 300 mM imidazole to buffer A. Proteins were subsequently gel-filtered on a Superdex S200 16/60 column equilibrated against buffer B (10 mM HEPES (pH 7.5), 150 mM NaCl, 5% glycerol, 2 mM TCEP).

2.2.2.13 Spindly purification

Recombinant mCherry-Spindly protein was purified in-house as described previously (Mosalaganti et al., 2017). The purification was performed by our lab member Sabine Wohlgemuth.

2.2.2.14 MAD2 purification and Sortase labeling

The expression pellets from bacterial cells were lysed by sonication in 20 mM Hepes (pH 7.5), 150mM NaCl, 5% glycerol, 10 mM imidazole and Roche Complete EDTA-free protease inhibitor cocktail). After clearing, the lysate was loaded on a Hi-Trap metal chelating column (GE Healthcare). After wash with 20 column volumes of low imidazole buffer, bound proteins were eluted with an imidazole gradient. Mad2

containing fractions were pooled, diluted with a low salt buffer and loaded onto an anion-exchange (AE) Resource-Q column (GE Healthcare) equilibrated in 20 mM Hepes (pH 7.5), 50 mM NaCl, 5% glycerol. The protein was eluted using a NaCl gradient, from 50 mM to 500 mM in 40ml volume. The O-MAD2 fraction that elutes around 150 mM NaCl concentration is collected and concentrated. We used Sortase A transpeptidase enzyme to label MAD2 C-terminally with a TAMRA fluorophore. Sortase catalyses the cleavage of a short five-amino-acid recognition sequence (LPETG) at MAD2 C-terminus with the concomitant formation of an amide linkage with the oligoglycine peptide conjugated to TAMRA (from GenScript). For the labeling reaction, we mixed 50 µM MAD2–LPETG with 150 µ M sortase A and 500 µM of TAMRA-conjugated peptide. The reactants were mixed in 20 mM Hepes (pH 7.5), 50 mM NaCl and 5% glycerol and incubated overnight at 4 °C. To purify MAD2 in the open conformation (O-MAD2), the labelling reaction was followed by ion-exchange chromatography (ResQ column, GE Healthcare) to remove the sortase A and excess of peptide.

2.2.2.15 p31^{COMET} purification

The expression pellets from bacterial cells were lysed by sonication in 30 mM Tris pH 7.4, 150 mM NaCl, 5% glycerol, 2 mM β-mercaptoenthanol and Roche Complete EDTA-free protease inhibitor cocktail). After clearing, the lysate was loaded on a Hi-Trap metal chelating column (GE Healthcare). After wash with 20 column volumes of 1 mM ATP+ 400 mM KCl solution, bound proteins were eluted with an imidazole gradient. Relevant fractions were concentrated in 10 kDa molecular mass cut-off Amicon concentrators and applied to a Superose 6 16/60 column equilibrated in size-exclusion chromatography buffer (30 mM Tris pH 7.4, 50 mM NaCl, 5% glycerol, 2 mM β-mercaptoenthanol). Peak fractions containing the p31^{COMET} protein were collected and further concentrated in a 10 kDa cut-off Amicon concentrator before being flash frozen in liquid N$_2$ and stored at −80 °C.

2.2.2.16 TRIP13 purification

Bacterial cells transformed with 'pET28A- His-TEV-TRIP13' construct was treated for expression conditions as described earlier. Cell pellets from the expression culture

were lysed in buffer A (30 mM Tri psH 7.4, 150 mM NaCl, 5% glycerol, 2 mM β-mercaptoenthanol). Soluble lysates were passed over a 5 ml Ni-NTA column followed by washing with 20 column volumes buffer A and elution with a gradient of imidazole. Eluted fractions were collected, concentrated in a 30 kDa cut-off Amicon concentrator, and incubated with TEV protease to cleave the N-terminal His-tag. Proteins were subsequently gel-filtered on a Superdex S200 16/60 column equilibrated against buffer B (30 mM Tris pH 7.4, 30 mM NaCl, 5% glycerol, 2 mM β-mercaptoenthanol).

2.2.3 Cell biological methods

2.2.3.1 Cell culture conditions

The following cell lines were cultured in DMEM (PAN Biotech) supplemented with 10% FBS (Clontech), penicillin, streptomycin (GIBCO) and 2 mM L-glutamine (PAN Biotech): HeLa, mCherry-H2B HeLa, U2OS, MDCK, HEK293, and RPE-Tir1. The following cell lines were grown in the indicated media (supplemented as above): Human A2780 and B65 in RPMI 1640, SK-N-SH and RCSN3 in DMEM-Ham's F-12 and SH-SY5Y in DMEM. All experiments requiring live imaging were performed in complemented CO_2-independent medium (GIBCO) at 37 °C. Cells were grown in cell culture dishes (Sarstedt) at 37 °C in the presence of 5% CO_2 and were passaged when cell confluency reached 90 %. All experiments and cell treatments were performed under sterile conditions in laminar flow cabinets (NuAire).

2.2.3.2 RNA interference

Lipofectamine RNAiMax (ThermoFisher) was used for all the siRNA transfections reported in this study. While seeding the cells at a density of 1.3 x 10^5 cells/mL, 3 µl/ml RNAiMax transfection reagent and the RNA oligos at 10 nM are added. For the MIS12C depletion transfection of 3 combined siRNA duplexes were used for 48 hr. The RNA oligos sequence for DSN1 is GUCUAUCAGUGUCGAUUUA; for NSL1 is CAUGAGCUCUU UCUGUUUA; (Sigma-Aldrich) and for MIS12 is GACGUUGA CUUUCUUUGAU; (GE Healthcare Dharmacon). After 48 hrs, cells were analyzed for phenotypes using Immunoblotting experiments. For the co-depletion of BUBR1 and MAD2, a smart pool of oligos from Dharmacon (UUACUCGAGUGCAGAAAUA, CUACUGAUCUUGAGCUCAU, GGUUGUAGUUAUCUCAAAU, GAAUCCGUUCAGU

GAUCA) is used for MAD2 depletion and for BUBR1 depletion, a previously described oligo (CGGGCAUUUGAAUAUGAAA) (Lampson and Kapoor, 2005) is used; all at 10 nM concentration for 24 hr. Depleted cells were processed for electroporation coupled lifetime imaging experiments afterwards.

2.2.3.3 Immunoprecipitation

We performed anti-GFP immunoprecipitation (IP) experiments from mitotic cell lysates of either HeLa cells electroporated with GFP or GFP-NDC80C. Mitotic cells were then harvested by shake off after nocodazole treatment and resuspended in lysis buffer [150 mM KCl, 75 mM Hepes, pH 7.5, 1.5 mM EGTA, 1.5 mM MgCl2, 10% glycerol, and 0.075 % NP-40 supplemented with protease inhibitor cocktail (Serva) and PhosSTOP phosphatase inhibitors (Roche)]. A total of 4 mg of protein extract per sample was then incubated with GFP-Traps beads (ChromoTek; 3 µl/mg of extract) for 3 hr at 4°C. Immunoprecipitates were washed with lysis buffer and resuspended in sample buffer, boiled and analyzed by SDS- PAGE and Western blotting.

2.2.3.4 Immunofluorescence

For immunofluorescence (IF) analysis, cells were fixed with PBS/Paraformaldehyde 4% for 20 mins in room temperature followed by extraction using PBS +0.5% TritonX-100 for 5mins. After a quick rinse with PBS, cells were blocked in PBST (PBS +0.1% TritonX-100) solution supplemented with 4 % BSA for 40 min. Primary antibodies (refer table 2-7) diluted in blocking solution are added and incubated for 2hrs inside a wet chamber at room temperature. Afterwards, coverslips are washed three times with PBST followed by secondary antibody (refer table 2-8) incubation for 1 hr at room temperature. Afterwards, the coverslips were washed thrice with PBS and were mounted with Mowiol (made inhouse using standard recipe). The samples were let dry at room temperature for at least 16 h and subsequently stored at 4 °C protected from light.

2.2.3.5 Electroporation of recombinant proteins

This is a general outline for the electroporation of mammalian cells with recombinant proteins used in this study. To electroporate recombinant proteins into cells, the Neon

Transfection System Kit (Thermo Fisher) was used. 3 x 10^6 cells were trypsinized, washed with PBS and resuspended in electroporation Buffer R (Thermo Fisher) to a final volume of 90 µl. Recombinant protein was diluted 1:2 in buffer R to reach a final concentration range of 10-50µM and 30 µl of the mixture was added to the 90 µl cell suspension. This mixture is what we call electroporation slurry. The slurry is loaded into a Neon Pipette Tip (Thermo Fisher) and electroporated by applying two consecutive 35 ms pulses with an amplitude of 800 V. The sample was subsequently added to 50 ml of pre-warmed PBS, centrifuged at 500 g for 3 min and trypsinized for 7 minto remove protein aggregates on membrane. After one additional PBS washing step and centrifugation, the cell pellet was resuspended in DMEM and allowed to recover in a cell culture plate of ideal size at 37 ºC.

2.2.3.6 Image acquisition and analysis

Three microscopes were used in this study. For imaging IF slides, a customized 3i Marianas system (Intelligent Imaging Innovations) equipped with an Axio Observer Z1 microscope chassis (Zeiss), a CSU-X1 confocal scanner unit (Yokogawa Electric Corporation), Plan-Apochromat 63×/1.4 NA objectives (Zeiss) and an Orca Flash 4.0 sCMOS Camera (Hamamatsu) was used. Images were acquired as *Z* sections (using Slidebook Software six from Intelligent Imaging Innovations) and converted into maximal-intensity-projection TIFF files for illustrative purposes. For live cell time-lapse imaging, a Deltavision Elite System (GE Healthcare) equipped with an IX-71 inverted microscope (Olympus), a UPlanFLN 40×/1.3 NA objective (Olympus) and a sCMOS camera (PCO-TECH Inc) was used. For the FLIM-FRET microscopy, an Olympus FV1000 laser scanning confocal microscope coupled with a single-photon counting avalanche photodiode (PDM Series, MPD; PicoQuant) and timed by using a time-correlated single-photon counting module (PicoHarp 300; PicoQuant) was used. For FLIM data analysis an in-house developed software JediFLIM (Bastiaens lab, MPI-Dortmund) was used. For the data analysis of IF and time-lapse images, FIJI is used. The quantification of kinetochore signals of proteins was done by selecting manual ROIs and subtracting the background intensities. Measurements were plotted with GraphPad Prism software.

2.2.3.7 Flow cytometry

Flow-cytometry and quantification (fluorescence intensity median analysis) of αSYN containing cells were performed with lysine-to-Atto488 fluorophore-coupled recombinant protein as described (Theillet et al., 2016). After electroporation, Atto488-tagged protein (530 nm) containing cells were collected and prior to analysis on the BD Accuri C6 flow cytometer (BD Biosciences), samples were subjected to sonication for 10 seconds at the lowest output on a Branson sonifier 450 to disrupt cell clumps. Over greater than 10,000 recorded events were detected for each sample. Median αSYN-Atto fluorescence from all events was determined with FlowJo 8.8.6 for each sample.

3. Results

3.1 Establishing electroporation of recombinant proteins into mammalian cells as tool for *in vivo* functional studies

Our laboratory focuses predominantly on the biochemical and structural characterization of recombinant kinetochore proteins, but we often face the problem of establishing functional assays to characterize several protein constructs also in mammalian cells. In this study, we aim to standardize *batch electroporation* (EP) as a tool for delivering recombinant proteins directly into mammalian cells and explore its potential cell biology applications. We mostly used proteins part of the kinetochore structure and SAC proteins for testing the applications of EP. A very recognizable localization pattern inside cells (punctuate pattern at kinetochores) along with extensive previous biochemical characterizations (Musacchio, 2017) made these proteins ideal targets for our studies.

3.1.1 EP as a technique to deliver recombinant proteins into cells

As outlined in Figure 3-1A and as described in detail in the Methods section, EP is a rather simple experimental procedure. Briefly, to be ready for EP, cells can be treated according to the required experimental design before being harvested, washed and resuspended in the electroporation buffer containing the diluted recombinant protein; this sample is called *EP slurry*. The EP slurry is subjected to multiple electric pulses that will transiently create reversible ruptures in the cell membrane to allow intracellular protein delivery. Following EP, cells are treated with trypsin protease and washed, to remove proteins that may have aggregated on the cell membrane. Electroporated cells are, then, given time to recover (minimum of 5 hours) before being prepared for the desired analysis, such as live imaging, immunofluorescence or western blotting.

We initially validated the success of this technique using two well characterized SAC proteins. The recombinant CFP-BUBR1$^{1-571}$, a minimal BUBR1 construct reported to be sufficient for SAC and kinetochore recruitment (Faesen et al., 2017), and MAD2^{TAMRA}, where the TAMRA fluorophore is added to the C-terminus of MAD2 via sortase ligation, were introduced into HeLa cells by independent EP experiments. In mitotically arrested cells, both proteins distinctly localized to kinetochores, as revealed by the co-localization with CREST signal, an established kinetochore marker (Figure

3-1B, C). Thus, EP is successful in delivering recombinant proteins and they achieve native localization once inside the cells.

A

B

C
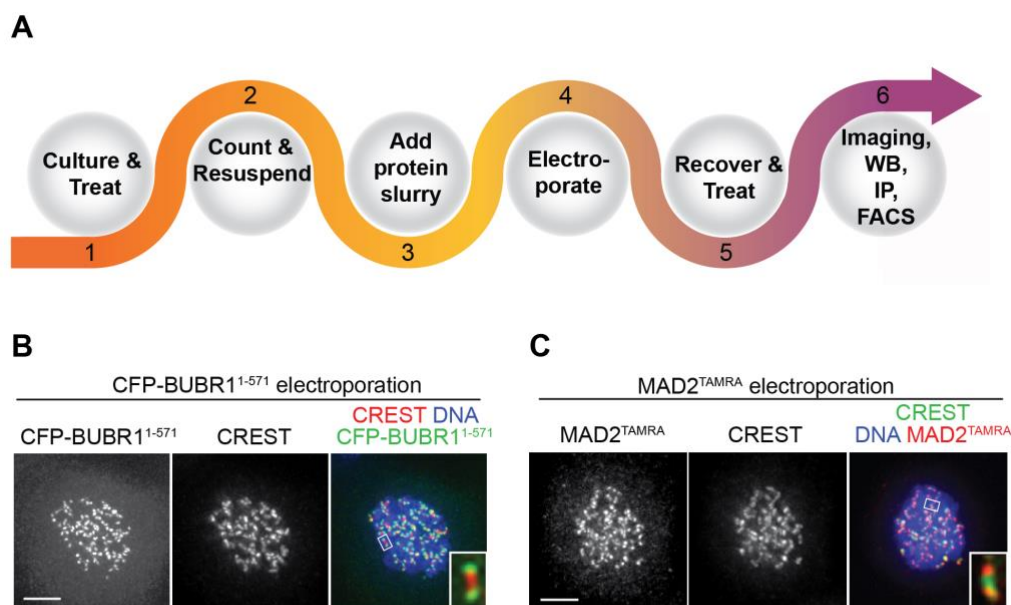
Figure 3-1 EP as a tool to deliver recombinant proteins into cells

A) Schematic showing the work-flow of EP using adherent cells. **B)** Immunofluorescent (IF) images of cells after the electroporation of CFP-BUBR1$^{1-571}$. Kinetochores were stained with the marker CREST and DNA with SiR-Hoechst-647. Insets represent magnifications of the boxed kinetochores. Scale bar = 5 μm. EP slurry concentration of CFP-BUBR1$^{1-571}$ = 10 μM **C)** IF images of cells after the electroporation of MAD2^{TAMRA}. Kinetochores were stained with the marker CREST and DNA with DAPI. Scale bar = 5 μm. EP slurry concentration of MAD2^{TAMRA}= 5 μM **(B, C)** Cells were given over-night recovery time after EP, and treated for 6 hours with nocodazole before sample preparation for IF.

Next, we addressed some important concerns to further validate this technique such as: 1) protein uptake efficiency; 2) cell viability; 3) homogeneity of protein delivery across cell population. The protein uptake efficiency for different cell types has been determined using a model recombinant protein called α-synuclein (αSYN), a synaptic and nuclear protein involved in Parkinson's disease. Using flow cytometry of EP-processed cells, we determined that the intracellular uptake scaled linearly with input concentrations, despite cell-type specific differences in uptake efficiency (Figure 3-2A, B). Experiments with αSYN were performed in the laboratory of our collaborator Prof. Dr. Philipp Selenko (Weizmann Institute, Rehovot, Israel). A similar trend in uptake efficiency was observed in fluorometric analysis of HeLa cell lysates after electroporation of the mCherry fluorescent protein (Figure 3.2C). EP is efficient across multiple cell lines and imparts only limited cytotoxicity, as tested by delivering αSYN

under different electroporation conditions (Figure 3-2 D, E). A comparison of the effects of changing the EP parameters, such as the composition of the EP buffer or the settings of the EP pulse (voltage strength, duration, and number of repetitions), on electroporation efficiency is described in details in *Alex et al., 2019*, Supplementary Figure 2D-H.To test the homogeneity of protein delivery across cells, we electroporated HeLa cells with the recombinant outer kinetochore component MIS12 complex (MIS12C) containing the MIS12 subunit fused to the fluorescent CFP protein (refer section 1.2.3 for details of MIS12C). CFP-MIS12C was clearly visible at kinetochores in the large majority of electroporated cells and with remarkably similar kinetochore levels within the same cell and between different cells (Figure 3-2 F, G). This result suggests that EP can be used for cell biology applications where phenotypes across a large population of cells need to analyzed.
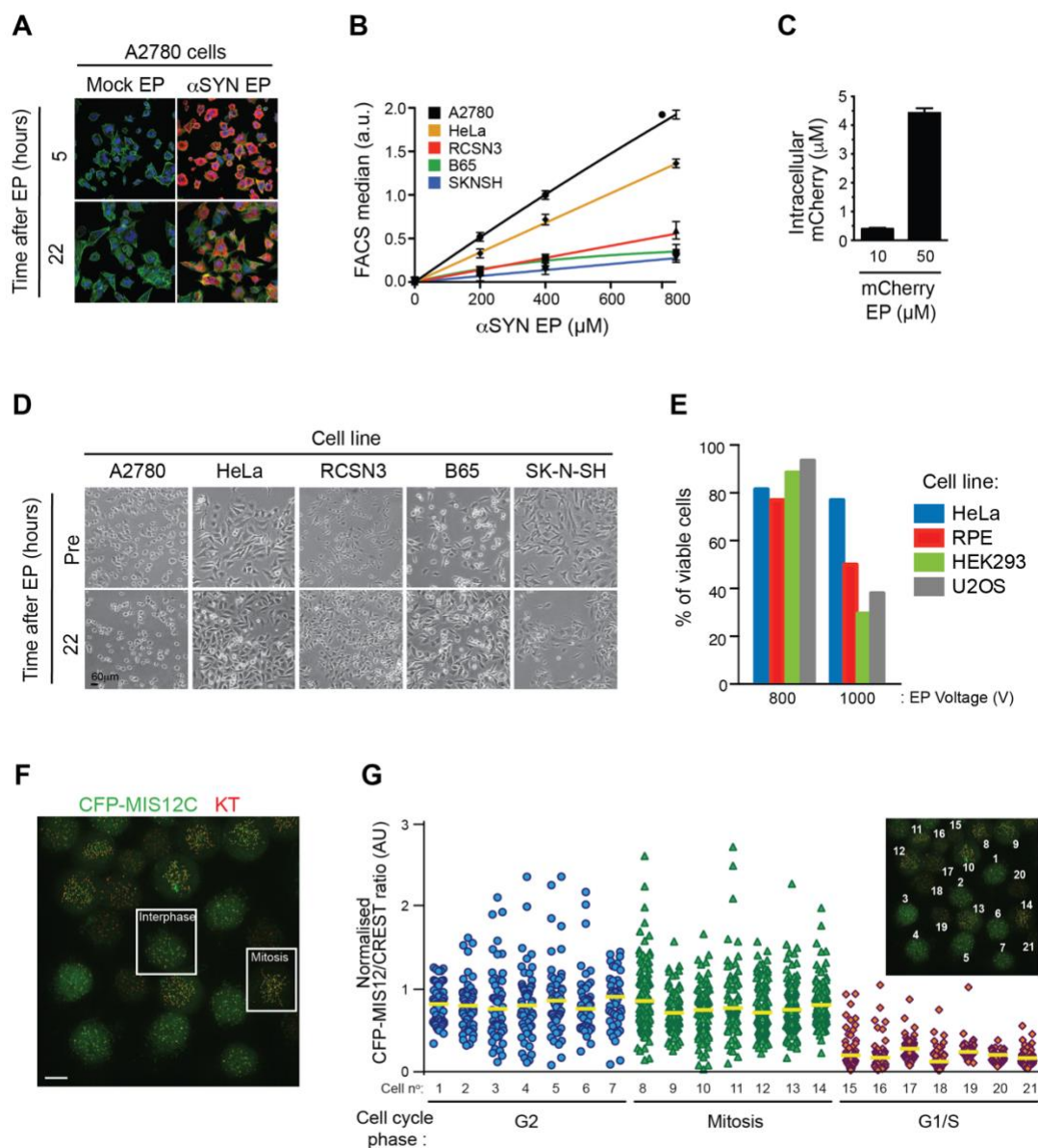
Figure 3-2 Characterization of the EP technique for functional applications

A) IF images of cells after EP of αSYN. DNA is shown in blue (DAPI), actin in green (phalloidin) and αSYN in red. Mock EP was carried out without recombinant αSYN in the EP mixture. **B)** Quantification of EP-mediated protein uptake by flow cytometry across different cell lines. Median fluorescence intensities (MFI) determined by flow cytometry of EP-processed cells harboring Atto488-labeled αSYN plotted against αSYN input concentrations in the respective EP slurries. MFI values were corrected for average cell sizes and corresponding volumes. Lines correspond to linear fits connecting individual measurement points; error bars represent the SDM from four independent experiments. **C)** Fluorescence measurements of EP-mediated protein uptake in extracts from HeLa cells electroporated with mCherry. The values obtained were subtracted for the intensity values measured from a mock EP sample. Graph represents mean values ± SD. **D)** Bright field images of neuronal (RCSN-3, B65, SK-N-SH) and non-neuronal (A2780, HeLa) cell lines to compare cell morphology and viability before and after EP with αSYN. **E)** Quantification of the viability of different cell lines after EP with αSYN. **F)** Imaging field shows HeLa cells electroporated with CFP-MIS12C after recovery, treated with nocodazole for 4 hours. Kinetochores were stained with the marker CREST. Scale bar = 5 µm. **G)** Quantification of kinetochore levels for electroporated CFP-MIS12C from cells in panel F. Individual cell numbers are indicated in the small inset. Each symbol represents a single kinetochore. Yellow lines indicate the median.

3.1.2 Electroporated recombinant proteins interacts with endogenous binding partners

Next, we investigated whether the electroporated proteins specifically interacts with previously characterized binding partners in cells. We used the electroporation of the SAC protein BUBR1 and the outer kinetochore NDC80 complex for this purpose. BUBR1 recruitment at kinetochores in human cells requires its dimerization with the BUBR1 paralog kinetochore-bound BUB1, through segments that encompass a predicted helical domain in the two proteins (Overlack et al., 2015). In agreement with the previous observations, CFP-BUBR1$^{1-571}$ localized to kinetochores whereas CFP-BUBR1$^{1-571-\Delta Helix}$, a mutant lacking the BUB1 binding helix, was unable to localize to kinetochores after electroporation (Figure 3-3A, C). Western blot analysis indicates similar protein uptake efficiency, disregarding any concentration dependent phenotype variations (Figure 3-3B).

We purified the four-subunit NDC80C complex (~180 kDa), with one of the subunits (NUF2) GFP tagged as described previously (Huis In 't Veld et al., 2016). After EP, the recombinant GFP-NDC80 complex localized stably to kinetochores (Figure 3-3D). This confirms that EP is also compatible with the delivery of large multi-subunit protein

complexes. To test whether recombinant GFP-NDC80C is able to interact with previously known binding partners, we performed GFP-immunoprecipitation (GFP-IP) assays on protein extracts generated from mitotic HeLa cells electroporated with GFP-NDC80C. IP assays demonstrated that the GFP-NDC80C but not GFP alone was able to interact with MIS12 and BUB1 (two of the known direct and indirect interactors of NDC80, respectively, Figure 3-3E). Thus, electroporated proteins are able to establish physiological interactions with their endogenous binding partners, demonstrating the versatility of EP as a technique to probe protein interactions in living cells.
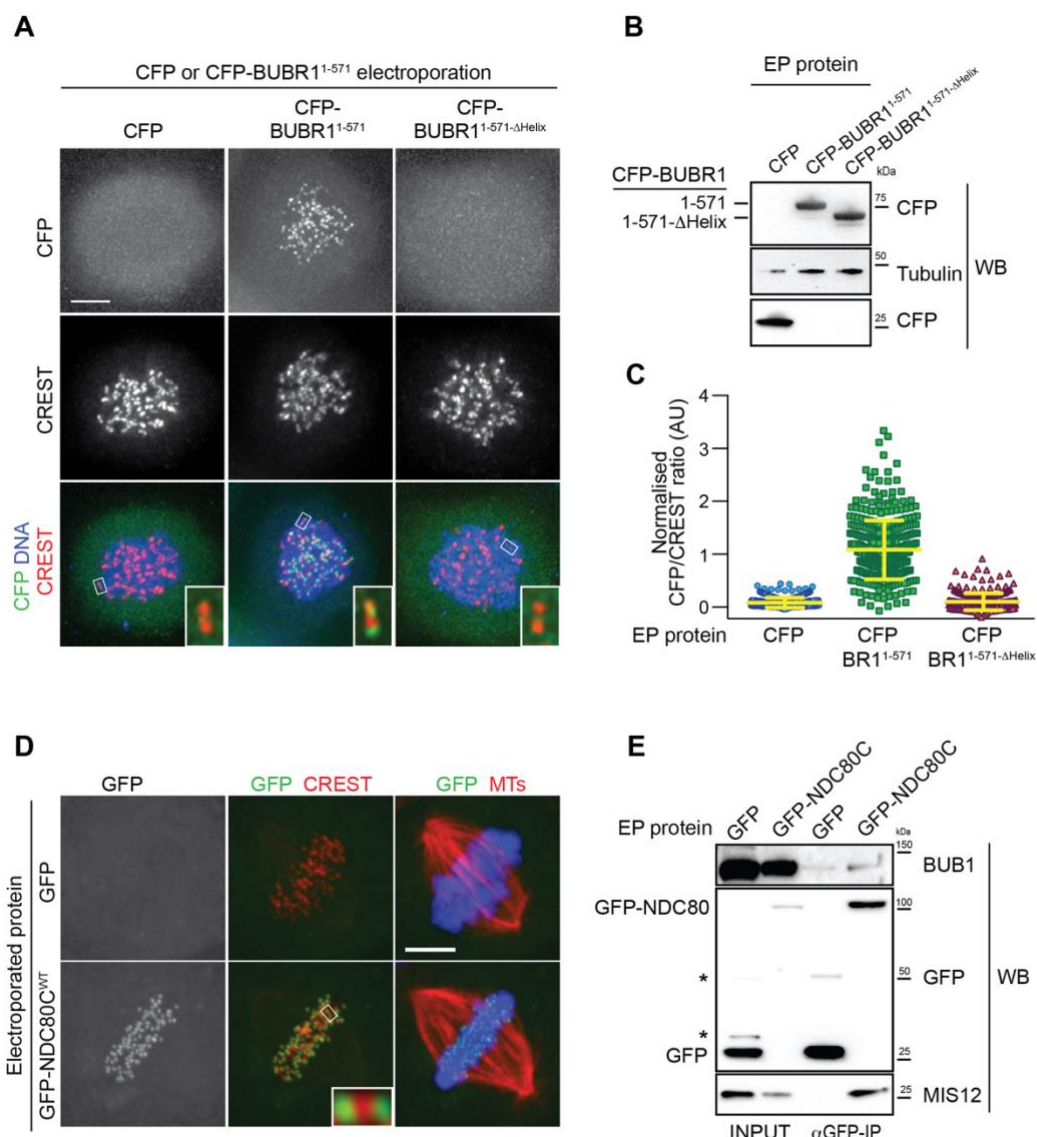
Figure 3-3 Electroporated proteins physically interact with endogenous binding partners

A) IF images of HeLa cells after EP with either CFP alone, CFP-BUBR1[1-571] or CFP-BUBR1[1-571-ΔHelix]. Kinetochores were stained with the marker CREST and DNA with SiR-Hoechst-647. Scale bar = 5 μm **B)** Western blot analysis with indicated antibodies of cell lysates from conditions described in panel A. **C)** Quantification of kinetochore levels for electroporated CFP-fused proteins from panel A. Each symbol represents a single cell. Yellow lines indicate median values ± interquartile range. **D)** IF images of HeLa

cells after EP with either GFP alone or GFP-NDC80C. Electroporated HeLa cells were treated with STLC, followed by STLC washout, released into MG132 (proteasome inhibitor that prevents mitotic exit), and fixed 150 min after STLC-release. Kinetochores were labeled with anti-CREST, microtubules (MT) with an anti-TUBULIN antibody and DNA with DAPI. Insets represent magnifications of the indicated kinetochores. Scale bar = 5 µm. **E)** IP analysis of protein extracts from cells treated as described in panel D. Western blots were performed with α-GFP beads and probed with the indicated antibodies.

3.1.3 Electroporated recombinant protein functionally complements depletion of the endogenous protein

MIS12C is a four-subunit kinetochore complex with DSN1, NSL1, MIS12, and PMF1 subunits with a total molecular mass of ~120 kDa. We co-expressed these subunits in insect cells (with a CFP tag fused to the PMF1 subunit) and purified following the previously described protocol (Petrovic et al., 2014; Petrovic et al., 2016). As described earlier in Figure 3-2F, the electroporation of the CFP-MIS12 complex in HeLa cells shows the recruitment of the complex to kinetochores with homogenous levels across cells. Here, we wanted to test whether the recombinant CFP-MIS12C is able to functionally replace endogenous MIS12 complex. Being an important structural element of the outer kinetochore, MIS12C is necessary for timely chromosome segregation and SAC activity. We performed a complementation assay in HeLa cells depleted of the endogenous MIS12 complex (RNAi protocol described in Kim and Yu, 2015) by electroporating either CFP alone or CFP-MIS12C. Western blot analysis from these cell lysates indicates the depletion of MIS12 subunits by RNAi and the delivery of recombinant MIS12C subunits (Figure 3-4A). As shown by live-cell microscopy, EP delivery of CFP-MIS12C into depleted cells, but not of the CFP alone, rescued chromosome congression defects (Figure 3-4B, C), indicating that the recombinant complex is functionally active. CFP-MIS12C was able to rescue the SAC defects caused by MIS12 complex RNAi depletion, indicated by the restoration of mitotic duration to values similar to those observed in control cells under nocodazole treatment (Figure 3-4D). Collectively, these results indicate EP can be used for biological complementation assays in combination with siRNA-mediated knockdown of the target protein. This can be recognized as a general feature of this approach, largely independent of the protein used. Electroporation experiments with MIS12C were performed in collaboration with my colleagues Dr. Soumitra Polley and Dr. Stefano Maffini.
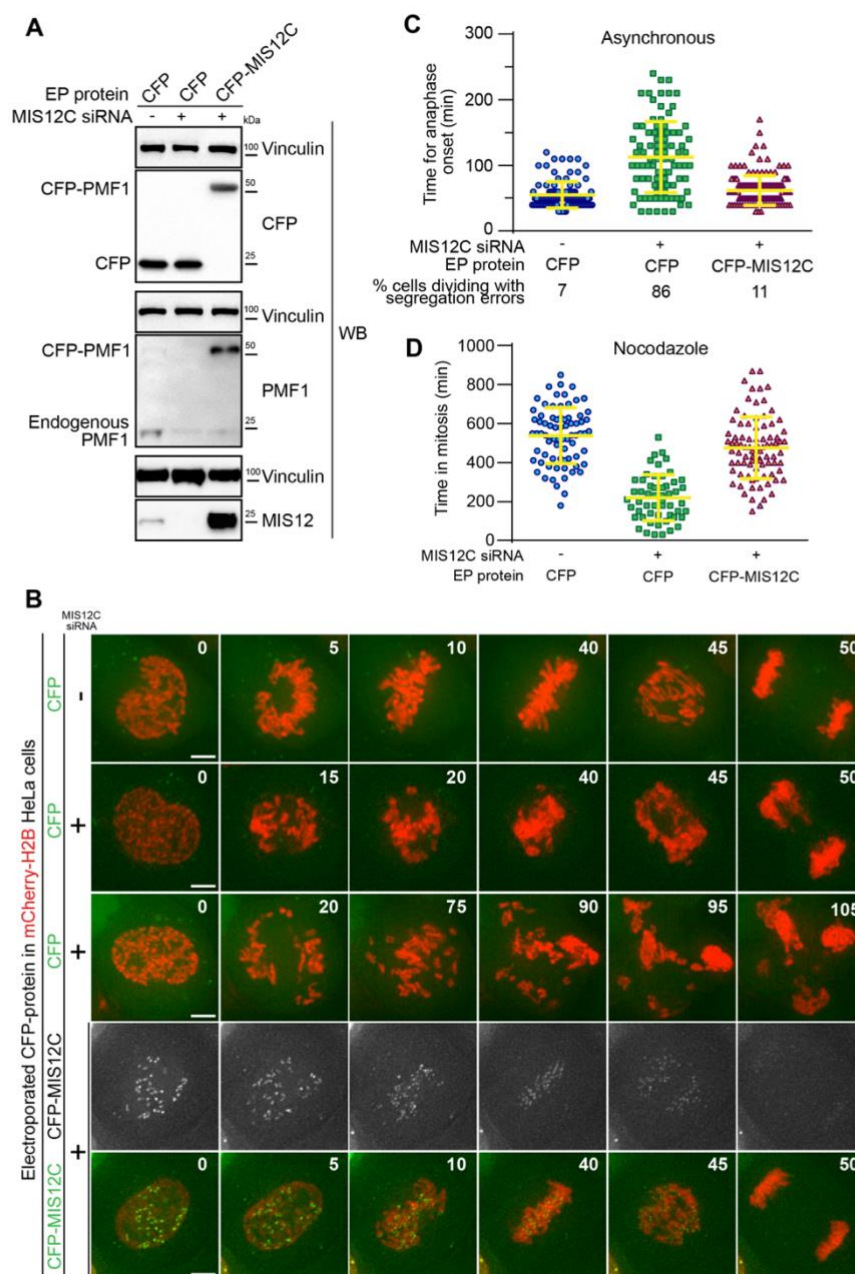
Figure 3-4 Electroporated MIS12 complex targets kinetochores and functionally complements depletion of the endogenous complex. A) mCherry-H2B-expressing HeLa cells, previously treated with siRNAs to deplete the endogenous MIS12C, were electroporated with either CFP or CFP-MIS12 complex. Western blot of cell extracts from the indicated conditions, against MIS12 and PMF subunits of MIS12C. **B)** Frames collected at the indicated time points (min) of time-lapse live-cell fluorescence microscopy movies of cells described in Panel A. The second and third rows show two representative phenotypes observed in cells depleted for MIS12C and concomitantly electroporated with CFP. Green and red signal represent, respectively, CFP-fused proteins and DNA. Scale bar = 5 µm **C)** Quantification of chromosome segregation timing and defects in cells from panel A-B. Each symbol represents a measure of mitotic duration until anaphase onset (based on DNA and cell morphology) of a single cell. Yellow lines indicate mean values ± SD. **D)** Quantification of mitotic duration of individual cells treated as in panel A but imaged in the presence of nocodazole 0.3 µM.

3.1.4 EP allows chemically modified recombinant proteins to complement functional modifications in cells

Spindly, a constituent of the kinetochore corona, is an adaptor protein that promotes the interaction of Dynein with its processivity factor Dynactin (Gassman et al., 2008). At the corona, Spindly interacts directly with the RZZ complex and this is critical for the kinetochore recruitment of Spindly. Spindly-RZZ interaction requires the irreversible post-translational isoprenylation of Spindly with a farnesyl moiety on a cysteine residue near the C-terminus (Holland et al., 2015; Mosalaganti et al., 2017). We purified two versions of recombinant Spindly one fused to GFP and another fused to mCherry tag, both at the N-terminus. Recombinant mCherry-Spindly electroporated in HeLa cells was detected at the periphery of kinetochores, comparable to the localization described for endogenous Spindly (Holland et al., 2015) (Figure 3-5A). mCherry-Spindly[C602A], a mutant that cannot be farnesylated, failed to localize at kinetochores after electroporation in mitotic arrested cells (Figure 3-5A). Thus, we reiterated the farenesylation dependency of Spindly for kinetochore localization in cells, this time with electroporated recombinant protein.

When we treated cells with FTI-227, a selective farnesyl-transferase inhibitor, localization of mCherry-Spindly to kinetochores was greatly reduced (Figure 3-5B, C). Because farnesylation of Spindly has been reconstituted *in vitro* with purified components (Mosalaganti et al., 2017), we reasoned that we could exploit this reaction to promote kinetochore localization of recombinant Spindly in cells experiencing a long-term inhibition of farnesyltransferase (FT) activity. mCherry-Spindly was treated *in vitro* with recombinant FT, resulting in farnesylated mCherry-Spindly (mCherry-Spindly[F]). We then co-electroporated mCherry-Spindly[F] and untreated GFP-Spindly into HeLa cells that had been treated with FTI-227 for the previous 24 hours. Remarkably, mCherry-Spindly[F], but not GFP-Spindly, successfully targeted kinetochores (Figure 3-5B, C), showing that the FT activity *in vitro* had bypassed and complemented the inhibition of endogenous FT activity by FTI-227. These experiments demonstrate that electroporation can be used to deliver chemically modified recombinant proteins into cells and study their functions *in vivo*. Electroporation experiments with Spindly were performed together with my colleagues Dr. Stefano Maffini and Beate Voss.
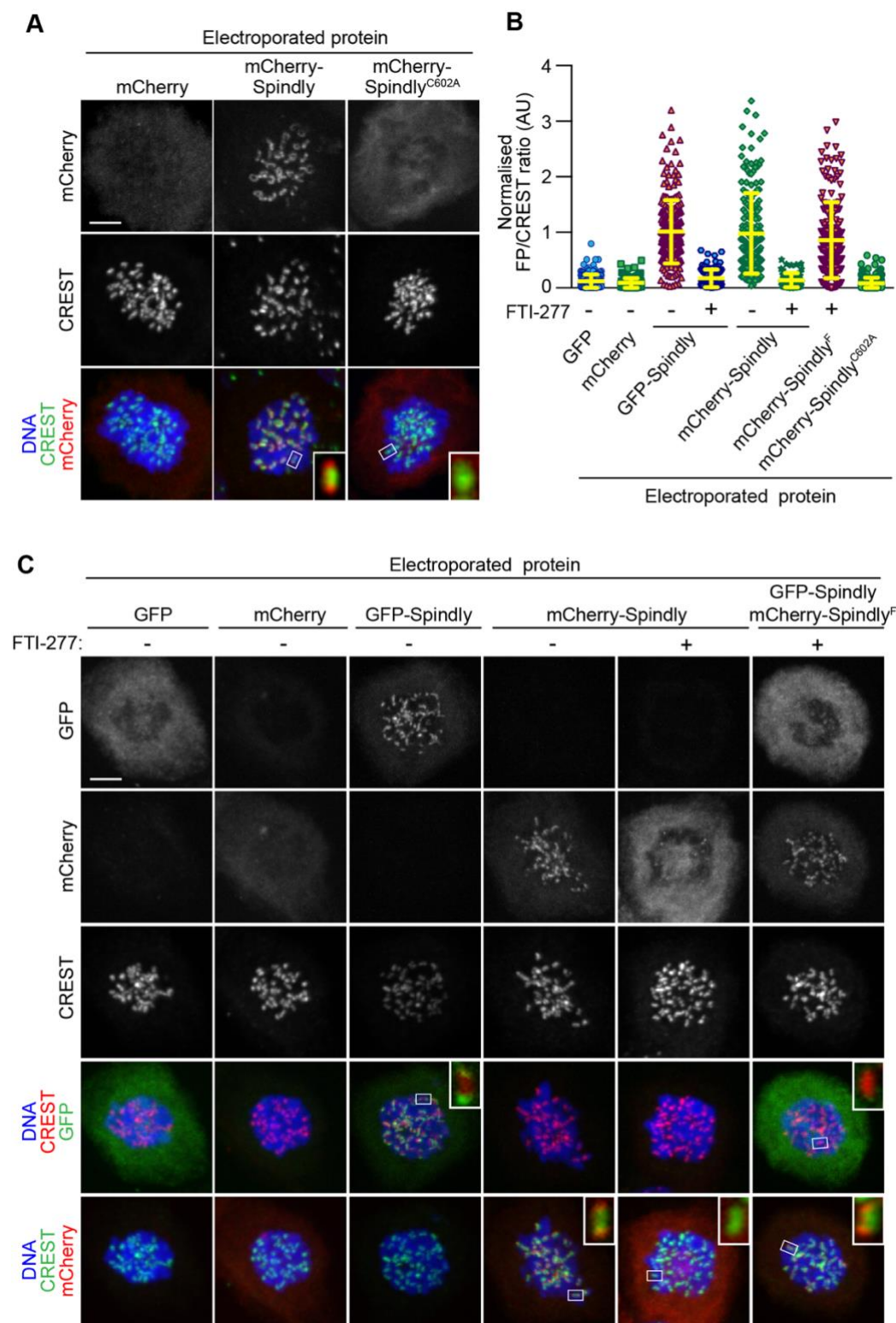
Figure 3-5 In vitro farnesylation allows Spindly localization when farnesyl transferase is inhibited. A) Immunofluorescent images of cells electroporated with proteins, mCherry as control or mCherry-Spindly constructs as indicated. Kinetochores were stained with CREST antibodies and DNA with DAPI. Insets represent magnifications of the indicated kinetochores. Scale bar = 5 µm **B)** Quantification of KT levels for electroporated Spindly from cells shown in panels A and C. Each symbol represents a single cell. Yellow lines indicate mean values ± SD **C)** Cells treated with the farnesyl-transferase inhibitor FTI-277 were electroporated with either GFP, GFP-Spindly, mCherry, mCherry-

Spindly, or in vitro pre-farnesylated mCherry-Spindly (mCherry-Spindly^F) and then processed for immunofluorescence analysis. Kinetochores were stained for CREST and DNA with DAPI. Insets represent magnifications of the indicated KT. FP = Fluorescent protein. Scale bar = 5 µm.

3.1.5 Electroporation of fluorescent proteins for quantitative spectroscopic applications

We wanted to demonstrate that EP-delivery of fluorescently labeled samples can be used for spectroscopic applications such as fluorescence lifetime imaging microscopy (FLIM)-FRET to study the spatial distribution of protein complexes in cells. Our laboratory has previously reported the development of a FRET sensor to monitor MCC assembly *in vitro* (Faesen et al., 2017). The FRET sensor consists of the recombinant CFP tagged BUBR1 (BUBR1^{CFP}) and MAD2 labelled with TAMRA via sortase mediated ligation (MAD2^{TAMRA}). The assembly of these proteins into MCC, along with CDC20, results in FRET signaling between CFP:TAMRA fluorophore pairs (Figure 3-6A). What we wanted to understand is where the MCC is assembled and its spatial distribution in the mitotic cells. To address this question, we decided to introduce the MCC FRET-sensor inside cells using electroporation, and study MCC assembly using FLIM-FRET. After electroporation, both BUBR1^{CFP} and MAD2^{TAMRA} are recruited to kinetochores in microtubule depolymerized mitotic cells (Figure 3-6D). We verified that the FRET sensor is working *in vitro*, indicated by the quenching of CFP emission coupled with excitation of TAMRA in the spectral scan (Figure 3-6B).

For FLIM experiments, we used Olympus FV1000 coupled with PicoQuant TCSPC modules for data acquisition and Jedi FLIM software package for data analysis, thanks to the technical support of the laboratory of Prof. Bastiaens, MPI Dortmund. The expected outcome of such experiment would be that the fluorescence life-time of the donor would decrease upon FRET. The average life-time map of the donor fluorophore across the sample would represent an indirect measurement of the localization of the protein-protein interaction, in this case MCC formation. As a proof of principle, we first measured the lifetime of the donor fluorophore (BUBR1^{CFP}) in solution. We observed a significant drop in the average life-time of the donor (~20%) when the FRET pair was incorporated within the MCC, compared to the control where un labelled MAD2 was used to assemble the MCC (Figure 3-6C).
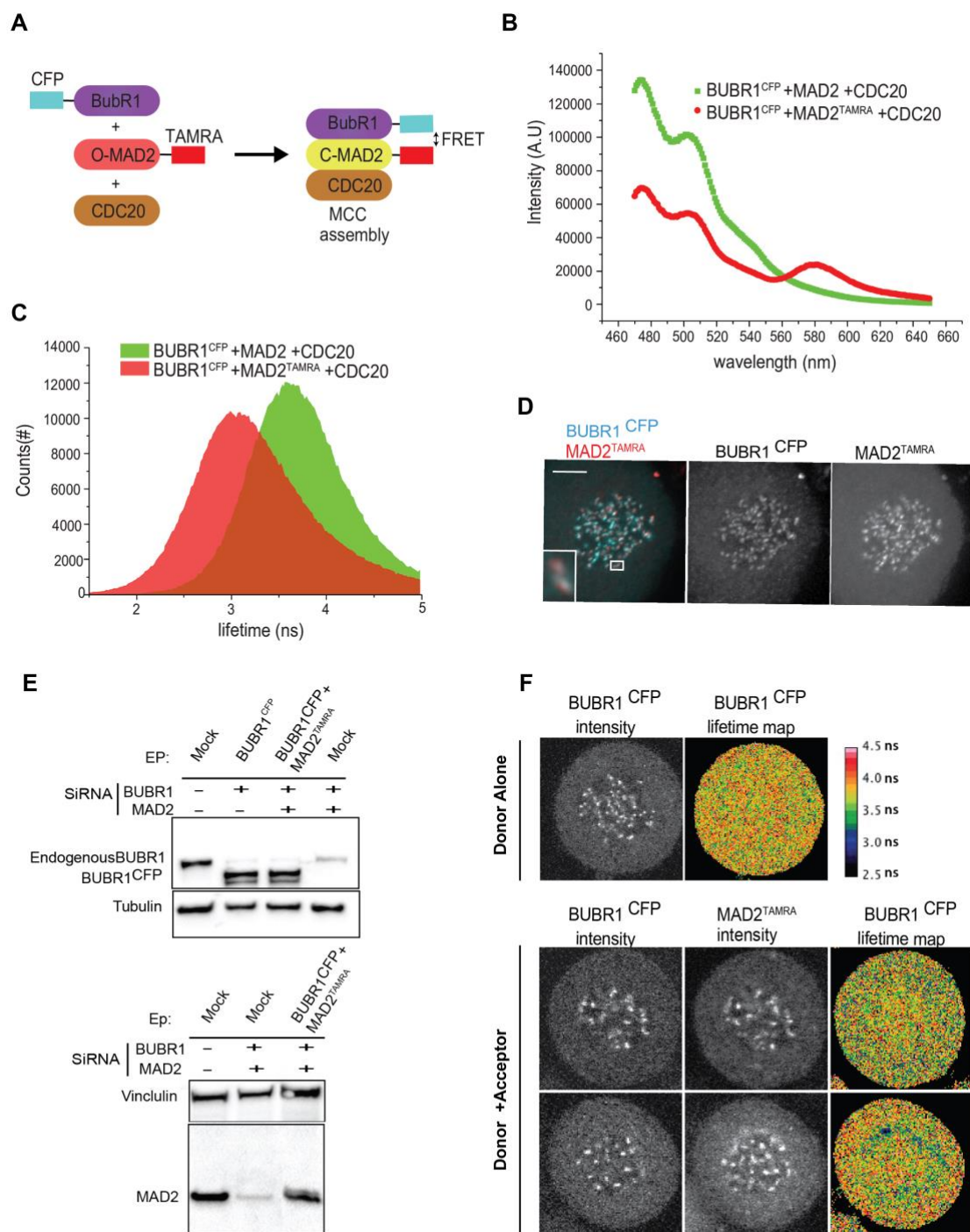
Figure 3-6 Electroporation coupled with FLIM-FRET to study MCC assembly in cells

A) Schematic of the MCC[FRET] sensor. BUBR1[CFP] and MAD2[TAMRA] when added along with CDC20 to form MCC, and as a result when the CFP fluorophore is excited at 430 nm, it produces FRET signal with TAMRA at 580 nm. **B)** Fluorescence emission spectral scans after exciting at the CFP absorbance maximum wavelength (430 nm) for the indicated sample conditions. **C)** The histogram plot shows drop in the average life-time of CFP fluorophore when the MCC is formed with MAD2[TAMRA] *in vitro*, measured using FLIM. **D)** Co-electroporation of BUBR1[CFP] and MAD2[TAMRA] results in localization of both recombinant proteins at kinetochores in mitotic cells. Cells were kept in 0.3 μM nocodazole for 6 hours

before imaging. Scale bar = 5 μm **E)** Western blot showing the rescue of electroporated BUBR1 and MAD2 proteins to levels comparable to their endogenous counterparts after depleting endogenous proteins by siRNA **F)** Color coded lifetime maps of CFP fluorophore in cells co-electroporated with BUBR1^{CFP}, together with either MAD2 not labelled or with MAD2^{TAMRA}. The fluorescence intensities of BUBR1^{CFP}, MAD2^{TAMRA} are also shown.

We depleted endogenous MAD2 and BUBR1 by RNAi and rescued their cellular levels using electroporated BUBR1^{CFP} and MAD2^{TAMRA} (Figure 3-6E), to avoid the incorporation of endogenous counterparts into MCC causing a decreased FRET efficiency. A drop in average lifetime of BUBR1^{CFP} (donor fluorophore) in mitotic cells having MAD2^{TAMRA} was observed, compared to cells having unlabeled MAD2 (Figure 3-6F). The decrease in donor lifetime was observed in cytosol and not at kinetochores, suggesting that the MCC assembly/distribution is spread across cytosol when SAC is active. Our observation is reasonable considering that MCC is a diffusible effector complex and its target APC/C is dispersed in the cytosol. These results confirm EP as a valuable tool for cellular studies and open up exciting future possibilities in the study of the spatio-temporal regulation of MCC assembly and disassembly in living cells. In agreement with this, we also demonstrated that EP is suitable for FLIM in live cells, using a previously described KRAS FRET sensor (refer to Alex et al., 2019, Supplementary Figure 5). The spectroscopic applications of EP mediated protein delivery are not just limited to FLIM-FRET as we exhibited, but also for general photobleaching and photoactivation microscopic techniques (data not shown here).

3.2 Studying the regulation of MCC disassembly during mitosis

The assembly of the MCC increases proportionally to the number of unattached kinetochores, reflecting the accumulation of catalytic machinery at unattached kinetochores (Faesen et al., 2017). TRIP13:p31^{COMET} is an enzymatic machinery that can disassemble MCC (Eytan et al., 2014; Ye et al., 2017). Both MCC assembly and disassembly occur simultaneously during mitosis, and the resultant MCC levels at any point of time determine whether a cell remains in, or exits, mitosis. Regulating the steady state MCC levels in accordance with the number of unattached kinetochores appears to be essential for the robustness of SAC signaling. In this part of my studies, we aimed to investigate how cells regulate TRIP13-mediated MCC disassembly process in harmony with the increase/decrease of MCC assembly catalysis. These findings shed light on some fundamental mechanisms decisive for the success of SAC signaling.

3.2.1 Recombinant TRIP13 hexamer binds to p31^{COMET}

The purification of both TRIP13 and p31^{COMET} were established in our laboratory from available protocols (Ye et al., 2015), and I purified both proteins to high purity (> 92%). Details for the expression and purification of these proteins are described in sections 2.2.2.15 and 2.2.2.16. In agreement with previous reports, after purification TRIP13 is present in multiple oligomeric states, which shift to higher molecular weight oligomers, up to hexamer, upon addition of ATP (Chen et al.,2013; Ye et al., 2015). Because of the basal ATP hydrolysis activity of TRIP13^{WT} that causes rapid dissociation of the oligomers, at any point of time only a fraction of total monomers would be present in the active hexamer state. For this reason, the ATP hydrolysis-defective TRIP13^{E253Q} mutant is used for all protein binding studies in this report unless mentioned otherwise. TRIP13^{E253Q} hexamer is able to bind its cofactor p31^{COMET} as shown in Figure 3-7.
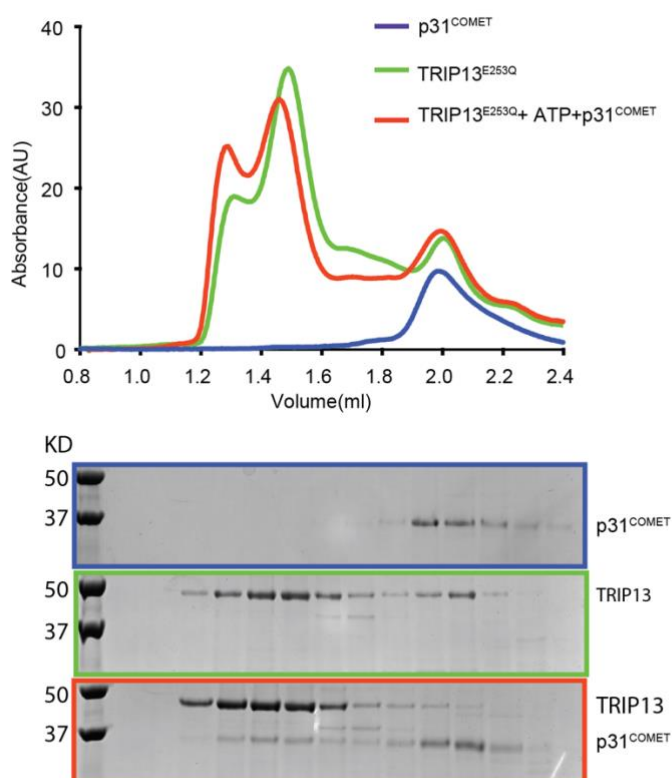
Figure 3-7 Purified TRIP13 oligomerize and binds p31^{COMET} in presence of ATP.

Analytical SEC elution profiles of three different conditions: TRIP13[E253Q], p31[COMET], TRIP13[E253Q] + p31[COMET] + ATP. The corresponding elution fractions of individual profiles were loaded on 12% SDS-PAGE and stained with Coomassie blue to further confirm the interactions.

3.2.2 Recombinant TRIP13: p31^{COMET} complex disassembles C-MAD2:CDC20 complex

C-MAD2:CDC20 complex is a known substrate for TRIP13:p31[COMET] activity. The conversion of MAD2 conformation from closed to open by TRIP13 results in the dissociation of the C-MAD2:CDC20 complex (Eytan et al., 2104). To test the activity of our recombinant TRIP13 on C-MAD2:CDC20 substrate, we setup a pulldown assay. We used the GST-MIM, a peptide including the MAD2 binding region of CDC20, assembled with C-MAD2 as substrate. We performed a GST-pulldown assay under various conditions, where the substrate is treated with the catalytic components. TRIP13[WT], but not the mutant TRIP13[E253Q], is able to dissociate the C-MAD2: GST-MIM substrate bound to the beads (Figure 3-8). The results show that the recombinant TRIP13[WT] is catalytically active and ATP hydrolysis is necessary for its function as previously reported (Ye et al., 2015).
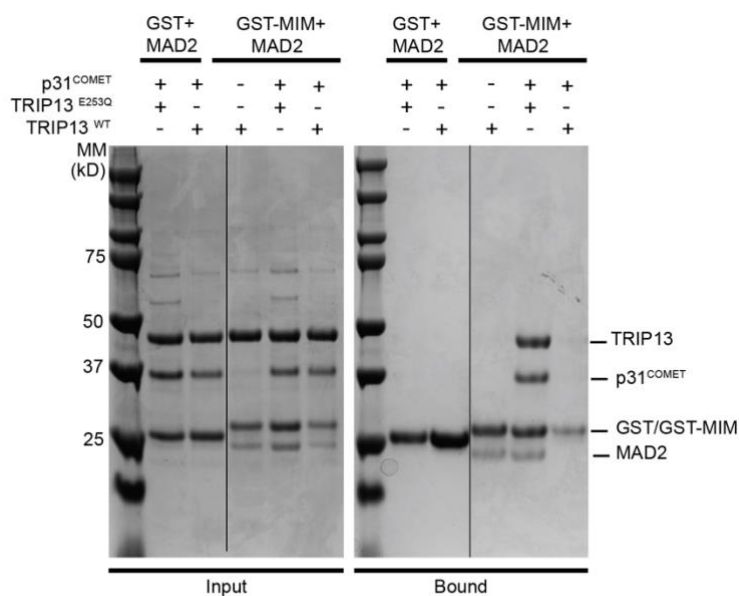
Figure 3-8 TRIP13 disassembles C-MAD2: CDC20 complex

GST-based pulldown to visualize the release of MAD2 from GST-MIM:C-MAD2 complex upon TRIP13 activity. GST-MIM:C-MAD2 complex is preassembled overnight at 4 $^\circ$C. Final concentrations used: GST/GST-MIM:C-MAD2 = 4 µM, p31^{COMET} = 5 µM, TRIP13^{WT}/ TRIP13^{E253Q} = 15 µM, ATP = 2 mM (in all conditions).

3.2.3 Fluorescent Polarization (FP) assay to monitor real-time TRIP13 activity

A fluorescent polarization (FP) based multi-well plate reader assay has been established to study the activity of TRIP13 on C-MAD2:CDC20 complex. O-MAD2 protein with FAM-labelled CDC20 MIM peptide (MIM^{FAM}) is incubated overnight at 4 $^\circ$C to form the C-MAD2:MIM^{FAM} complex. The ability of the MIM^{FAM} peptide to polarize light is high in the C-MAD2 bound state and it is lower in the free, unbound state (Figure 3-9A). Therefore, we measure the decrease of FP intensity of the MIM^{FAM} in real-time as a proxy for the C-MAD2 to O-MAD2 conversion that causes the MIM^{FAM} release and its dissociation from MAD2. We report that TRIP13 is able to disassemble C-MAD2:MIM^{FAM} in a strictly ATP, Mg^{2+} and p31^{COMET} dependent manner (Figure 3-9B). Next, the FP assay was performed by titrating the TRIP13 and p31^{COMET} concentrations in independent experiments while keeping the substrate concentration constant. The initial rate of disassembly of the substrate showed linear dependency for a certain range of TRIP13 and p31^{COMET} concentrations, confirming the enzymatic behaviour of the reaction (Figure 3-9C). Additional control experimental conditions were performed to further validate the robustness of the FP assay. The mutant TRIP13^{E253Q} is unable to act on the substrate. A previously reported p31^{COMET} mutant (described in Yang et al., 2007) that affects its binding to C- MAD2, is shown to

dramatically decrease the rate of C-MAD2:MIM dissociation (Figure 3-9D). Altogether, these observations demonstrate that the FP assay is ideally suited to study MAD2 remodelling by TRIP13 *in vitro*.
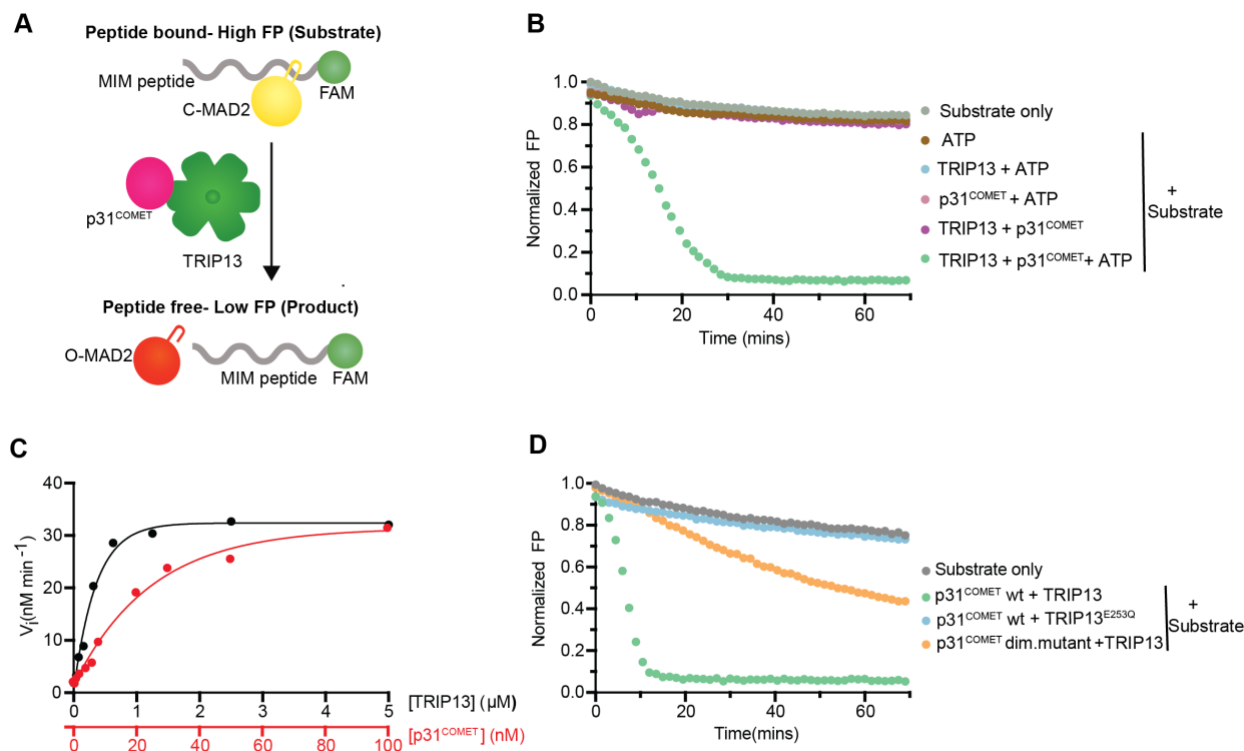
Figure 3-9 FP assay to monitor TRIP13 activity on C-MAD2:CDC20 substrate
A) Schematic displaying the working principle behind the FP assay. **B)** FP assay showing the disassembly of C-MAD2:MIM^{FAM} substrate under different conditions. MAD2 is incubated with MIM^{FAM} peptide overnight at 4 $^\circ$C to form the substrate. Unless otherwise specified, here and in other figures depicting real-time FP assays, [MAD2: MIMFAM] = 100 nM is used. For this experiment, [TRIP13] = 500 nM, [p31^{COMET}] = 50 nM. The Y axis represents the normalized FP of the FAM fluorophore. **C)** Plot showing the effect of titration of either TRIP13 or its cofactor p31^{COMET} on the initial rates of substrate disassembly in FP assay. **D)** FP assay monitoring MAD2 remodeling in the presence of TRIP13^{WT}, TRIP13^{E253Q} or p31^{COMET} dim. mutant (substitution mutant of two residues: p31^{COMET} Q83A-F191A).

3.2.4 CDK1 and Aurora B kinases phosphorylate p31^{COMET} *in vitro*

To investigate whether any of the mitotic kinases can regulate TRIP13 or p31^{COMET} activity, we tested the ability of PLK1, CDK1-CyclinB, Aurora B and MPS1 to phosphorylate these proteins *in vitro*. Among these four different mitotic kinases we tested, none of them phosphorylated TRIP13 as observed from SDS-PAGE gel stained with ProQ-diamond (Figure 3-10A, the phosphorylation conditions are described in the

figure legend). We observed that all four kinases phosphorylated p31^{COMET}, instead (Figure 3-10A). Mass spectrometry (MS) analysis showed that the N-terminal region of p31^{COMET} (residues 1 to 55) is phosphorylated non-specifically by all four kinases. The N-terminal portion of p31^{COMET} is structurally disordered and non-conserved across species and, so far, no functional role is known.
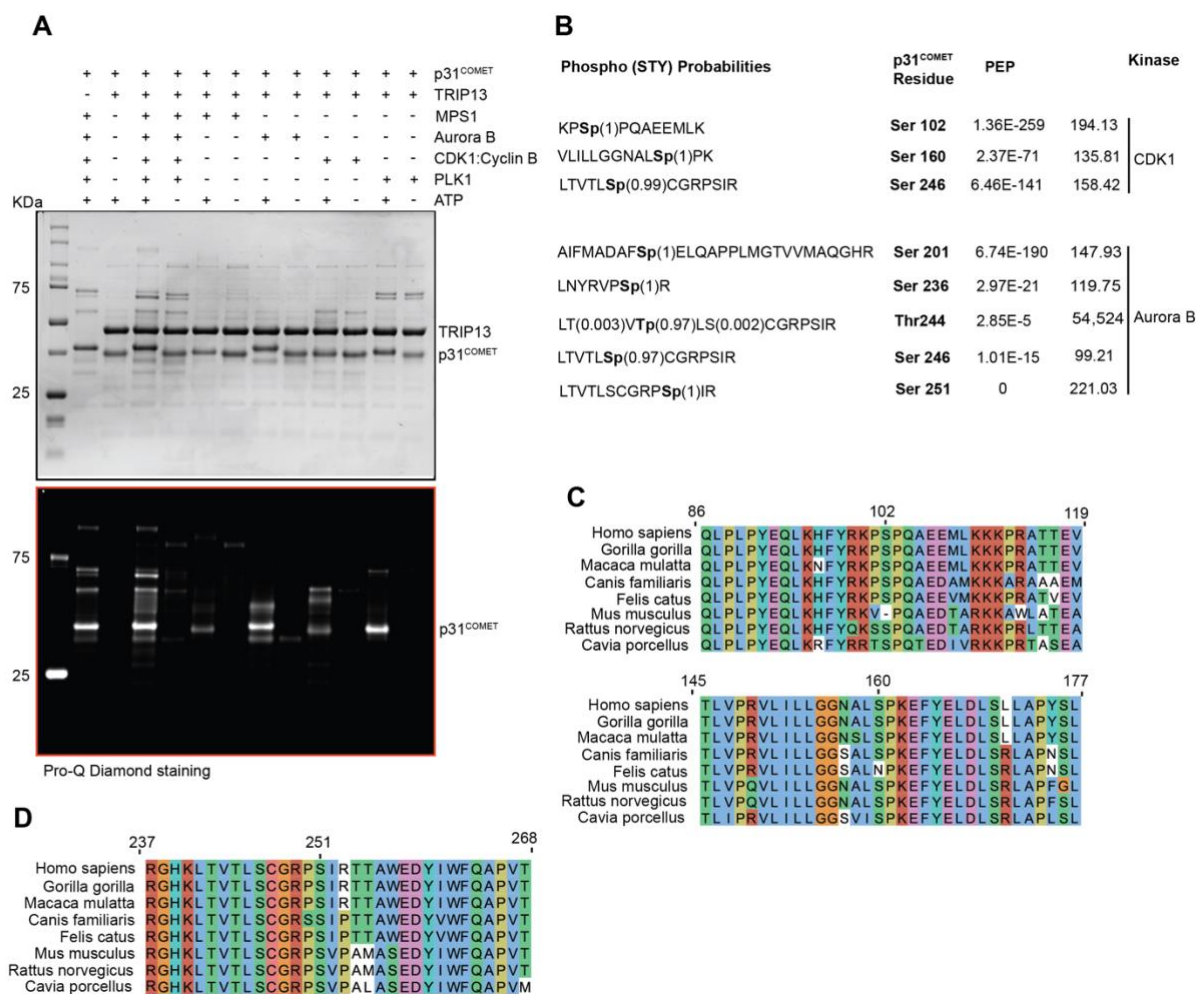
Figure 3-10 Mitotic kinases phosphorylate p31^{COMET} *in vitro*

A) Coomassie staining and ProQ diamond staining of SDS-PAGE gel showing that mitotic kinases phosphorylate p31^{COMET} but not TRIP13. TRIP13 (10 µM) and p31^{COMET} (10µM) were phosphorylated overnight at 4 ⁰C with individual kinases (500 nM) or kinase mix, as indicated. **B)** Table showing the phosphorylation sites identified by MS analysis of the phosphorylated samples. The table represents the sites detected at least once in MS analysis after three independent experiments for the CDK1 and Aurora B phosphorylation samples. **C)** Multiple sequence alignment of p31^{COMET} of the regions containing the Ser102 and Ser160 residues. **D)** Multiple sequence alignment of p31^{COMET} of the region containing the Ser251 residue.

For the samples phosphorylated with CDK1-CyclinB and Aurora B, multiple phosphorylated sites of p31^{COMET} were detected by MS analysis. All sites that were identified by MS analysis are listed in Figure 3-10B. Among these, the following residues were detected in three independent samples with high intensity values and localization probabilities: Ser102 and Ser160, phosphorylated by CDK1-CyclinB, and Ser251, phosphorylated by Aurora B kinase. The multiple sequence alignments show that the regions encompassing these residues are well conserved across mammals (Figure 3-10C, D).

3.2.5 CDK1-CyclinB negatively regulates TRIP13 activity on MAD2

Next, we wanted to investigate whether the identified phosphorylation sites have functional relevance in regulating TRIP13 activity. To address this question, we relied on FP assay to compare TRIP13 activity on C-MAD2:MIM^{FAM} under conditions where p31^{COMET} is phosphorylated by different mitotic kinases. We performed the FP assay in which TRIP13, p31^{COMET} and substrate concentrations are kept constant, but p31^{COMET} is pre-phosphorylated with the individual kinases and added to the final reaction volume just before starting the experimental reading. The rate of C-MAD2:MIM^{FAM} disassembly was unaffected by MPS1, Aurora B and PLK1 incubation with p31^{COMET}, whereas a reduction in rate of disassembly (compared to p31^{COMET} untreated) occurred when p31^{COMET} was pre-incubated with CDK1-CyclinB (Figure 3-11A). This reduction was not observed in the absence of ATP, suggesting indeed the CDK1-CyclinB phosphorylation, and not physical interaction, of p31^{COMET} is the cause for the reduced rate of disassembly (data not shown here). To show that p31^{COMET} N-terminus is dispensable for its function, we created truncation mutant (p31$^{COMET\ \Delta N53}$) and tested its activity in FP assay. This experiment demonstrated that rate of C-MAD2:MIM^{FAM} disassembly by TRIP13 is unaltered by p31^{COMET} lacking the first 53 amino acids compared to the p31^{COMET} wild-type (Figure 3-11B). This observation gives us confidence that the non-specific phosphorylation sites identified in the p31^{COMET} N-terminal region are of no functional importance for TRIP13 activity.

To further validate the exact residues involved in the phospho-regulation of p31^{COMET} by CDK1-CyclinB, we created mutants both at the Ser102 and Ser160 residues. The phospho-null mutants Ser102Ala, Ser160Ala and the phospho-mimetic mutants

Ser102Asp, Ser160Asp were tested for their efficiency in substrate disassembly. Using the FP assay, only the S160D mutant showed a decreased catalytic efficiency compared to p31^{COMET} wild-type (Figure 3-11C). To delineate the contribution of the two identified CDK1 phosphorylation sites to the regulation of TRIP13 activity, we performed FP assays using p31^{COMET} wild-type, S102A, S160A with and without CDK1-CyclinB pre-phosphorylation. Both p31^{COMET}- S102A and -S160A showed a decreased rate of substrate disassembly upon CDK1-CyclinB phosphorylation (Figure 3-11D), indicating, that both S102 and S160 residues of p31^{COMET} upon CDK1-CyclinB phosphorylation, contribute to the negative regulation of TRIP13 activity on substrates.
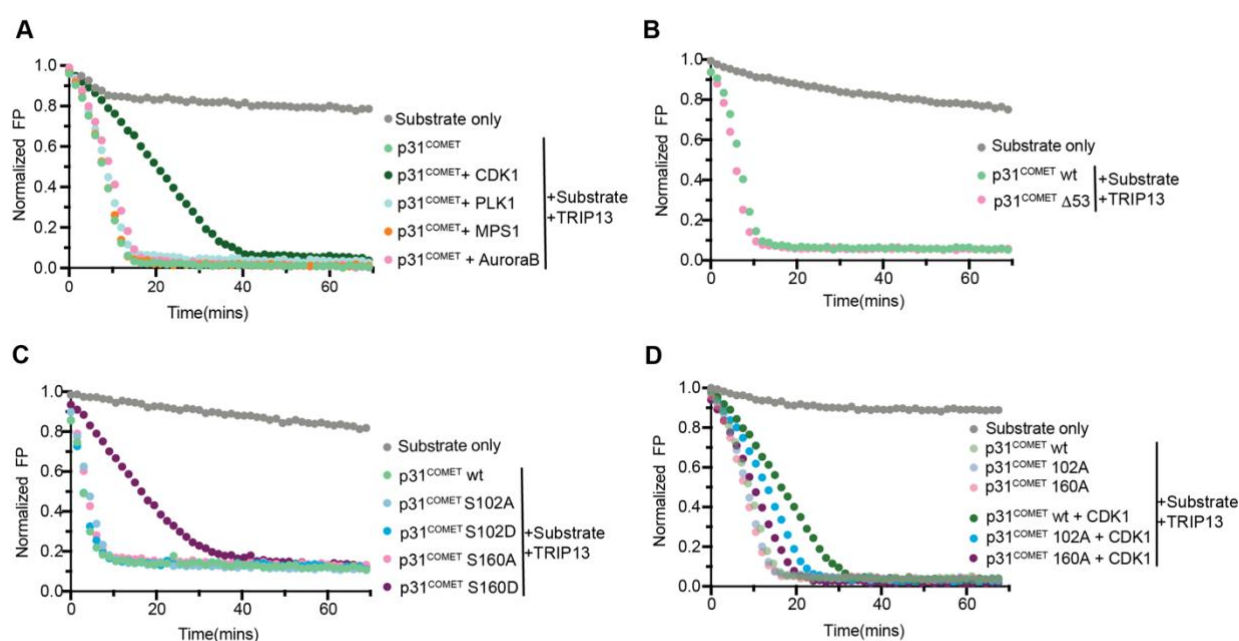
Figure 3-11 CDK1-CyclinB phosphorylation of p31^{COMET} negatively regulates TRIP13 activity on MAD2. A) FP assay showing MAD2:MIM^{FAM} dissociation with p31^{COMET} phosphorylated by different mitotic kinases such as with CDK1, MPS1, PLK1, Aurora B compared to non-phosphorylated p31^{COMET}. p31^{COMET} (2 µM) is phosphorylated overnight with individual kinases (100 nM) at 8 °C, with shaking at 450 rpm. Final concentrations of proteins [MAD2:MIM^{FAM}] = 100 nM, [TRIP13] = 500 nM, [p31^{COMET}] = 50 nM for all the panels in this figure. **B)** FP assay monitoring MAD2:MIM^{FAM} dissociation with N-terminal deletion construct of p31^{COMET} or full-length p31^{COMET}. **C)** FP assay comparing MAD2:MIM^{FAM} dissociation with p31^{COMET} wild-type , p31^{COMET} S102A, p31^{COMET} S102D, p31^{COMET} S160A, p31^{COMET} S160D **D)** FP assay showing MAD2:MIM^{FAM} dissociation with p31^{COMET} wild-type, p31^{COMET} S102A, p31^{COMET} S160A, p31^{COMET} wt + CDK1-CyclinB, p31^{COMET} S102A + CDK1-CyclinB, p31^{COMET} S160A+ CDK1-CyclinB.

Next, we set out to demonstrate the activity of the recombinant TRIP13 on MCC disassembly to further show that CDK1-CyclinB phosphorylation of p31^{COMET} negatively regulate TRIP13 activity. We used the previously characterized FRET-sensor developed to monitor the MCC assembly *in vitro* (for details about the sensor, refer to section 3.1.4 of this report). The FRET-sensor consists of the donor BUBR1^{CFP} and the acceptor MAD2^{TAMRA} pair, that, upon their incorporation into the MCC with CDC20, and excitation at 430nm produce FRET coupling between CFP and TAMRA.
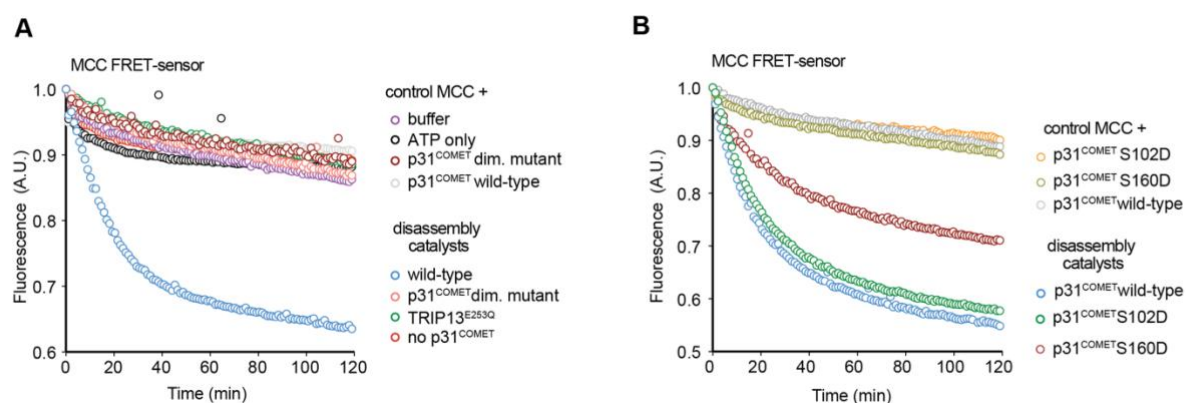
Figure 3-12 p31^{COMET} mutants reduce TRIP13 mediated disassembly of MCC

A) FRET assay showing the disassembly of MCC by TRIP13 and p31^{COMET} using the wild-type recombinant proteins or the mutants as indicated. [Preassembled MCC]= 100 nM, [TRIP13] = 1 μM, [p31^{COMET}] = 25 nM. **B)** FRET assay comparing the disassembly of MCC with p31^{COMET} wild-type, p31^{COMET} S102D or p31^{COMET} S160D.The concentrations of MCC, p31^{COMET} (both wt and mutant) and TRIP13 similar to panel A.

Recombinant TRIP13 can dissociate the pre-assembled MCC FRET-sensor only if the ATPase activity of TRIP13 and the p31^{COMET} dimerization with C-MAD2 are retained, as shown in Figure 3-12A. Similar to the experiments shown in Figure 3-11C, the Ser160Asp mutant of p31^{COMET} negatively regulated the MCC disassembly (Figure 3-12B). Further investigations are necessary to understand the mechanism behind the negative regulation of TRIP13 activity by CDK1-CyclinB, which we address in the course of this project.

3.2.6 Understanding the biochemical mechanism behind CDK1-CyclinB regulation of TRIP13 activity

There are no previous studies describing a regulatory role of CDK1-CyclinB on TRIP13 activity. We aimed to dissect the molecular mechanism at the basis of the effect observed in our FP assay of CDK1-CyclinB phosphorylation of p31^{COMET} on TRIP13 activity. p31^{COMET} Ser102 residue has been previously reported in an *in vivo* study to

be phosphorylated during mitosis, and it was proposed that the phosphorylation of this residue weakens C-MAD2:p31^{COMET} binding (Date et al., 2014). A more recent study reported that PLK1 phosphorylates p31^{COMET} on the Ser102 residue *in vitro* and this phosphorylation inhibits the activity of p31^{COMET}:TRIP13 complex on MCC disassembly in mitotic lysates (Kaisari et al., 2019). In our experiments, however, we observed that the phosphorylation of Ser102, with the resulting decrease in TRIP13 activity, is obtained with CDK1-CyclinB and not PLK1 *in vitro*. Furthermore, the authors did not explore the biochemical mechanism behind the decrease in TRIP13 activity. To delineate the mechanism behind CDK1-CyclinB regulation of TRIP13 activity, we asked whether the p31^{COMET} interaction with either C-MAD2 or TRIP13 is affected upon phosphorylation.

3.2.6.1 The effect of CDK1-CyclinB phosphorylation on C-MAD2:p31^{COMET} binding

As mentioned earlier, previous studies claimed that the C-MAD2: p31^{COMET} interaction is weakened upon Ser102 phosphorylation (Date et al., 2014). For this reason, we set out to investigate whether p31^{COMET} phosphorylation by the mitotic kinases, in particular CDK1-CyclinB, affects its interaction with C-MAD2. GST-based pulldown experiments show that p31^{COMET} phosphorylation by none of the mitotic kinases impaired its interaction with C-MAD2 (Figure 3-13A). To further examine possible effects of CDK1-CyclinB phosphorylation, we performed analytic SEC analysis of p31^{COMET} binding with C-MAD2. SEC analysis indicated that the direct binding of p31^{COMET} with C-MAD2 is unaffected by CDK1-CyclinB phosphorylation of p31^{COMET} (Figure 3-13B).

Isothermal titration calorimetry (ITC) assays were performed to measure the binding affinity between C-MAD2 and p31^{COMET}. ITC is a quantitative technique that allows to measure the binding affinities between biomolecules by detecting the heat that is either released or absorbed during the binding events. Recombinant p31^{COMET} (either wild-type, S102A or S102D mutants) was loaded into the sample cell at a concentration of 10 µM. C-MAD2 (purified MAD2 incubated with the MIM peptide to ensure the closed conformation) at 120 µM concentration, was aspirated into the syringe, injected stepwise at regular intervals of 2 seconds and the binding events were measured. As shown in Figure 3-13C, the dissociation constant (K_d) of p31^{COMET}: C-MAD2 interaction

is approximately 90 nM. The K_d value was similar also for the mutants on the Ser102, further corroborating the previous observations.
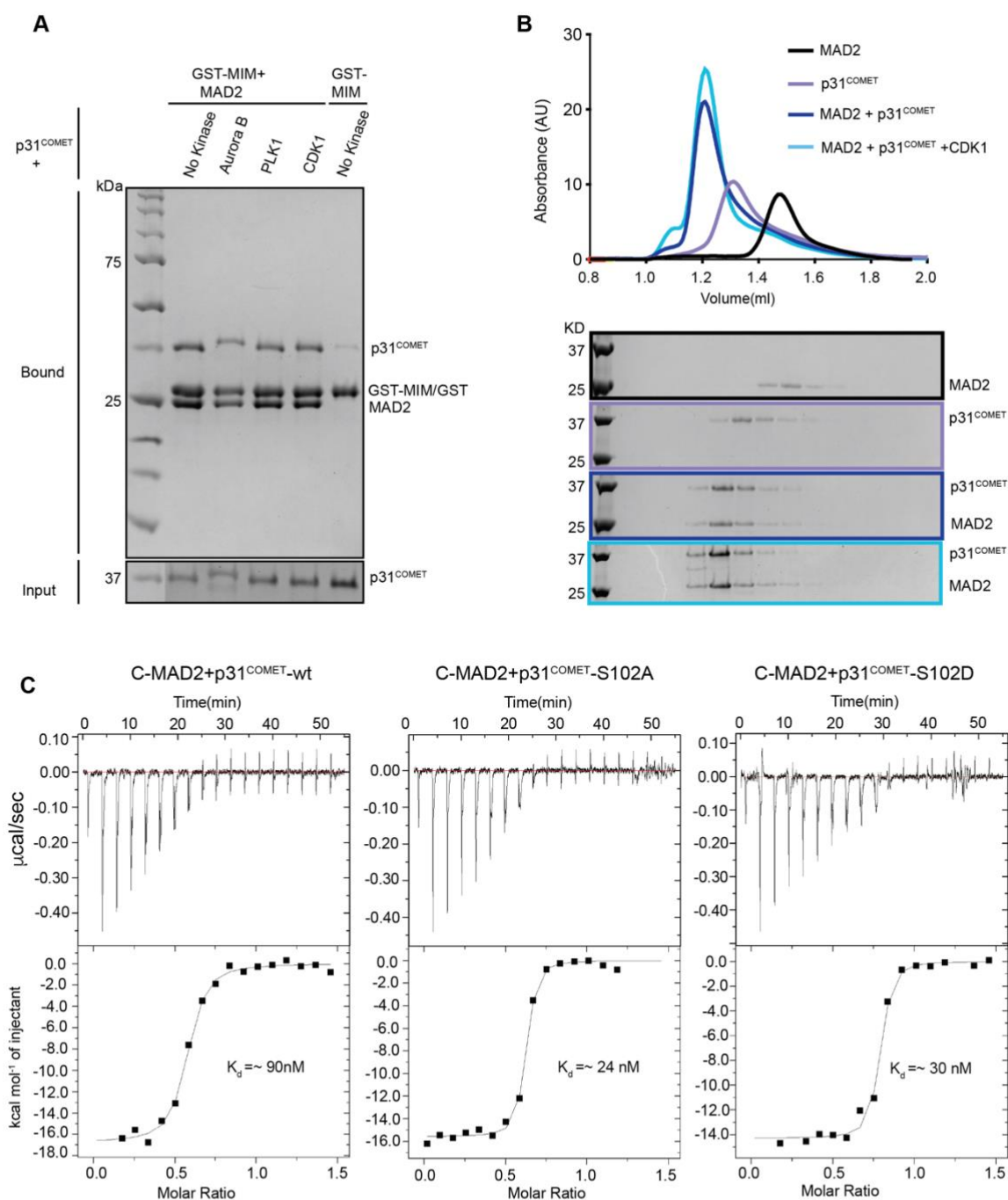
Figure 3-13 C-MAD2: p31COMET interaction is unaffected by CDK1-CyclinB phosphorylation
A) GST-based pulldown to monitor the binding of C-MAD2 and p31COMET. GST-MIM or GST-MIM+C-MAD2 were immobilized on GSH resin as bait. p31COMET was added as prey, either alone or phosphorylated by mitotic kinases, as marked above each lane. [GST MIM/GST-MIM + MAD2] = 4 µM, [p31COMET] =5 µM. **B)** SEC elution profile on a Superdex200 column of MAD2 with p31COMET (both at 5 µM, CDK1-CyclinB preincubated at 200 nM with p31COMET overnight at 4 °C). **C)** Binding isotherms by ITC detecting the physical interaction of C-MAD2 with p31COMET wild-type, S102A or S102D mutants.

To further support the above observations, we performed SEC analysis to monitor the binding of C-MAD2:MIM with p31^{COMET}. Both the mutants, S012A and S102D of p31^{COMET} bind C-MAD2 comparably to p31^{COMET} wild-type (Figure 3-14). Altogether, our observations disagree with the previous claim that Ser102 phosphorylation by-
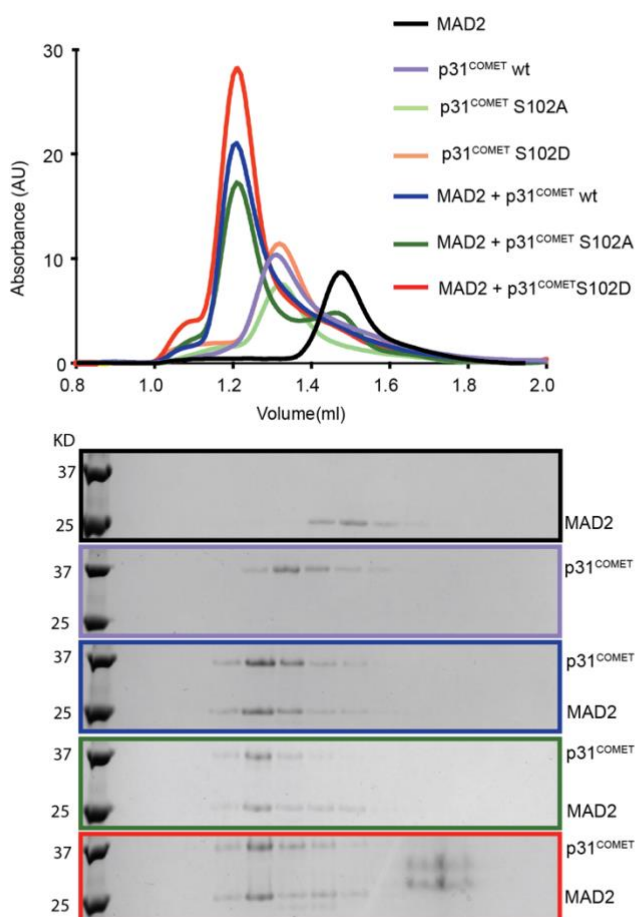
Figure 3-14 p31^{COMET} mutants of Ser102 can bind to C-MAD2 similarly to p31^{COMET} wt

SEC elution profile on a Superdex200 column of C-MAD2 with p31^{COMET} wild-type or Ser102 mutants (all proteins are at 5 µM).

PLK1 weakens C-MAD2: p31^{COMET} interaction (Date et al., 2014, Kaisari et al., 2019). We rather show that the Ser102 residue of p31^{COMET} is phosphorylated by CDK1-CyclinB and that it does not impair the interaction between p31^{COMET} and C-MAD2.

3.2.6.2 CDK1-CyclinB phosphorylation of p31^{COMET} reduces TRIP13: p31^{COMET} interaction *in vitro*

To understand the mechanism behind CDK1-CyclinB regulation of TRIP13 activity, we hypothesized that TRIP13:p31^{COMET} interaction is weakened upon p31^{COMET} phosphorylation by CDK1-CyclinB complex. Structural information available of the

TRIP13: p31^{COMET}:C-MAD2 complex (PDB: 6F0X) shows that the Ser160, one of the CDK1-CyclinB phosphorylation site that we identified, is located at the binding interface between TRIP13 and p31^{COMET}, and that, in particular, the TRIP13 interface has several negatively charged residues. The Ser102 residue, the other CDK1-CyclinB site that we found, is, instead, located on a flexible elongated loop (α3–4 loop, missing in the structure), that has been modelled upon cross-linking-MS analysis which suggests an interaction between the p31^{COMET} α3-4 loop with the TRIP13 NTD (refer to Figure S7 of Alfieri et al., 2018). To test our hypothesis, we relied on an MBP-based pulldown assay, shown schematically in Figure 3-15A. MBP or MBP-MAD1:C-MAD2 were immobilized on amylose resin as bait. p31^{COMET} and TRIP13^{E253Q} were added as prey, either alone or with p31^{COMET} pre-phosphorylated by individual mitotic kinases. As expected, there is no difference in the extent of p31^{COMET} binding to MAD1:C-MAD2 complex after phosphorylation, whereas TRIP13 binding to MAD1:C-MAD2:p31^{COMET} complex is reduced significantly upon p31^{COMET} phosphorylation by CDK1-CyclinB (Figure 3-15B).

To further corroborate our hypothesis, we tested various mutants of p31^{COMET}, such as S102A, S102D, S160A, S160D, S102A-S160A, S102D-S160D, in the MBP-based pulldown assay. The double phospho-mimetic mutant S102D-S160D was unable to recapitulate the drastic decrease in TRIP13 binding to MAD1:C-MAD2:p31^{COMET} complex after CDK1-CyclinB phosphorylation of p31^{COMET} (Figure 3-15C). The inability of the aspartic acid residues to recapitulate to the same extent the phosphorylation of the serine residues might be the reason for the observed weaker effect. Nevertheless, we performed a MBP-based pulldown assay with p31^{COMET} phospho-null mutants of the aforementioned residues to uncover the contribution of individual residues on p31^{COMET}:TRIP13 interaction. As shown in Figure 3-15D, the single phospho-null mutants of p31^{COMET} S102A and S160A behaved similarly to p31^{COMET} wild-type and the phosphorylation by CDK1-CyclinB reduced the interaction of both mutants with TRIP13. Contrary to this, the double mutant p31^{COMET}-S102A-S160A showed invariant TRIP13 binding with and without CDK1-CyclinB phosphorylation. These results suggest a complementary behavior of S102 and S160 residues, where both residues need to be phosphorylated by CDK1-CyclinB to weaken the interaction with TRIP13. Altogether, the collected *in vitro* data demonstrate that TRIP13: p31^{COMET} interaction

is reduced by the CDK1-CyclinB phosphorylation of p31^{COMET} and, presumably, this is sufficient to explain the negative regulation of CDK1-CyclinB on TRIP13 activity.
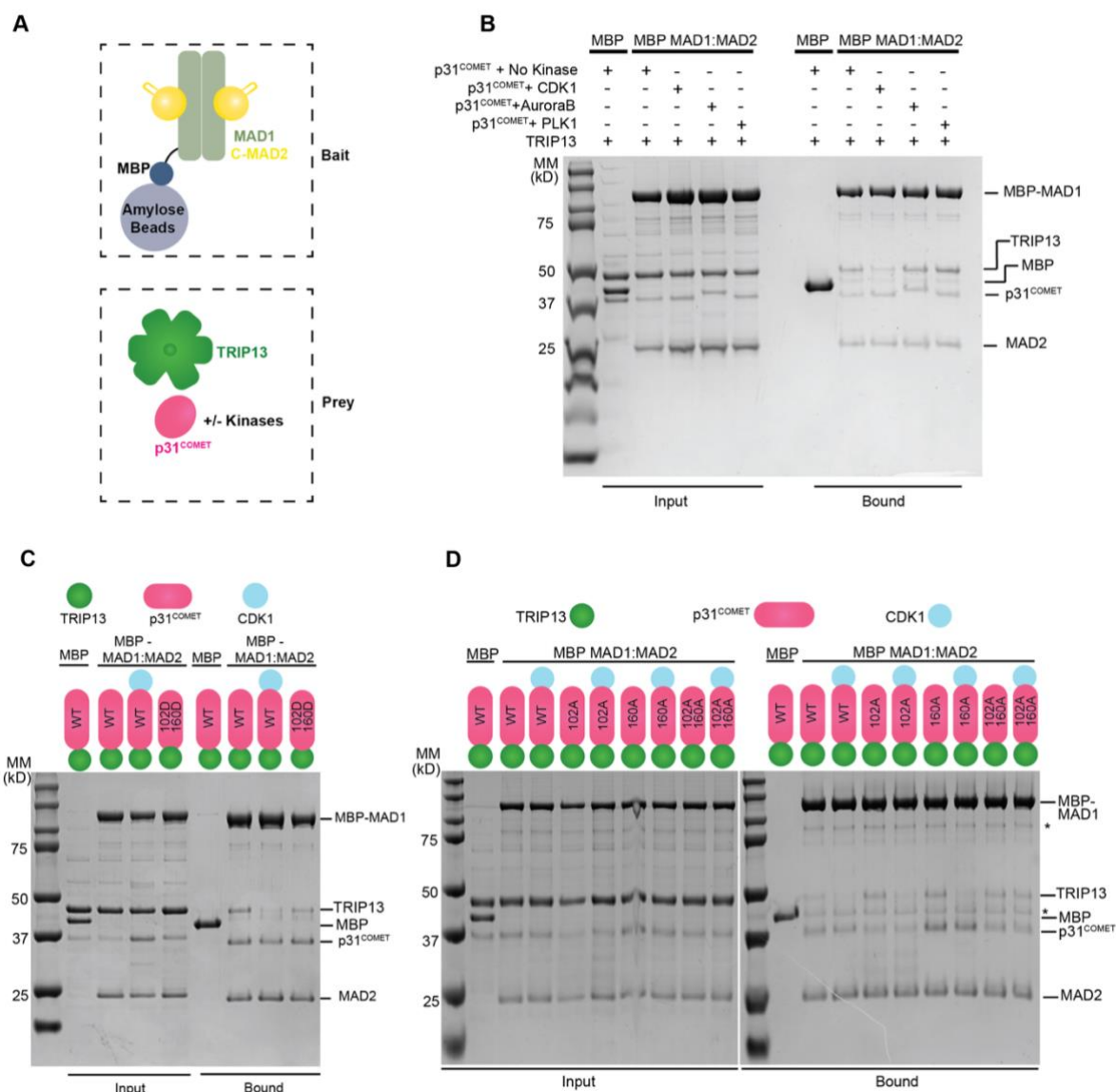
Figure 3-15 p31^{COMET} phosphorylation by CDK1 reduces TRIP13 binding

 A.) Schematic of the performed amylose-resin pull-down assays. MBP and MBP-MAD1:C-MAD2 were immobilized on amylose resin as bait. p31^{COMET} and TRIP13^{E253Q} were added as prey, either alone or with p31^{COMET} phosphorylated by mitotic kinases where indicated. **B)** Result of the amylose-resin pull-down experiment in which p31^{COMET} is pre-phosphorylated by kinases as indicated above each lane. The left SDS-PAGE gel shows the input fractions, the right gel shows the bound fractions. [MBP/MBP-MAD1:C-MAD2] = 4 μM, [p31^{COMET}] = 5 μM, [TRIP1] = 15 μM, [ATP] = 2 mM (in all conditions)**.** p31^{COMET} (20 μM) is phosphorylated overnight at 10 °C with the indicated mitotic kinases at 1 μM. **C, D)** SDS-PAGE gels of the MBP pull-down experiment with the p31^{COMET} mutants of identified CDK1-CyclinB sites (Ser102, Ser160) are tested as indicated above the lanes to compare with p31^{COMET} wild-type.

3.2.7 MAD1:C-MAD2 is a TRIP13 pseudo-substrate that stimulates CDK1-CyclinB phosphorylation of p31[COMET]

As discussed in the Introduction, whether TRIP13 can dissociate the MAD1:C-MAD2 complex remains an unanswered question. MAD1:C-MAD2 can be a potential TRIP13 substrate as 1) the interaction between MAD2 and MAD1 is structurally similar to the C-MAD2:CDC20, a well-characterized TRIP13 substrate (Luo et al.,2002; Sironi et al., 2002; Xia et al., 2004); 2) p31[COMET] can dimerize with both MAD1:C-MAD2 and C-MAD2:CDC20 complexes (Yang et al., 2007). Moreover, MAD1:C-MAD2:p31[COMET] complex is able to bind TRIP13[E253Q] and form a stable complex with it, as shown by pulldowns in Figure 3-15.

We first asked whether the MAD1:C-MAD2 complex can stimulate the TRIP13 consumption of ATP like the other known C-MAD2 substrates. We established a NADH-based ATP consumption assay (Hackney et al., 2001; Kilanista et al., 2002) to monitor the TRIP13 stimulation by different C-MAD2 containing substrates. The working principle behind the assay is shown schematically in Figure 3-16A. This coupled enzymatic assay measures the consumption of ATP by converting the ADP produced by the ATPase back to ATP via the phosphoenolpyruvate (PEP) kinase (PK), which in turn accumulates pyruvate that can be used by the lactate-dehydrogenase (LDH) to convert it into lactate while consuming NADH. The final readout is the decrease of NADH, monitored by its absorbance at 340 nm. Every molecule of ATP converted to ADP corresponds to a molecule of NADH oxidized to NAD (decreasing absorbance at 340 nm). We observed that in presence of TRIP13 or with the addition of p31[COMET] there is a limited hydrolysis of ATP, whereas upon addition of known substrates, such as C-MAD2:MIM and MCC, the ATPase activity of Trip13 is stimulated by almost 4-fold, as previously reported with *M. musculus* TRIP13 (Ye et al., 2015). We observed that MAD1:C-MAD2 complex also stimulated TRIP13 ATPase activity similarly to other known MAD2 substrates (Figure 3-16B). NADH coupled ATPase assays were performed in collaboration with my colleague Dr. Valentina Piano.
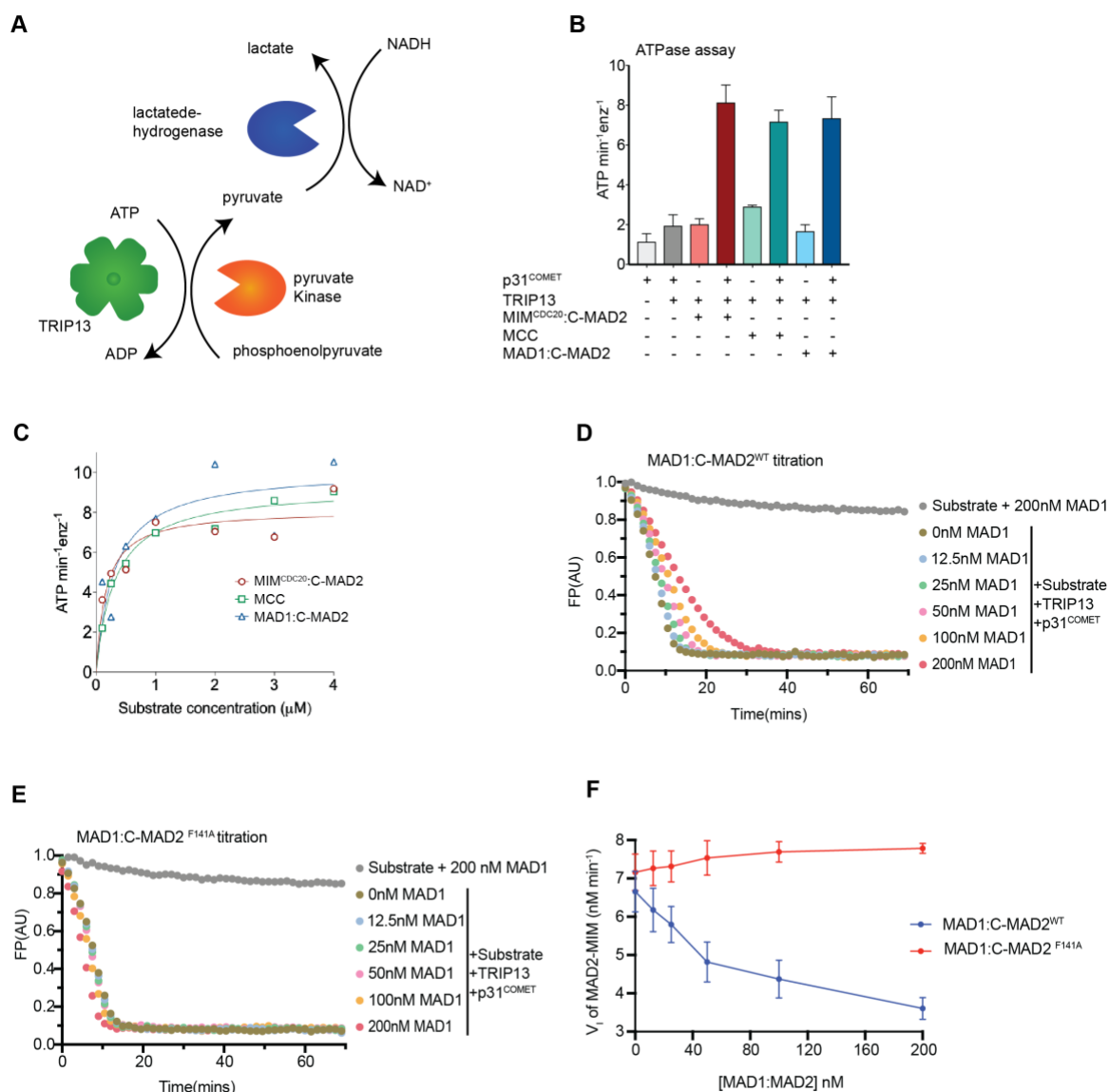
Figure 3-16 MAD1:C-MAD2 is a substrate of the TRIP13:p31^COMET enzymatic machinery

A) Schematic illustration of the NADH-coupled ATP consumption assay. **B)** Bar plots showing the consumption of ATP by TRIP13 (ATP min⁻¹enz⁻¹) in presence of different C-MAD2 containing substrates. The error bars show the SEM from three independent experiments. The velocity of the reaction, expressed in ATP min⁻¹enz⁻¹ (considering the concentration of hexamer, not monomer of TRIP13), is corrected for the spontaneous ATP hydrolysis in absence of TRIP13. The concentration of NADH is calculated interpolating the measured absorbance with our standard curve (not shown here). **C)** Michaelis–Menten kinetics of TRIP13 activity with the different substrates. **D, E)** FP assay showing the inhibition by MAD1:C-MAD2 (wild-type or F141A mutant) on the TRIP13 activity on C-MAD2:MIM^FAM. MAD1:C-MAD2 is titrated from 200 nM to 12.5 nM as indicated, and C-MAD2:MIM^FAM is constant at 100 nM. **F)** Plot showing the initial velocities of the FP assay with titration of MAD1:C-MAD2^WT and MAD1:C-MAD2^F141A. Error bars show mean +/- SEM of three independent technical replicates.

We fitted the experimental data of ATP consumption with a Michaelis–Menten curve for each of the individual substrates. Similar kinetics were observed for all the

substrates, with a resulting K_m value of approximately 0.2 µM and V_{max} of about 9 ATP min^{-1} enzyme^{-1} (Figure 3-16C), supporting the hypothesis that MAD1:C-MAD2 is also a substrate of TRIP13, like the MCC and C-MAD2:MIM^{CDC20}, at least to the extent that it promotes the catalytic activity of the enzyme. To further validate this idea, we tested whether MAD1:C-MAD2 is able to compete with the C-MAD2:MIM^{FAM} substrate for TRIP13:p31^{COMET} activity in the FP assay. For this competition assay, we kept the MAD2:MIM^{FAM} concentration constant at 100 nM and titrated MAD1:C-MAD2, as represented in Figure 3-16D. The initial velocities (V_i) of the MAD2:MIM^{FAM} substrate disassembly decreased with the amount of MAD1:C-MAD2 added to the reaction, confirming that MAD1:C-MAD2 competes for the C-MAD2:MIM^{FAM} substrate (Figure 3-10D,F). The competitive behavior was not observed for MAD1:C-MAD2^{F141A}, a mutant of MAD2 that is defective in p31^{COMET} binding, excluding any off-target effects (Figure 3-16E, F). As of now, our data suggests that MAD1:C-MAD2 is a TRIP13 substrate analogous to CDC20:C-MAD2.

MAD2 structural remodeling by TRIP13 results in the dissociation of MAD2 from its binding partners (Eytan et al., 2014). Therefore, the MAD1:C-MAD2 complex should also be dissociated by TRIP13 enzyme for it to qualify as a substrate. Even though both TRIP13 and p31^{COMET} bind to MAD1:C-MAD2 complex, the enzyme machinery could not dissociate the complex, as shown in the MBP-based pulldown assay in Figure 3-17. This observation is in contrast with our previous experiments that claim MAD1:C-MAD2 is a TRIP13 substrate (Figure 3-16). Nevertheless, the ability of MAD1:C-MAD2 to stimulate TRIP13 ATPase activity and compete with MAD2:MIM^{CDC20} substrate should not be neglected. Therefore, we hypothesize that MAD1:C-MAD2 is a pseudo-substrate of TRIP13 that binds and induce futile ATP hydrolysis cycles, without allowing MAD2 to undergo its conformational change to O-MAD2. However, this appears to be a heavily energy wasteful process that the cell needs to regulate.

CDK1-CyclinB binds to an acidic patch in the N-terminal region of MAD1 and this interaction is necessary for its recruitment to unattached kinetochores (Alfonso-Perez et al., 2019). CDK1-CyclinB interaction with MAD1:C-MAD2 complex is crucial for the release of MAD1:C-MAD2 from the nuclear pore complex (NPC) on the nuclear envelop at the onset of mitosis (Jackman and Marcozzi et al., 2020), and for the

subsequent MAD1:C-MAD2 kinetochore and corona localization to ensure robust SAC signaling (Allan et al., 2020). Other than its dependency on MAD1 recruitment to the corona, so far there has been no physiological relevance attributed to kinetochore localization of CDK1-CyclinB. When localized at NPC or at the kinetochore during mitosis, MAD1:C-MAD2 was observed to be bound to p31^{COMET} (Fava et al., 2011). Taken all these observations into consideration, we asked whether CDK1-CyclinB phosphorylation of p31^{COMET} is enhanced by the presence of MAD1:C-MAD2 complex. As discussed in the previous paragraphs, the binding of TRIP13 to MAD1:C-MAD2:p31^{COMET} complex and the resulting futile ATP consumption cycles are likely to be reduced in cells to conserve energy. If CDK1-CyclinB interaction with MAD1:C-MAD2 enhances the p31^{COMET} phosphorylation, this can prevent TRIP13 binding and the subsequent ATP hydrolysis.
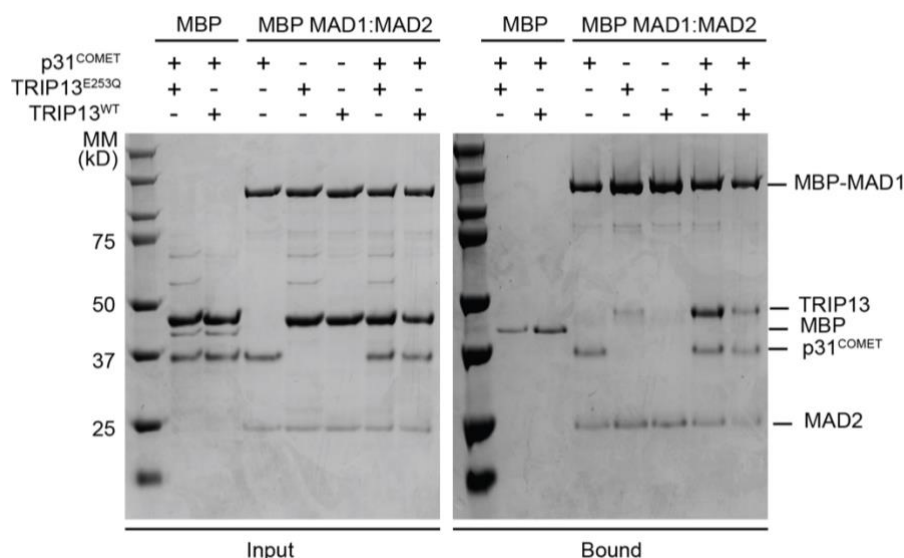
Figure 3-17 TRIP13 is unable to disassemble MAD1:C-MAD2 complex

MBP-based pulldown assay to test the release of C-MAD2 from MBP-MAD1:C-MAD2 complex. [MBP/MBP-MAD1:C-MAD2] = 4 µM, [p31^{COMET}] = 5 µM, [TRIP13] = 15 µM, [ATP] = 2 mM (in all conditions).

In order to address this question, we compared CDK1-CyclinB dependent phosphorylation of p31^{COMET} in the presence and absence of MAD1:C-MAD2. Samples were collected at fixed time intervals from both conditions and analyzed with SDS-PAGE using ProQ- diamond staining. MAD1:C-MAD2 enhanced the CDK1-CyclinB phosphorylation of p31^{COMET} only slightly compared to the CDK1-CyclinB alone condition (Figure 3-18A, B). Note that we used the p31^{COMET}ΔN53 truncated proteinto avoid the unspecific N-terminal phosphorylation shown earlier in this report. MS

analysis of the phosphorylated samples (after 90 min of incubation) identified the Ser102 residue being phosphorylated both with and without MAD1:C-MAD2, whereas the Ser160 residue was phosphorylated only in the presence of MAD1:C-MAD2 (Figure 3-18C).
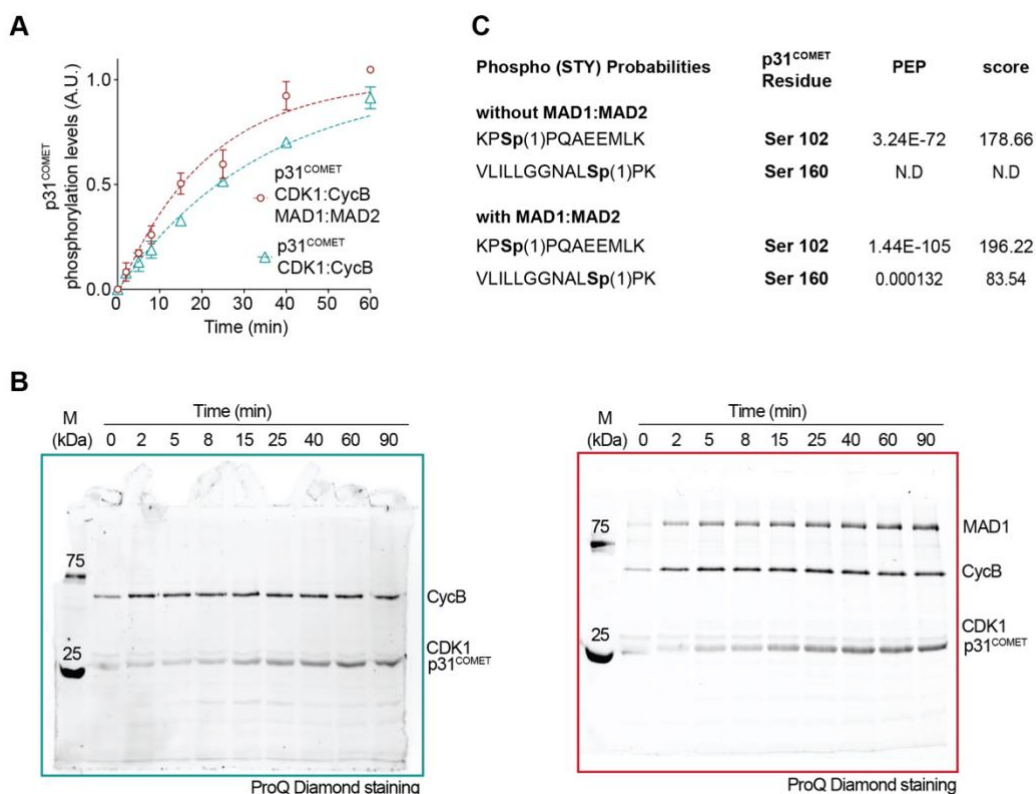
Figure 3-18 MAD1:C-MAD2 enhances the phosphorylation of p31^{COMET} by CDK1-CyclinB

A) Phosphorylation of p31^{COMET} by CDK1-CyclinB is performed under two conditions: with and without the addition of MAD1:C-MAD2. The plot shows the mean with SD of quantification of the ProQ diamond staining intensity of three technical triplicates of each condition at regular time intervals. [p31^{COMET}] = 4 µM, [MAD1:C-MAD2] = 1 µM, [CDK1-CyclinB] = 1 µM. **B)** Representative ProQ diamond staining of SDS-PAGE gels used in the quantifications in panel A. **C)** Phosphorylation sites identified by MS analysis of samples described in panel A, B.

To summarize the experiments reported so far, these are the main observations: 1) MAD1:C-MAD2 is a pseudo-substrate of the TRIP13:p31^{COMET} enzymatic machinery; 2) CDK1-CyclinB phosphorylation of p31^{COMET} reduces its binding to TRIP13; 3) MAD1:C-MAD2 stimulates CDK1-CyclinB phosphorylation of p31^{COMET}. These three main observations lead us to hypothesize that CDK1-CyclinB phosphorylation of p31^{COMET} is required to prevent TRIP13 interaction with MAD1:C-MAD2:p31^{COMET} complex during mitosis. This proposed mechanism and its cellular implications are discussed in greater detail in Section 4.2.2.

3.2.8 MCC assembly catalysts displaces p31^{COMET} to recruit O-MAD2 at SAC signaling kinetochores

MAD2:CDC20 interaction is the rate limiting step of MCC assembly, which is accelerated by the identified catalytic components MAD1:C-MAD2, BUB1:BUB3 and MPS1 (Faesen et al., 2017). A recent study from our laboratory and an accompanying study from the laboratory of Prof. Desai described the molecular mechanism underlying the MCC assembly catalysis (Piano et al., 2021; Lara- Gonzalez et al., 2021). The studies report that MPS1 phosphorylation-dependent interaction of MAD1, BUB1 and CDC20, specifically happening at unattached kinetochores, is crucial for the MCC assembly catalysis. These interactions geometrically constrain CDC20 and MAD2 positions at kinetochore to favor their effective binding. The O-MAD2 recruitment to kinetochores through dimerization with MAD1:C-MAD2 is fundamental for the catalysis, as depicted in Figure 3-19A. The binding of p31^{COMET} to MAD1:C-MAD2 at kinetochores (as reported in Fava et al., 2011) is detrimental for the MCC catalysis as it does not allow O-MAD2 recruitment (Figure 3-19A). Additionally, C-MAD2: p31^{COMET} interaction (K_d = 50 nM, this study) has much higher affinity than C-MAD2:O-MAD2 dimerization (K_d = 1 µM, Hara et al., 2015). So, it remains mysterious how kinetochores selectively render MAD1:C-MAD2 available for O-MAD2 dimerization to activate the SAC signaling.

Mutants of MAD1, BUB1 or CDC20 that impaired catalytic MCC formation also failed in recruiting O-MAD2 to unattached kinetochores (Lara-Gonzalez et al., 2021). This observation remains unexplained, but we hypothesize that the MPS1 mediated interaction of the catalytic components favors O-MAD2 recruitment to kinetochores and displaces p31^{COMET} bound to MAD1:C-MAD2. To prove our hypothesis *in vitro*, we designed an MBP-based pulldown assay to detect the binding of O-MAD2 and p31^{COMET} with MBP-MAD1:C-MAD2. At equimolar concentrations, p31^{COMET} prevented O-MAD2 binding to MAD1:C-MAD2. Upon addition of the other components of the MCC catalytic machinery, BUB1:BUB3 and CDC20, the binding of O-MAD2 significantly increased (Figure 3-19B). Also, a significant decrease in p31^{COMET} binding to MAD1:C-MAD2 was observed, when the MCC catalysts and an excess of O-MAD2 were added (Figure 3-19C). The MAD1:C-MAD2 complex is the lone identified receptor for p31^{COMET} recruitment at kinetochores. If no other receptors for p31^{COMET} at kinetochores are present, then the competition for MAD1:C-MAD2 receptor implies

that O-MAD2 can be recruited to kinetochore only by displacing p31[COMET]. We have confirmed that p31[COMET] does not directly interact with BUB1:BUB3 and CDC20 (data not shown here), further justifying the competition between O-MAD2 and p31[COMET] for a single kinetochore receptor.
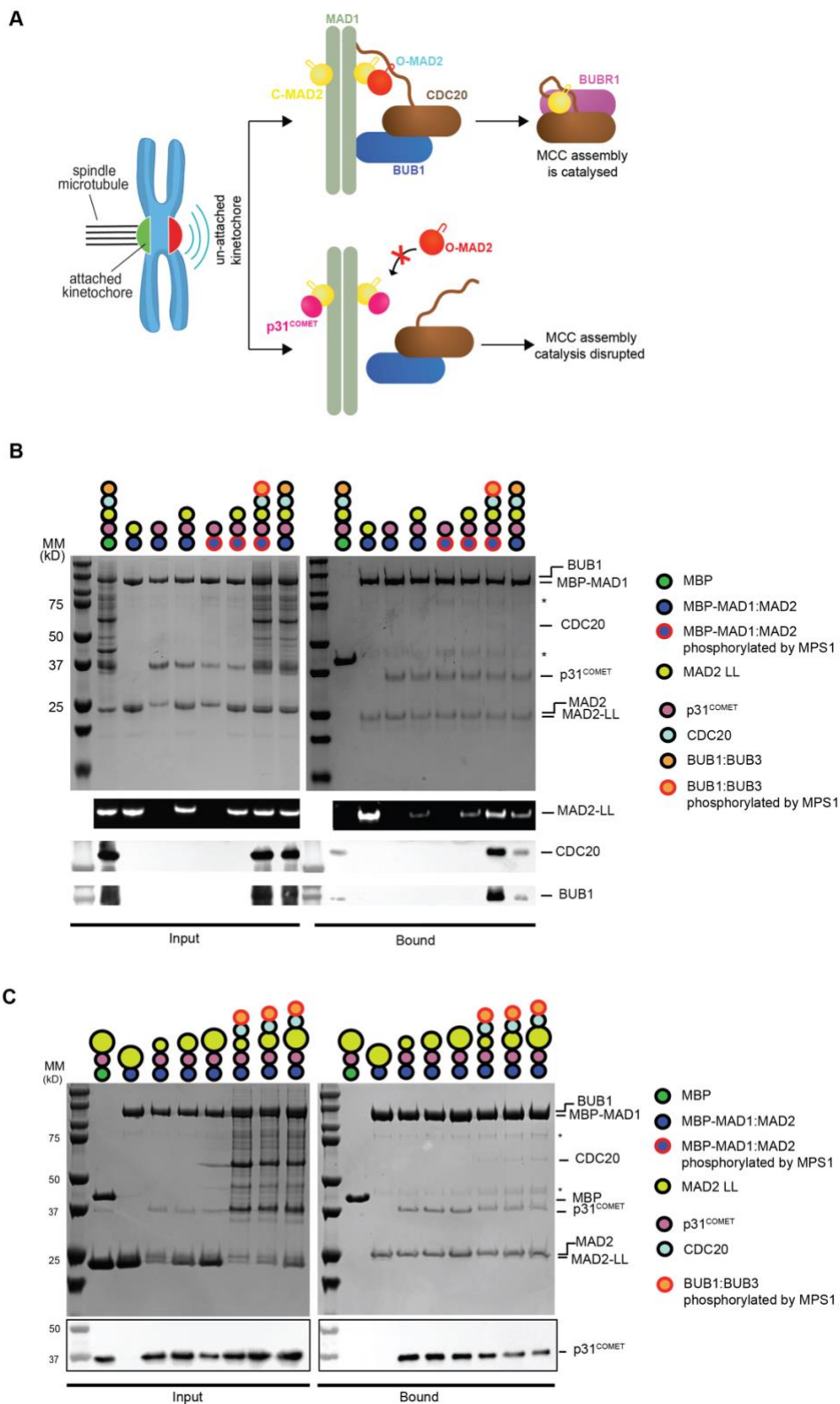
Figure 3-19 MCC catalysts favor O-mad2 over p31COMET for MAD1:C-MAD2 binding

 A) Schematic illustration of the interactions among the MCC assembly catalysts (BUB1:BUB3, CDC20, MAD1:C-MAD2) at kinetochore necessary for MCC formation (top). Blocking of the dimerization interface of MAD1:C-MAD2 complex by p31COMET prevents O-MAD2 recruitment and MCC catalysis. **B**) MBP-based pulldown to compare the binding of O-MAD2 and p31COMET to MBP-MAD1:C-MAD2 (bait), with or without adding MCC assembly catalysts. Coomassie stained protein gels on the top, fluorescence emission of TAMRA labelled MAD2LL mutant (loop mutant of MAD2 locked in open conformation) in the middle, and western blots against CDC20 and BUB1 at the bottom. [MBP]/[MBP-MAD1:C-MAD2] = 4 µM, [p31COMET] = 4 µM, [MAD2-LL] = 4 µM, [CDC20] = 6 µM, [BUB1:BUB3] = 6 µM. In conditions where MPS1 phosphorylation is performed, MAD1:C-MAD2 and BUB1:BUB3 (20 µM) are phosphorylated overnight at 4^0 C with MPS1 (1 µM). **C**) MBP-based pulldown similar to panel B, except the MAD2-LL concentration is titrated compared to p31COMET. [MAD2-LL] = 4 µM / 8 µM / 12 µM (represented by the increasing radius of yellow circle). Concentrations of other proteins are kept constant as in previous pulldown. Coomassie stained protein gels showing the input and bound fractions on top, and western blot against p31COMET at bottom.

To further support the described observations, we tested the ability of p31COMET to inhibit MCC catalysis by blocking the dimerization interface of MAD1:C-MAD2 complex in our FRET-based assay using the sensor monitoring CDC20:C-MAD2 formation (CFP-CDC20 as donor and MAD2TAMRA as acceptor, refer to section 1.3.4 for details). At equimolar concentrations, p31COMET did not inhibit MCC catalysis (Figure 3-20 A, B), further corroborating the idea that MCC catalysts disrupt p31COMET binding to MAD1:C-MAD2. All together our observations demonstrate a novel mechanism by which MCC catalysts displace p31COMET from unattached kinetochores to favor O-MAD2 recruitment. How this proposed mechanism would help to regulate steady state MCC levels and robustness of SAC signaling is discussed in detail in section 4.2.3.
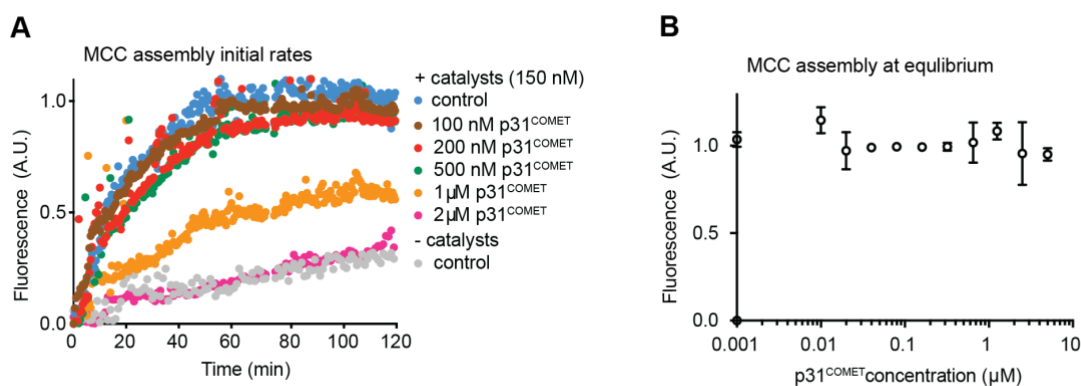

Figure 3-20 p31COMET is unable to inhibit MCC assembly catalysts at equimolar concentration
A) FRET-based assay detecting the effect of p31COMET titration on MCC assembly catalysis. **B)** Equilibrium plot showing that FRET efficiency of the sensor is unaffected by p31COMET titration at indicated concentrations.

4. Discussion

4.1 The applications of electroporation as a tool for protein functional studies in mammalian cells

In recent years, the demand for robust methods to deliver modified synthetic or semi-synthetic macromolecules into cells has been growing. Rapid development of new methodologies in synthetic biology enables addition of chemical functionalities into proteins and lipids. High-throughput approaches that can deliver recombinant protein into large number of cells, thus, hold advantage over traditional DNA transfection-based approaches. While electroporation has been long recognized for its potential as a delivery approach, there have been concerns about the cellular toxicity it can cause (Torchilin, 2008). In the studies described here, we assessed the suitability of batch EP for delivering recombinant proteins into living mammalian cells for various applications in cell biology. We used mainly kinetochore and SAC related proteins for the studies, because their characteristic localization pattern and previously established phenotypes make them ideal for *in vivo* functional studies. Our results identify EP as a rapid, efficient, and semi-quantitative technique that enables the delivery into various cultured mammalian cell lines of proteins and protein complexes of variable mass and hydrodynamic radius. Our experiments show that EP delivered proteins remain largely structurally and functionally intact in cells, interact with endogenous binding partners and are able to complement siRNA-based depletion of corresponding protein. Since it is a batch method, cell lysates from large cohorts of electroporated cells can be obtained and, therefore, EP is compatible with many macromolecular interaction approaches, from mass spectrometry to immuno-precipitation.

In our study, for example, using Spindly protein we demonstrated that *in vitro* addition of a lipid group bypassed the requirement of the specific lipid transferase enzyme in cells. In the future, this approach may be extended to study the functional roles of specific lipid-modified proteins in cells. Another clear advantage of *in vitro* modification of proteins is that it allows precision labeling of recombinant proteins with small fluorescent dyes, and, thus, enables the expansion of the toolbox for live-cell photo-manipulation techniques. We envision that EP can be used for the detection of low affinity interactions between elusive binding partners in cells, if the recombinant proteins that are introduced are modified with suitable chemical handles, such as photo-activatable crosslinking groups. In summary, we conclude that EP has the

potential to become a method of choice for delivery of synthetic or semi-synthetic recombinant proteins into mammalian cells for various functional studies.

4.2 The regulation of TRIP13-p31^{COMET} enzymatic machinery during mitosis

Accurate chromosome segregation into daughter cells is ensured during mitosis through the spindle assembly checkpoint (SAC). An unattached/improperly attached kinetochore during prometaphase is the signaling hub for SAC, that recruits SAC proteins and accelerate assembly of the effector complex called mitotic checkpoint complex (MCC). The spatial interaction of many of these SAC proteins that specifically happens at kinetochore is vital for the catalysis of MCC assembly (Faesen et al., 2017; Piano et al., 2021). Thus, the SAC strength is proportional to the number of signaling kinetochores. The continuous disassembly of MCC takes place along with the assembly to ensure steady recruitment of O-MAD2, BUBR1-BUB3 and CDC20 to SAC signaling kinetochores (Uzunova et al., 2012; Kim et al., 2018). One of the major pathways for MCC disassembly is mediated by the AAA+ ATPase TRIP13 along with its cofactor p31^{COMET}. It remains unanswered whether the TRIP13 mediated MCC disassembly is regulated during the SAC to control the steady state MCC levels. In this study, I show that mitotic kinase CDK1-CyclinB phosphorylate p31^{COMET}, and these phosphorylation events reduce the binding efficiency of p31^{COMET} with TRIP13. I also report that MAD1:C-MAD2 is a TRIP13 pseudo-substrate and is able to increase the efficacy of the identified phosphorylation by CDK1 on p31^{COMET}. I propose a physiological mechanism by which CDK1 phosphorylation of p31^{COMET} prevents TRIP13 interaction with MAD1:C-MAD2:p31^{COMET} pseudo-substrate, making TRIP13 available for other C-MAD2-containing substrates in the cytosol, rather than at kinetochores. Our study also reports that MCC assembly catalysts favor O-MAD2 recruitment to unattached kinetochore by displacing p31^{COMET} bound to MAD1:C-MAD2 complex. Altogether, our study provides mechanistic insights into how MCC disassembly is regulated in harmony with the number of SAC signaling kinetochores.

4.2.1 CDK1 phosphorylation of p31^{COMET} reduce TRIP13 binding

The initial goal of our study was to understand whether TRIP13 mediated MCC disassembly is regulated via post-translational modifications. Previous studies report

phosphorylation of Ser102 residue of p31^{COMET} from mitotic lysates (Date et al., 2014). A more recent study reported that PLK1 phosphorylates p31^{COMET} Ser102 residue *in vitro* and this phosphorylation results in the suppression of TRIP13 activity to disassemble MCC (Kaisari et al., 2019). A mechanistic explanation for the decreased TRIP13 activity on substrates, however, has not been provided. In our study, we identified that CDK1 phosphorylates two residues of p31^{COMET}, Ser102 and Ser160, and together these modifications weaken the interaction of TRIP13 with p31^{COMET}. In accordance with the previous literature, I showed that recombinant TRIP13-p31^{COMET} disassembles C-MAD2:CDC20 complex (Eytan et al., 2014; Ye et al., 2015). Nonetheless, the phosphorylation of p31^{COMET} by CDK1 reduced the rate of TRIP13 mediated substrate disassembly. We attribute the reduced p31^{COMET}-TRIP13 interaction after CDK1 phosphorylation of p31^{COMET} as the prime reason for TRIP13 activity suppression on substrates *in vitro*. We disproved the previous study claiming that phosphorylation of p31^{COMET} by mitotic kinases weaken p31^{COMET}-MAD2 interaction (Date et al., 2014). Also, in contrast to the previous study reporting PLK1 phosphorylation of p31^{COMET} S102 residue (Kaisari et al., 2019), we demonstrate that CDK1-CyclinB phosphorylates this residue *in vitro*. p31^{COMET} S102 residue is enclosed in a classic CDK1 phosphorylation consensus motif (S/TP) and p31^{COMET} lacks a motif for polo box domain (PBD) binding. Thus, our data suggests a mechanism by which CDK1, the master regulator of mitosis, modulates TRIP13 activity at least *in vitro*. The physiological relevance of this proposed CDK1 mediated regulation of p31^{COMET}-TRIP13 interaction will be discussed in next section.

4.2.2 Physiological relevance of CDK1 mediated regulation of p31^{COMET}- TRIP13 interaction

To understand why modulating p31^{COMET}-TRIP13 interaction is important for proper SAC signaling in cells, a few observations need to be put into context. First, CDK1-CyclinB binds to MAD1:C-MAD2 during mitosis (Alfonso-Perez et al., 2019, Allan et al., 2020), and this interaction helps to enhance the CDK1 phosphorylation of p31^{COMET}. Second, we identified that MAD1:C-MAD2 complex as a pseudo-substrate of TRIP13. MAD1:C-MAD2 is able to bind p31^{COMET}- TRIP13 enzyme complex and stimulate the ATPase activity of TRIP13 *in vitro*, similarly to other known substrates. However, unlike CDC20:C-MAD2 substrates, TRIP13 is incapable to disassemble the MAD1:C-MAD2 complex by remodeling MAD2 bound to MAD1. Therefore, TRIP13

interaction with MAD1:C-MAD2:p31^{COMET} complex during mitosis would be detrimental in cells, due to wasteful energy consumption and limiting TRIP13 availability for C-MAD2 substrates in the cytosol, and, therefore, it should be prevented. In this context, we propose that CDK1 phosphorylation of p31^{COMET} occurs when both proteins are bound to MAD1:C-MAD2 at kinetochores and it prevents the recruitment of TRIP13 to this complex (Figure 4-1). Why CDK1, a ubiquitous mitotic kinase, actively phosphorylates p31^{COMET} only when it is bound to MAD1:C-MAD2 needs to be further investigated. We speculate that the p31^{COMET} binding to MAD1:C-MAD2 might result in a topological rearrangement of p31^{COMET}, which would make Ser102 and Ser160 residues (or any one of them) more accessible to CDK1 phosphorylation. Also, in a cellular perspective, the CDK1 localized onto MAD1:C-MAD2 and the removal of phosphatases that occurs at SAC signaling kinetochores (Saurin, 2018) would create a distinct spatial hub where CDK1 activity on p31^{COMET} might be high and not counteracted.
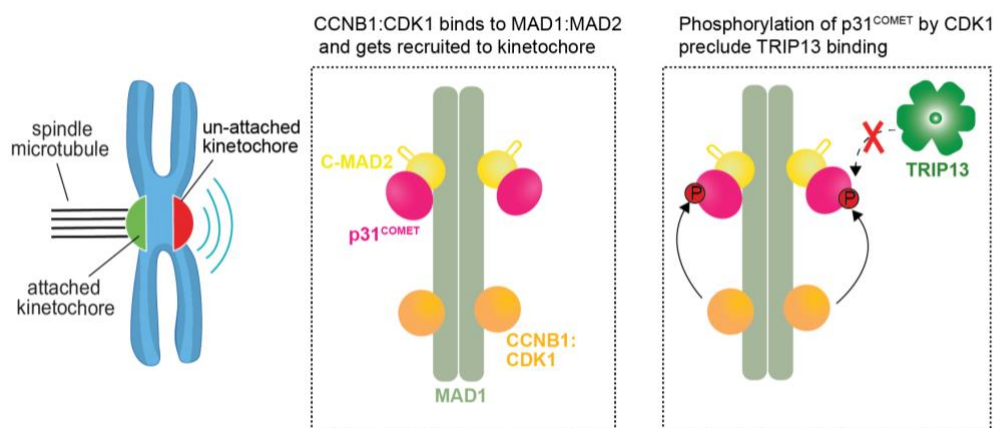
Figure 4-1 Model for the CDK1 mediated regulation of TRIP13 binding to MAD1:C-MAD2
The CDK1 catalytic activity at kinetochores prevents TRIP13 binding to MAD1:C-MAD2. CCNB1= CyclinB1

CDK1-CyclinB binding to MAD1 is required for the proper release of MAD1:C-MAD2: p31^{COMET} complex from the TPR at the nuclear pores, so that it can be recruited to kinetochores before nuclear envelope breakdown (Jackman et al., 2020). We don't know yet, however, whether CDK1-CyclinB remains bound to MAD1:C-MAD2 complex after its removal from kinetochore upon proper microtubule attachment. When at kinetochores, the CDK1 activity ensures that TRIP13 binding to MAD1:C-MAD2 is prevented. Thus, TRIP13 is more available for acting on the MCC and control its disassembly. The proposed regulation mechanism imposes that TRIP13 mediated

MCC disassembly at cytosol is modulated in a co-dependent manner with the number of unattached kinetochores. Cell biology studies are necessary to further prove the observations from our *in vitro* experiments. Functional studies are currently ongoing to analyze CDK1 phosphorylation of p31[COMET] and its regulation of TRIP13 interaction with MAD1:C-MAD2 complex in cells.

4.2.3 MCC assembly catalysts promote O-MAD2 recruitment to kinetochores by displacing p31[COMET]

A recent study from our laboratory demonstrated that MAD2 and CDC20 must bind concomitantly to the *catalyst* - MAD1:C-MAD2 and BUB1:BUB3 phosphorylated by MPS1 – to allow the acceleration of MCC assembly (Piano et al., 2021). In cells, kinetochores act as the spatial hub where all these proteins are recruited and can specifically interact with each other. An accompanying study from the Desai research group reported an orthogonal analysis of SAC signaling in *C. elegans* (Lara-Gonzalez et al., 2021) whose conclusions were entirely consistent with our *in vitro* analysis. A puzzling observation from the Lara-Gonzalez et al. study is that mutations that impair the interaction of the *catalysts* also failed to recruit O-MAD2 to kinetochores. p31[COMET] and O-MAD2 compete for C-MAD2 dimerization and the former has a higher binding affinity for this interaction than the latter. However, our *in vitro* experiments
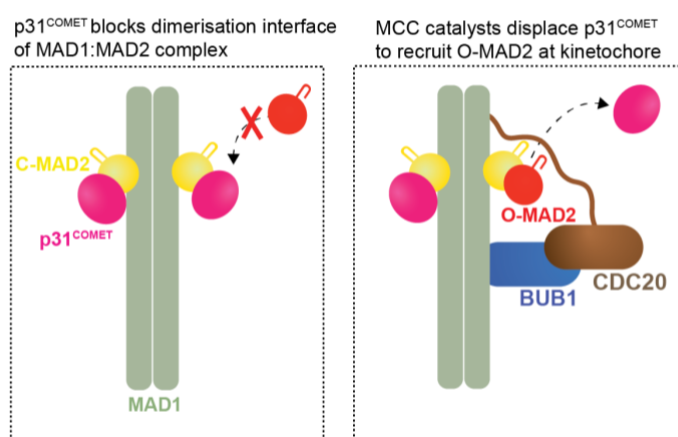
Figure 4-2 Model for MCC catalysts mediated O-MAD2 recruitment at kinetochore. The MAD1:C-MAD2 complex during mitosis is bound to p31[COMET] through the dimerization interface of C-MAD2 and thus prevent O-MAD2 dimerization, which is essential for the catalytic acceleration of MCC assembly. The interaction of CDC20 and BUB1 with MAD1 at kinetochores, promote O-MAD2 recruitment by displacing p31[COMET]. This ensure free p31[COMET] availability in the cytosol.

demonstrated that the interaction between MCC catalysts favors O-MAD2 over p31^{COMET} for dimerization with MAD1:C-MAD2 complex (Figure 3-19). We propose that the MAD1:C-MAD2 interaction with CDC20 and BUB1:BUB3, taking place at SAC signaling kinetochores, cooperatively increases the affinity of O-MAD2 for MAD1:C-MAD2 binding. Additional *in vitro* experiments with mutants of BUB1, CDC20 and MAD1 (described in Piano et al., 2021) are in progress to delineate the specific interactions vital for this mechanism. Our model predicts proper catalysis of C-MAD2:CDC20 assembly at kinetochores and simultaneously predicts the availability of p31^{COMET} for TRIP13 mediated MCC disassembly in the cytosol (Figure 4-2).

4.2.4 MCC disassembly is regulated in unison with the number of SAC signaling kinetochores

The components of the catalytic machinery converting O-MAD2 to C-MAD2 and assembling the MCC are tightly spatially and temporally regulated. However, little is understood about the regulation of TRIP13:p31^{COMET} on the MCC disassembly. During mitosis, the simultaneous MCC assembly and disassembly reactions must be fine-tuned to *a)* maintain a sufficient O-MAD2 pool to sustain SAC signaling; *b)* control steady state MCC levels to ensure SAC robustness. I try to conceptualize this in a hypothetical plot showing MCC concentration at different stages of cell cycle (Figure 4-3A). During mitosis, the MCC assembly is proportional to the number of unattached kinetochores signaling for SAC. Remarkably, a single SAC signaling kinetochore is able to catalyze the production of enough MCC to maintain the SAC. The strength of the SAC increases with the number of unattached kinetochores according to previous reports (Dick and Gelrich, 2013; note that in our plot mitotic duration is shown the same for all conditions to simplify). Based on our findings, also the MCC disassembly increases proportional to the number of unattached kinetochores. Accordingly, we propose that the actual MCC concentration does not increase proportionally to the increasing number of signaling kinetochores, but rather that the cell SAC machinery maintains the steady-state MCC levels within a certain dynamic range (indicated by the green region), in such a way that the amount of MCC is sufficient to inhibit the APC/C and stop mitotic progression. This mechanism would ensure *a)* quick SAC silencing upon microtubule attachment as previously reported (Collins et al., 2014; Henze et al., 2017), by preventing over-accumulation of MCC, and *b)* robustness of

the SAC mechanism, because both assembly and disassembly of the effector complex is augmented by the same entity, the unattached kinetochores (Figure 4-3B).
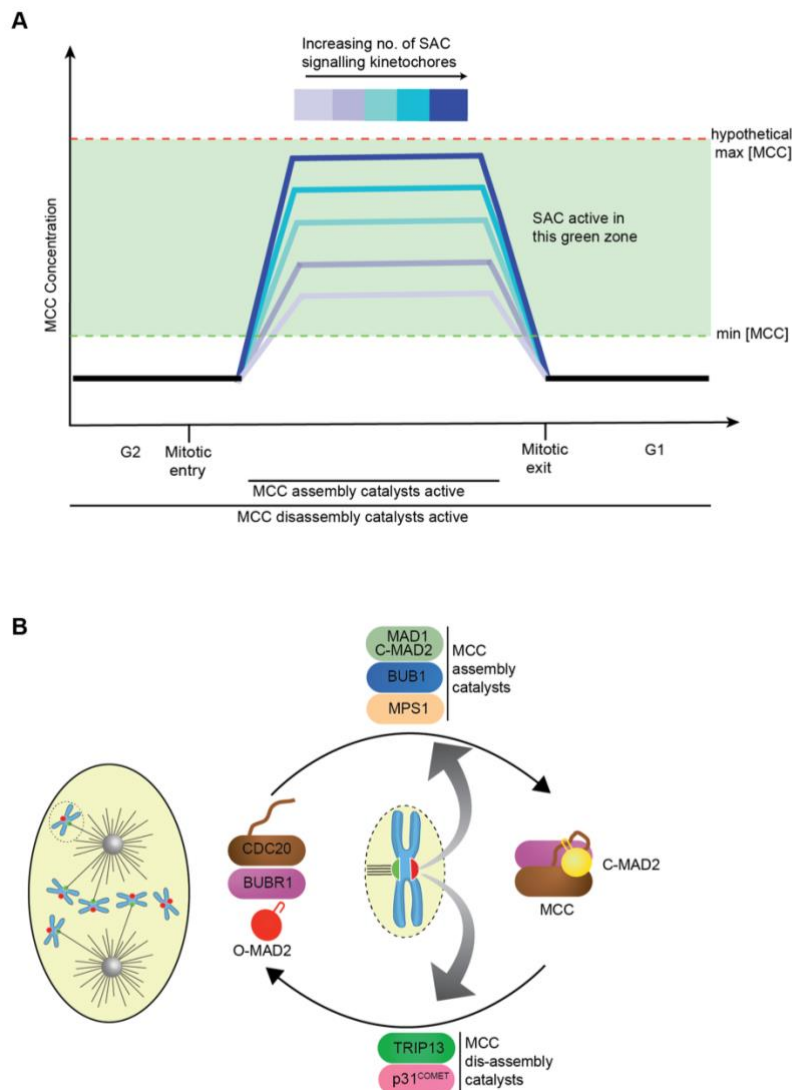
Figure 4-3 Unattached kinetochores during mitosis accelerate MCC assembly and disassembly
A) Hypothetical plot showing the amount of MCC at different stages of the cell cycle. **B)** Unattached kinetochores favor i) MCC assembly by acting as the structural platform for the interaction between assembly catalysts ii) MCC disassembly by promoting the accumulation of active TRIP13: p31[COMET]

To summarize, our *in vitro* experiments shed light on a previously unrecognized mechanism by which the SAC signaling kinetochores can control simultaneously the MCC assembly and disassembly and effectively ensure the correct segregation of chromosomes.

5. Summary

During mitosis, the accurate segregation of chromosomes to daughter cells is ensured by the Spindle Assembly Checkpoint (SAC). Incorrect attachments of spindle microtubules with kinetochores triggers the SAC signaling and results in the assembly of an effector complex called Mitotic Checkpoint Complex (MCC). Recent studies have identified that the SAC signaling kinetochores provide a catalytic platform for the MCC assembly. To ensure the timely activation and inactivation of SAC signaling, MCC disassembly occurs in parallel with its assembly. TRIP13, a AAA$^+$ ATPase along with its cofactor p31^{COMET} catalyzes the MCC disassembly mainly in cells. My PhD work aim to provide some mechanistic insights into the regulation of both MCC assembly and disassembly processes.

During this work, I established electroporation (EP) as a method to deliver recombinant proteins into mammalian cells for the purpose of functional studies using kinetochore and SAC proteins. Our data provides a better comprehension of the spatial distribution of MCC in SAC signaling cells. MCC disassembly was characterized *in vitro* using biochemical assays. I demonstrated that CDK1 phosphorylation of p31^{COMET} impaired its interaction with TRIP13. Additionally, this study showed for the first time that MAD1:C-MAD2 complex is a TRIP13 pseudo-substrate and the interaction between this substrate-enzyme pair is negatively regulated by the CDK1 phosphorylation of p31^{COMET}. *In vitro* experiments showed that the previously identified MCC assembly catalysts displace p31^{COMET} from MAD1:C-MAD2 complex in order to favor O-MAD2 dimerization. In a cellular context, this would help to increase the p31^{COMET} accumulation in cytosol for MCC disassembly during checkpoint. Collectively, my PhD work demonstrates that MCC disassembly is regulated in unison with the number of SAC signaling kinetochores. This proposed mechanism of regulation would ensure that SAC signaling is both adaptive and robust.

6. Zusammenfassung

Während der Mitose wird die korrekte Segregation der Chromosomen auf die Tochterzellen durch den Spindle Assembly Checkpoint (SAC) sichergestellt. Falsche Bindungen der Spindel-Mikrotubuli an Kinetochore lösen die SAC-Signalisierung aus und führen zur Bildung eines Effektor-Komplexes, der Mitotic Checkpoint Complex (MCC) genannt wird. Neue Studien haben gezeigt, dass Kinetochore, die den SAC signalisieren, eine katalytische Plattform für die MCC-Assemblierung darstellen. Um die rechtzeitige Aktivierung und Inaktivierung der SAC-Signalisierung zu gewährleisten, erfolgt der Abbau des MCC parallel zu seinem Aufbau. TRIP13, eine AAA+ ATPase katalysiert zusammen mit seinem Kofaktor p31^{COMET} hauptsächlich den MCC-Abbau in Zellen. Das Ziel dieser Arbeit ist es einige mechanistische Einblicke in die Regulation des MCC-Aufbaus als auch des MCC-Abbaus zu gewinnen.

Während dieser Arbeit etablierte ich die Elektroporation (EP) als Methode um rekombinante Proteine in Säugetierzellen einzubringen. Dies ermöglichte die Durchführung funktioneller Studien mit Kinetochore und SAC-Proteinen in vivo. Unsere Daten liefern ein besseres Verständnis für die räumliche Verteilung des MCC in SAC-signalisierenden Zellen. Der Abbau des MCC wurde in vitro mit biochemischen Assays charakterisiert. Ich konnte zeigen, dass die CDK1-Phosphorylierung von p31^{COMET} die Interaktion mit TRIP13 beeinträchtigt. Außerdem erwies diese Studie zum ersten Mal, dass der MAD1:C-MAD2-Komplex ein TRIP13-Pseudosubstrat ist und die Interaktion zwischen diesem Substrat-Enzym-Paar durch die CDK1-Phosphorylierung von p31^{COMET} negativ reguliert wird. In vitro-Experimente zeigten, dass p31^{COMET} durch die zuvor identifizierten MCC-Assembly-Katalysatoren aus dem MAD1:C-MAD2-Komplex verdrängt wird. Dies wiederum begünstigt die O-MAD2-Dimerisierung. In einem zellulären Kontext würde dies dazu beitragen, die p31^{COMET}-Akkumulation im Zytosol für den MCC-Abbau während des Checkpoints zu steigern. Insgesamt zeigt meine Doktorarbeit, dass der MCC-Abbau im Einklang mit der Anzahl der SAC-signalisierenden Kinetochore reguliert wird. Dieser Mechanismus der Regulierung würde sicherstellen, dass die SAC-Signalisierung sowohl adaptiv als auch robust ist.

7. Bibliography

Abrieu, A. *et al.* Mps1 Is a Kinetochore-Associated Kinase Essential for the Vertebrate Mitotic Checkpoint. *Cell* 106, 83–93 (2001).

Alfieri, C., Chang, L. & Barford, D. Mechanism for remodelling of the cell cycle checkpoint protein MAD2 by the ATPase TRIP13. *Nature* 559, 274 (2018).

Alfieri, C. *et al.* Molecular basis of APC/C regulation by the spindle assembly checkpoint. *Nature* 536, 431–436 (2016).

Alfonso-Pérez, T., Hayward, D., Holder, J., Gruneberg, U. & Barr, F. A. MAD1-dependent recruitment of CDK1-CCNB1 to kinetochores promotes spindle checkpoint signaling. *Journal of Cell Biology* 218, 1108–1117 (2019).

Allan, L. A. *et al.* CyclinB1 scaffolds MAD1 at the kinetochore corona to activate the mitotic checkpoint. *EMBO J* 39, (2020).

Aloy, P. *et al.* Structure-based assembly of protein complexes in yeast. *Science* 303, 2026–2029 (2004).

Alushin, G. M. *et al.* Multi-modal microtubule binding by the Ndc80 kinetochore complex. *Nat Struct Mol Biol* 19, 1161–1167 (2012).

Alushin, G. M. *et al.* The Ndc80 kinetochore complex forms oligomeric arrays along microtubules. *Nature* 467, 805–810 (2010).

Aravamudhan, P., Goldfarb, A. A. & Joglekar, A. P. The kinetochore encodes a mechanical switch to disrupt spindle assembly checkpoint signalling. *Nature Cell Biology* 17, 868–879 (2015).

Babst, M., Wendland, B., Estepa, E. J. & Emr, S. D. The Vps4p AAA ATPase regulates membrane association of a Vps protein complex required for normal endosome function. *EMBO J* 17, 2982–2993 (1998).

Bajaj, R., Bollen, M., Peti, W. & Page, R. KNL1 Binding to PP1 and Microtubules Is Mutually Exclusive. *Structure* 26, 1327-1336.e4 (2018).

Bancroft, J., Auckland, P., Samora, C. P. & McAinsh, A. D. Chromosome congression is promoted by CENP-Q- and CENP-E-dependent pathways. *J Cell Sci* 128, 171–184 (2015).

Basilico, F. *et al.* The pseudo GTPase CENP-M drives human kinetochore assembly. *eLife* 3, e02978 (2014).

Bieniossek, C., Imasaki, T., Takagi, Y. & Berger, I. MultiBac: expanding the research toolbox for multiprotein complexes. *Trends Biochem Sci* 37, 49–57 (2012).

Black, B. E., Brock, M. A., Bédard, S., Woods, V. L. & Cleveland, D. W. An epigenetic mark generated by the incorporation of CENP-A into centromeric nucleosomes.

PNAS 104, 5008–5013 (2007).

Broad, A. J., DeLuca, K. F. & DeLuca, J. G. Aurora B kinase is recruited to multiple discrete kinetochore and centromere regions in human cells. *Journal of Cell Biology* 219, (2020).

Buffin, E., Lefebvre, C., Huang, J., Gagou, M. E. & Karess, R. E. Recruitment of Mad2 to the Kinetochore Requires the Rod/Zw10 Complex. *Current Biology* 15, 856–861 (2005).

Burton, J. L. & Solomon, M. J. Mad3p, a pseudosubstrate inhibitor of APCCdc20 in the spindle assembly checkpoint. *Genes Dev* 21, 655–667 (2007).

Caldas, G. V. *et al.* The RZZ complex requires the N-terminus of KNL1 to mediate optimal Mad1 kinetochore localization in human cells. *Open Biol* 5, (2015).

Carmena, M., Wheelock, M., Funabiki, H. & Earnshaw, W. C. The chromosomal passenger complex (CPC): from easy rider to the godfather of mitosis. *Nature Reviews Molecular Cell Biology* 13, 789–803 (2012).

Carroll, C. W., Milks, K. J. & Straight, A. F. Dual recognition of CENP-A nucleosomes is required for centromere assembly. *Journal of Cell Biology* 189, 1143–1155 (2010).

Carroll, C. W., Silva, M. C. C., Godek, K. M., Jansen, L. E. T. & Straight, A. F. Centromere assembly requires the direct recognition of CENP-A nucleosomes by CENP-N. *Nature Cell Biology* 11, 896–902 (2009).

Chakrabarti, R., Wylie, D. E. & Schuster, S. M. Transfer of monoclonal antibodies into mammalian cells by electroporation. *J Biol Chem* 264, 15494–15500 (1989).

Chan, Y. W. *et al.* Mitotic control of kinetochore-associated dynein and spindle orientation by human Spindly. *J Cell Biol* 185, 859–874 (2009).

Chao, W. C. H., Kulkarni, K., Zhang, Z., Kong, E. H. & Barford, D. Structure of the mitotic checkpoint complex. *Nature* 484, 208–213 (2012).

Cheerambathur, D. K., Gassmann, R., Cook, B., Oegema, K. & Desai, A. Crosstalk between microtubule attachment complexes ensures accurate chromosome segregation. *Science* 342, 1239–1242 (2013).

Cheeseman, I. M. & Desai, A. Molecular architecture of the kinetochore-microtubule interface. *Nat Rev Mol Cell Biol* 9, 33–46 (2008).

Ciferri, C. *et al.* Architecture of the human ndc80-hec1 complex, a critical constituent of the outer kinetochore. *J Biol Chem* 280, 29088–29095 (2005).

Clift, D. *et al.* A Method for the Acute and Rapid Degradation of Endogenous Proteins. *Cell* 171, 1692-1706.e18 (2017).

Collin, P., Nashchekina, O., Walker, R. & Pines, J. The spindle assembly checkpoint works like a rheostat rather than a toggle switch. *Nat Cell Biol* 15, 1378–1385

(2013).

Collins, K. A., Castillo, A. R., Tatsutani, S. Y. & Biggins, S. De novo kinetochore assembly requires the centromeric histone H3 variant. *Mol Biol Cell* 16, 5649–5660 (2005).

Coudreuse, D. & Nurse, P. Driving the cell cycle with a minimal CDK control network. *Nature* 468, 1074–1079 (2010).

Date, D. A., Burrows, A. C. & Summers, M. K. Phosphorylation Regulates the p31Comet-Mitotic Arrest-deficient 2 (Mad2) Interaction to Promote Spindle Assembly Checkpoint (SAC) Activity. *J Biol Chem* 289, 11367–11373 (2014).

Davenport, J., Harris, L. D. & Goorha, R. Spindle checkpoint function requires Mad2-dependent Cdc20 binding to the Mad3 homology domain of BubR1. *Exp Cell Res* 312, 1831–1842 (2006).

De Antoni, A. *et al.* The Mad1/Mad2 Complex as a Template for Mad2 Activation in the Spindle Assembly Checkpoint. *Current Biology* 15, 214–225 (2005).

DeLaBarre, B. & Brunger, A. T. Nucleotide dependent motion and mechanism of action of p97/VCP. *J Mol Biol* 347, 437–452 (2005).

DeLuca, J. G. *et al.* Kinetochore Microtubule Dynamics and Attachment Stability Are Regulated by Hec1. *Cell* 127, 969–982 (2006).

Di Fiore, B. *et al.* The ABBA motif binds APC/C activators and is shared by APC/C substrates and regulators. *Dev Cell* 32, 358–372 (2015).

Di Fiore, B., Wurzenberger, C., Davey, N. E. & Pines, J. The Mitotic Checkpoint Complex Requires an Evolutionary Conserved Cassette to Bind and Inhibit Active APC/C. *Molecular Cell* 64, 1144–1153 (2016).

Dick, A. E. & Gerlich, D. W. Kinetic framework of spindle assembly checkpoint signaling. *Nat Cell Biol* 15, 1370–1377 (2013).

Dou, Z. *et al.* Dynamic localization of Mps1 kinase to kinetochores is essential for accurate spindle microtubule attachment. *Proc Natl Acad Sci U S A* 112, E4546-4555 (2015).

Earnshaw, W. C. & Rothfield, N. Identification of a family of human centromere proteins using autoimmune sera from patients with scleroderma. *Chromosoma* 91, 313–321 (1985).

Espert, A. *et al.* PP2A-B56 opposes Mps1 phosphorylation of Knl1 and thereby promotes spindle assembly checkpoint silencing. *J Cell Biol* 206, 833–842 (2014).

Espeut, J., Cheerambathur, D. K., Krenning, L., Oegema, K. & Desai, A. Microtubule binding by KNL-1 contributes to spindle checkpoint silencing at the kinetochore. *J Cell Biol* 196, 469–482 (2012).

Etemad, B., Kuijt, T. E. F. & Kops, G. J. P. L. Kinetochore–microtubule attachment is sufficient to satisfy the human spindle assembly checkpoint. *Nature*

Communications 6, 8987 (2015).

Evans, T., Rosenthal, E. T., Youngblom, J., Distel, D. & Hunt, T. Cyclin: a protein specified by maternal mRNA in sea urchin eggs that is destroyed at each cleavage division. *Cell* 33, 389–396 (1983).

Eytan, E. *et al.* Disassembly of mitotic checkpoint complexes by the joint action of the AAA-ATPase TRIP13 and p31comet. *PNAS* 111, 12019–12024 (2014).

Fachinetti, D. *et al.* A two-step mechanism for epigenetic specification of centromere identity and function. *Nat Cell Biol* 15, 1056–1066 (2013).
\
Faesen, A. C. *et al.* Basis of catalytic assembly of the mitotic checkpoint complex. *Nature* 542, 498–502 (2017).

Falk, S. J. *et al.* Chromosomes. CENP-C reshapes and stabilizes CENP-A nucleosomes at the centromere. *Science* 348, 699–703 (2015).

Fava, L. L., Kaulich, M., Nigg, E. A. & Santamaria, A. Probing the in vivo function of Mad1:C-Mad2 in the spindle assembly checkpoint. *EMBO J* 30, 3322–3336 (2011).

Foley, E. A. & Kapoor, T. M. Microtubule attachment and spindle assembly checkpoint signalling at the kinetochore. *Nat Rev Mol Cell Biol* 14, 25–37 (2013).

Foltz, D. R. *et al.* The human CENP-A centromeric nucleosome-associated complex. *Nature Cell Biology* 8, 458–469 (2006).

Furuhata, Y. *et al.* A method using electroporation for the protein delivery of Cre recombinase into cultured Arabidopsis cells with an intact cell wall. *Sci Rep* 9, 2163 (2019).

Gama, J. B. *et al.* Molecular mechanism of dynein recruitment to kinetochores by the Rod-Zw10-Zwilch complex and Spindly. *J Cell Biol* 216, 943–960 (2017).

Gassmann, R. *et al.* A new mechanism controlling kinetochore-microtubule interactions revealed by comparison of two dynein-targeting components: SPDL-1 and the Rod/Zwilch/Zw10 complex. *Genes Dev* 22, 2385–2399 (2008)
.
Gassmann, R. *et al.* Removal of Spindly from microtubule-attached kinetochores controls spindle checkpoint silencing in human cells. *Genes Dev.* 24, 957–971 (2010).

Gibson, D. G. *et al.* Enzymatic assembly of DNA molecules up to several hundred kilobases. *Nat Methods* 6, 343–345 (2009).

Guo, L. Y. *et al.* Centromeres are maintained by fastening CENP-A to DNA and directing an arginine anchor-dependent nucleosome transition. *Nat Commun* 8, 15775 (2017).

Hackney, D. D. & Jiang, W. Assays for kinesin microtubule-stimulated ATPase activity. *Methods Mol Biol* 164, 65–71 (2001).

Hanson, P. I. & Whiteheart, S. W. AAA+ proteins: have engine, will work. *Nat Rev Mol Cell Biol* 6, 519–529 (2005).

Hänzelmann, P. & Schindelin, H. Structural Basis of ATP Hydrolysis and Intersubunit Signaling in the AAA+ ATPase p97. *Structure* 24, 127–139 (2016).

Hara, M., Özkan, E., Sun, H., Yu, H. & Luo, X. Structure of an intermediate conformer of the spindle checkpoint protein Mad2. *Proc Natl Acad Sci USA* 112, 11252–11257 (2015).

Hartwell, L. H. Saccharomyces cerevisiae cell cycle. *Bacteriol Rev* 38, 164–198 (1974).

Hashimoto, M. & Takemoto, T. Electroporation enables the efficient mRNA delivery into the mouse zygotes and facilitates CRISPR/Cas9-based genome editing. *Sci Rep* 5, 11315 (2015).

Heun, P. *et al.* Mislocalization of the Drosophila centromere-specific histone CID promotes formation of functional ectopic kinetochores. *Dev Cell* 10, 303–315 (2006).

Hiruma, Y. *et al.* Competition between MPS1 and microtubules at kinetochores regulates spindle checkpoint signaling. *Science* 348, 1264–1267 (2015).

Holland, A. J. *et al.* Preventing farnesylation of the dynein adaptor Spindly contributes to the mitotic defects caused by farnesyltransferase inhibitors. *Mol Biol Cell* 26, 1845–1856 (2015).

Honda, R. *et al.* The structure of Cyclin E1/CDK2: implications for CDK2 activation and CDK2-independent roles. *EMBO J* 24, 452–463 (2005).

Hori, T. *et al.* CCAN Makes Multiple Contacts with Centromeric DNA to Provide Distinct Pathways to the Outer Kinetochore. *Cell* 135, 1039–1052 (2008).

Hori, T., Okada, M., Maenaka, K. & Fukagawa, T. CENP-O Class Proteins Form a Stable Complex and Are Required for Proper Kinetochore Function. *MBoC* 19, 843–854 (2007).

Howell, B. J. *et al.* Cytoplasmic dynein/dynactin drives kinetochore protein transport to the spindle poles and has a role in mitotic spindle checkpoint inactivation. *J Cell Biol* 155, 1159–1172 (2001).

Huis in 't Veld, P. J. *et al.* Molecular basis of outer kinetochore assembly on CENP-T. *eLife* 5,.

Ingebritsen, T. S. & Cohen, P. The protein phosphatases involved in cellular regulation. 1. Classification and substrate specificities. *Eur J Biochem* 132, 255–261 (1983).

Inomata, K. *et al.* High-resolution multi-dimensional NMR spectroscopy of proteins in human cells. *Nature* 458, 106–109 (2009).

Izuta, H. *et al.* Comprehensive analysis of the ICEN (Interphase Centromere Complex) components enriched in the CENP-A chromatin of human cells. *Genes to Cells*

11, 673–684 (2006).

Jackman, M. *et al.* CyclinB1-Cdk1 facilitates MAD1 release from the nuclear pore to ensure a robust spindle checkpoint. *J Cell Biol* 219, (2020).

Jeffrey, P. D. *et al.* Mechanism of CDK activation revealed by the structure of a cyclinA-CDK2 complex. *Nature* 376, 313–320 (1995).

Jelluma, N., Dansen, T. B., Sliedrecht, T., Kwiatkowski, N. P. & Kops, G. J. P. L. Release of Mps1 from kinetochores is crucial for timely anaphase onset. *Journal of Cell Biology* 191, 281–290 (2010).

Ji, Z., Gao, H. & Yu, H. CELL DIVISION CYCLE. Kinetochore attachment sensed by competitive Mps1 and microtubule binding to Ndc80C. *Science* 348, 1260–1264 (2015).

Joglekar, A. P., Bloom, K. & Salmon, E. D. In vivo protein architecture of the eukaryotic kinetochore with nanometer scale accuracy. *Curr Biol* 19, 694–699 (2009).

Joshi, N., Barot, A., Jamison, C. & Börner, G. V. Pch2 Links Chromosome Axis Remodeling at Future Crossover Sites and Crossover Distribution during Yeast Meiosis. *PLoS Genet* 5, (2009).

Kaisari, S. *et al.* Role of Polo-like kinase 1 in the regulation of the action of p31comet in the disassembly of mitotic checkpoint complexes. *PNAS* 116, 11725–11730 (2019).

Kang, Y. H. *et al.* Mammalian polo-like kinase 1-dependent regulation of the PBIP1-CENP-Q complex at kinetochores. *J Biol Chem* 286, 19744–19757 (2011).

Kang, Y. H. *et al.* Self-regulated Plk1 recruitment to kinetochores by the Plk1-PBIP1 interaction is critical for proper chromosome segregation. *Mol Cell* 24, 409–422 (2006).

Karess, R. Rod–Zw10–Zwilch: a key player in the spindle checkpoint. *Trends in Cell Biology* 15, 386–392 (2005).

Kawashima, S. A., Yamagishi, Y., Honda, T., Ishiguro, K. & Watanabe, Y. Phosphorylation of H2A by Bub1 prevents chromosomal instability through localizing shugoshin. *Science* 327, 172–177 (2010).

Kiianitsa, K., Solinger, J. A. & Heyer, W.-D. Rad54 protein exerts diverse modes of ATPase activity on duplex DNA partially and fully covered with Rad51 protein. *J Biol Chem* 277, 46205–46215 (2002).

Kim, D. H. *et al.* TRIP13 and APC15 drive mitotic exit by turnover of interphase- and unattached kinetochore-produced MCC. *Nature Communications* 9, 4354 (2018).

Kim, S., Kim, D., Cho, S. W., Kim, J. & Kim, J.-S. Highly efficient RNA-guided genome editing in human cells via delivery of purified Cas9 ribonucleoproteins. *Genome Res* 24, 1012–1019 (2014).

Kim, S., Sun, H., Tomchick, D. R., Yu, H. & Luo, X. Structure of human Mad1 C-terminal domain reveals its involvement in kinetochore targeting. *PNAS* 109, 6549–6554 (2012).

Kim, T. K. & Eberwine, J. H. Mammalian cell transfection: the present and the future. *Anal Bioanal Chem* 397, 3173–3178 (2010).

Kiyomitsu, T., Obuse, C. & Yanagida, M. Human Blinkin/AF15q14 is required for chromosome alignment and the mitotic checkpoint through direct interaction with Bub1 and BubR1. *Dev Cell* 13, 663–676 (2007).

Klare, K. *et al.* CENP-C is a blueprint for constitutive centromere–associated network assembly within human kinetochores. *Journal of Cell Biology* 210, 11–22 (2015).

Koch, L. B. *et al.* Autophosphorylation is sufficient to release Mps1 kinase from native kinetochores. *PNAS* 116, 17355–17360 (2019).

Kops, G. J. P. L. *et al.* ZW10 links mitotic checkpoint signaling to the structural kinetochore. *Journal of Cell Biology* 169, 49–60 (2005).

Kramer, E. R., Gieffers, C., Hölzl, G., Hengstschläger, M. & Peters, J. M. Activation of the human anaphase-promoting complex by proteins of the CDC20/Fizzy family. *Curr Biol* 8, 1207–1210 (1998).

Krenn, V. & Musacchio, A. The Aurora B Kinase in Chromosome Bi-Orientation and Spindle Checkpoint Signaling. *Front Oncol* 5, (2015).

Kuijt, T. E. F., Omerzu, M., Saurin, A. T. & Kops, G. J. P. L. Conditional targeting of MAD1 to kinetochores is sufficient to reactivate the spindle assembly checkpoint in metaphase. *Chromosoma* 123, 471–480 (2014).

Kwon, M.-S., Hori, T., Okada, M. & Fukagawa, T. CENP-C Is Involved in Chromosome Segregation, Mitotic Checkpoint Function, and Kinetochore Assembly. *Mol Biol Cell* 18, 2155–2168 (2007).

Lambert, H., Pankov, R., Gauthier, J. & Hancock, R. Electroporation-mediated uptake of proteins into mammalian cells. *Biochem Cell Biol* 68, 729–734 (1990).

Lampson, M. A. & Cheeseman, I. M. Sensing centromere tension: Aurora B and the regulation of kinetochore function. *Trends Cell Biol* 21, 133–140 (2011).

Lan, W. & Cleveland, D. W. A chemical tool box defines mitotic and interphase roles for Mps1 kinase. *Journal of Cell Biology* 190, 21–24 (2010).

Lara-Gonzalez, P., Kim, T., Oegema, K., Corbett, K. & Desai, A. A tripartite mechanism catalyzes Mad2-Cdc20 assembly at unattached kinetochores. *Science* 371, 64–67 (2021).

Larsen, N. A., Al-Bassam, J., Wei, R. R. & Harrison, S. C. Structural analysis of Bub3 interactions in the mitotic spindle checkpoint. *PNAS* 104, 1201–1206 (2007).

Levine, M. S. & Holland, A. J. The impact of mitotic errors on cell proliferation and

tumorigenesis. *Genes Dev* 32, 620–638 (2018).

Li, D., Morley, G., Whitaker, M. & Huang, J.-Y. Recruitment of Cdc20 to the Kinetochore Requires BubR1 but Not Mad2 in Drosophila melanogaster. *Molecular and Cellular Biology* 30, 3384–3395 (2010).

Li, X. & Nicklas, R. B. Mitotic forces control a cell-cycle checkpoint. *Nature* 373, 630–632 (1995).

Lin, S., Staahl, B. T., Alla, R. K. & Doudna, J. A. Enhanced homology-directed human genome engineering by controlled timing of CRISPR/Cas9 delivery. *Elife* 3, e04766 (2014).

Lischetti, T. & Nilsson, J. Regulation of mitotic progression by the spindle assembly checkpoint. *Mol Cell Oncol* 2, (2015).

Liu, S.-T., Rattner, J. B., Jablonski, S. A. & Yen, T. J. Mapping the assembly pathways that specify formation of the trilaminar kinetochore plates in human cells. *J Cell Biol* 175, 41–53 (2006).

Liu, S.-T. & Zhang, H. The mitotic checkpoint complex (MCC): looking back and forth after 15 years. *AIMS Mol Sci* 3, 597–634 (2016).

Logsdon, G. A. *et al.* Both tails and the centromere targeting domain of CENP-A are required for centromere establishment. *J Cell Biol* 208, 521–531 (2015).

London, N. & Biggins, S. Mad1 kinetochore recruitment by Mps1-mediated phosphorylation of Bub1 signals the spindle checkpoint. *Genes Dev.* 28, 140–152 (2014).

London, N., Ceto, S., Ranish, J. A. & Biggins, S. Phosphoregulation of Spc105 by Mps1 and PP1 Regulates Bub1 Localization to Kinetochores. *Current Biology* 22, 900–906 (2012).

Loog, M. & Morgan, D. O. Cyclin specificity in the phosphorylation of Cyclin-dependent kinase substrates. *Nature* 434, 104–108 (2005).

Luo, X., Tang, Z., Rizo, J. & Yu, H. The Mad2 Spindle Checkpoint Protein Undergoes Similar Major Conformational Changes Upon Binding to Either Mad1 or Cdc20. *Molecular Cell* 9, 59–71 (2002).

Ma, H. T. & Poon, R. Y. C. TRIP13 Functions in the Establishment of the Spindle Assembly Checkpoint by Replenishing O-MAD2. *Cell Rep* 22, 1439–1450 (2018).

Maldonado, M. & Kapoor, T. M. Constitutive Mad1 targeting to kinetochores uncouples checkpoint signalling from chromosome biorientation. *Nature Cell Biology* 13, 475–482 (2011).

Malik, H. S. & Henikoff, S. Major Evolutionary Transitions in Centromere Complexity. *Cell* 138, 1067–1082 (2009).

Mansfeld, J., Collin, P., Collins, M. O., Choudhary, J. S. & Pines, J. APC15 drives the

turnover of MCC-Cdc20 to make the Spindle Assembly Checkpoint responsive to kinetochore attachment. *Nat Cell Biol* 13, 1234–1243 (2011).

Maresca, T. J. & Salmon, E. D. Intrakinetochore stretch is associated with changes in kinetochore phosphorylation and spindle assembly checkpoint activity. *Journal of Cell Biology* 184, 373–381 (2009).

McEwen, B. F., Dong, Y. & VandenBeldt, K. J. Using Electron Microscopy to Understand Functional Mechanisms of Chromosome Alignment on the Mitotic Spindle. in *Methods in Cell Biology* vol. 79 259–293 (Academic Press, 2007).

McKinley, K. L. *et al.* The CENP-L-N complex forms a critical node in an integrated meshwork of interactions at the centromere-kinetochore interface. *Mol Cell* 60, 886–898 (2015).

Miller, S. A., Johnson, M. L. & Stukenberg, P. T. Kinetochore attachments require an interaction between unstructured tails on microtubules and Ndc80(Hec1). *Curr Biol* 18, 1785–1791 (2008).

Morgan, D. O. Principles of CDK regulation. *Nature* 374, 131–134 (1995).

Mosalaganti, S. *et al.* Structure of the RZZ complex and molecular basis of its interaction with Spindly. *Journal of Cell Biology* 216, 961–981 (2017).

Moudgil, D. K. *et al.* A novel role of farnesylation in targeting a mitotic checkpoint protein, human Spindly, to kinetochores. *J Cell Biol* 208, 881–896 (2015).

Musacchio, A. The Molecular Biology of Spindle Assembly Checkpoint Signaling Dynamics. *Current Biology* 25, R1002–R1018 (2015).

Musacchio, A. & Desai, A. A Molecular View of Kinetochore Assembly and Function. *Biology (Basel)* 6, (2017).

Musacchio, A. & Salmon, E. D. The spindle-assembly checkpoint in space and time. *Nat. Rev. Mol. Cell Biol.* 8, 379–393 (2007).

Nelson, C. R., Hwang, T., Chen, P.-H. & Bhalla, N. TRIP13PCH-2 promotes Mad2 localization to unattached kinetochores in the spindle checkpoint response. *Journal of Cell Biology* 211, 503–516 (2015).

Nijenhuis, W. *et al.* A TPR domain–containing N-terminal module of MPS1 is required for its kinetochore localization by Aurora B. *Journal of Cell Biology* 201, 217–231 (2013).

Nishino, T. *et al.* CENP-T-W-S-X Forms a Unique Centromeric Chromatin Structure with a Histone-like Fold. *Cell* 148, 487–501 (2012).

141. O'Connell, C. B. *et al.* The spindle assembly checkpoint is satisfied in the absence of interkinetochore tension during mitosis with unreplicated genomes. *J Cell Biol* 183, 29–36 (2008).

Obuse, C. *et al.* Proteomics analysis of the centromere complex from HeLa interphase

cells: UV-damaged DNA binding protein 1 (DDB-1) is a component of the CEN-complex, while BMI-1 is transiently co-localized with the centromeric region in interphase. *Genes Cells* 9, 105–120 (2004).

Ogino, S. *et al.* Observation of NMR signals from proteins introduced into living mammalian cells by reversible membrane permeabilization using a pore-forming toxin, streptolysin O. *J Am Chem Soc* 131, 10834–10835 (2009).

Okada, M. *et al.* The CENP-H–I complex is required for the efficient incorporation of newly synthesized CENP-A into centromeres. *Nature Cell Biology* 8, 446–457 (2006).

Olszewski, M. M., Williams, C., Dong, K. C. & Martin, A. The Cdc48 unfoldase prepares well-folded protein substrates for degradation by the 26S proteasome. *Communications Biology* 2, 1–8 (2019).

Overlack, K. *et al.* A molecular basis for the differential roles of Bub1 and BubR1 in the spindle assembly checkpoint. *eLife* 4.

Pachis, S. T. & Kops, G. J. P. L. Leader of the SAC: molecular mechanisms of Mps1/TTK regulation in mitosis. *Open Biol* 8, (2018).

Pan, J. & Chen, R.-H. Spindle checkpoint regulates Cdc20p stability in Saccharomyces cerevisiae. *Genes Dev* 18, 1439–1451 (2004).

Pardee, A. B. A Restriction Point for Control of Normal Animal Cell Proliferation. *Proc Natl Acad Sci U S A* 71, 1286–1290 (1974).

Pentakota, S. *et al.* Decoding the centromeric nucleosome through CENP-N. *eLife* 6, e33442 (2017).

Perrakis, A., Musacchio, A., Cusack, S. & Petosa, C. Investigating a macromolecular complex: the toolkit of methods. *J Struct Biol* 175, 106–112 (2011).

Pesenti, M. E., Weir, J. R. & Musacchio, A. Progress in the structural and functional characterization of kinetochores. *Current Opinion in Structural Biology* 37, 152–163 (2016).

Pesenti, M. E. *et al.* Reconstitution of a 26-Subunit Human Kinetochore Reveals Cooperative Microtubule Binding by CENP-OPQUR and NDC80. *Molecular Cell* 71, 923-939.e10 (2018).

Petrovic, A. *et al.* Structure of the MIS12 Complex and Molecular Basis of Its Interaction with CENP-C at Human Kinetochores. *Cell* 167, 1028-1040.e15 (2016).

Petrovic, A. *et al.* Modular assembly of RWD domains on the Mis12 complex underlies outer kinetochore organization. *Mol Cell* 53, 591–605 (2014).

Petrovic, A. *et al.* The MIS12 complex is a protein interaction hub for outer kinetochore assembly. *J Cell Biol* 190, 835–852 (2010).

Piano, V. *et al.* CDC20 assists its catalytic incorporation in the mitotic checkpoint complex. *Science* 371, 67–71 (2021).

Pines, J. Cyclins: wheels within wheels. *Cell Growth Differ* 2, 305–310 (1991).

Primorac, I. & Musacchio, A. Panta rhei: The APC/C at steady state. *Journal of Cell Biology* 201, 177–189 (2013).

Primorac, I. *et al.* Bub3 reads phosphorylated MELT repeats to promote spindle assembly checkpoint signaling. *eLife* 2, e01030 (2013).

Przewloka, M. R. *et al.* CENP-C is a structural platform for kinetochore assembly. *Curr Biol* 21, 399–405 (2011).

Rago, F., Gascoigne, K. E. & Cheeseman, I. M. Distinct Organization and Regulation of the Outer Kinetochore KMN Network Downstream of CENP-C and CENP-T. *Current Biology* 25, 671–677 (2015).

Reddy, S. K., Rape, M., Margansky, W. A. & Kirschner, M. W. Ubiquitination by the anaphase-promoting complex drives spindle checkpoint inactivation. *Nature* 446, 921–925 (2007).

Reddy, S. K., Rape, M., Margansky, W. A. & Kirschner, M. W. Ubiquitination by the anaphase-promoting complex drives spindle checkpoint inactivation. *Nature* 446, 921–925 (2007).

Rieder, C. L., Cole, R. W., Khodjakov, A. & Sluder, G. The checkpoint delaying anaphase in response to chromosome monoorientation is mediated by an inhibitory signal produced by unattached kinetochores. *J Cell Biol* 130, 941–948 (1995).

Roig, I. *et al.* Mouse TRIP13/PCH2 Is Required for Recombination and Normal Higher-Order Chromosome Structure during Meiosis. *PLOS Genetics* 6, e1001062 (2010).

Rosenberg, J. S., Cross, F. R. & Funabiki, H. KNL1/Spc105 recruits PP1 to silence the spindle assembly checkpoint. *Curr Biol* 21, 942–947 (2011).

Rouiller, I. *et al.* Conformational changes of the multifunction p97 AAA ATPase during its ATPase cycle. *Nature Structural Biology* 9, 950–957 (2002).

Samejima, I. *et al.* Whole-proteome genetic analysis of dependencies in assembly of a vertebrate kinetochore. *Journal of Cell Biology* 211, 1141–1156 (2015).

Saurin, A. T. Kinase and Phosphatase Cross-Talk at the Kinetochore. *Front Cell Dev Biol* 6, (2018).

Saurin, A. T., van der Waal, M. S., Medema, R. H., Lens, S. M. A. & Kops, G. J. P. L. Aurora B potentiates Mps1 activation to ensure rapid checkpoint establishment at the onset of mitosis. *Nature Communications* 2, 316 (2011).

Screpanti, E. *et al.* Direct binding of Cenp-C to the Mis12 complex joins the inner and

outer kinetochore. *Curr Biol* 21, 391–398 (2011).

Shepperd, L. A. *et al.* Phosphodependent Recruitment of Bub1 and Bub3 to Spc7/KNL1 by Mph1 Kinase Maintains the Spindle Checkpoint. *Current Biology* 22, 891–899 (2012).

Silió, V., McAinsh, A. D. & Millar, J. B. KNL1-Bubs and RZZ Provide Two Separable Pathways for Checkpoint Activation at Human Kinetochores. *Developmental Cell* 35, 600–613 (2015).

Silva, P. M. A. *et al.* Dynein-dependent transport of spindle assembly checkpoint proteins off kinetochores toward spindle poles. *FEBS Lett* 588, 3265–3273 (2014).

Simonetta, M. *et al.* The Influence of Catalysis on Mad2 Activation Dynamics. *PLoS Biol* 7, (2009).

Singh, P. *et al.* BUB1 and CENP-U, Primed by CDK1, Are the Main PLK1 Kinetochore Receptors in Mitosis. *Molecular Cell* 81, 67-87.e9 (2021).

Sironi, L. *et al.* Crystal structure of the tetrameric Mad1–Mad2 core complex: implications of a 'safety belt' binding mechanism for the spindle checkpoint. *EMBO J* 21, 2496–2506 (2002).

Starr, D. A. *et al.* HZwint-1, a novel human kinetochore component that interacts with HZW10. *J Cell Sci* 113 (Pt 11), 1939–1950 (2000).

Stoler, S., Keith, K. C., Curnick, K. E. & Fitzgerald-Hayes, M. A mutation in CSE4, an essential gene encoding a novel chromatin-associated protein in yeast, causes chromosome nondisjunction and cell cycle arrest at mitosis. *Genes Dev* 9, 573–586 (1995).

Stucke, V. M., Silljé, H. H. W., Arnaud, L. & Nigg, E. A. Human Mps1 kinase is required for the spindle assembly checkpoint but not for centrosome duplication. *The EMBO Journal* 21, 1723–1732 (2002).

Sullivan, K. F., Hechenberger, M. & Masri, K. Human CENP-A contains a histone H3 related histone fold domain that is required for targeting to the centromere. *J Cell Biol* 127, 581–592 (1994).

Takahashi, K., Chen, E. S. & Yanagida, M. Requirement of Mis6 centromere connector for localizing a CENP-A-like protein in fission yeast. *Science* 288, 2215–2219 (2000).

Takeuchi, K. *et al.* The centromeric nucleosome-like CENP-T-W-S-X complex induces positive supercoils into DNA. *Nucleic Acids Res* 42, 1644–1655 (2014).

Tanaka, T. U. *et al.* Evidence that the Ipl1-Sli15 (Aurora kinase-INCENP) complex promotes chromosome bi-orientation by altering kinetochore-spindle pole connections. *Cell* 108, 317–329 (2002).

Tauchman, E. C., Boehm, F. J. & DeLuca, J. G. Stable kinetochore–microtubule attachment is sufficient to silence the spindle assembly checkpoint in human cells. *Nature Communications* 6, 10036 (2015).

Taylor, S. S., Ha, E. & McKeon, F. The Human Homologue of Bub3 Is Required for Kinetochore Localization of Bub1 and a Mad3/Bub1-related Protein Kinase. *Journal of Cell Biology* 142, 1–11 (1998).

Teng, K. W. *et al.* Labeling proteins inside living cells using external fluorophores for microscopy. *Elife* 5, (2016).

Theillet, F.-X. *et al.* Structural disorder of monomeric α-synuclein persists in mammalian cells. *Nature* 530, 45–50 (2016).

Uchida, K. S. K. *et al.* Kinetochore stretching inactivates the spindle assembly checkpoint. *Journal of Cell Biology* 184, 383–390 (2009).

Uzman, A. Essential Cell Biology, Third Edition. *Biochemistry and Molecular Biology Education* 38, 59–59 (2010).

Uzunova, K. *et al.* APC15 mediates CDC20 autoubiquitylation by APC/C MCC and disassembly of the mitotic checkpoint complex. *Nature Structural & Molecular Biology* 19, 1116–1123 (2012).

Vader, G. Pch2(TRIP13): controlling cell division through regulation of HORMA domains. *Chromosoma* 124, 333–339 (2015).

Valverde, R., Ingram, J. & Harrison, S. C. Conserved Tetramer Junction in the Kinetochore Ndc80 Complex. *Cell Rep* 17, 1915–1922 (2016).

Vidal, M., Cusick, M. E. & Barabási, A.-L. Interactome networks and human disease. *Cell* 144, 986–998 (2011).

Vienken, J., Jeltsch, E. & Zimmermann, U. Penetration and entrapment of large particles in erythrocytes by electrical breakdown techniques. *Cytobiologie* 17, 182–196 (1978).

Walstein, K. *et al.* Assembly principles and stoichiometry of a complete human kinetochore module. *bioRxiv* 2020.12.01.407130 (2020) doi:10.1101/2020.12.01.407130.

Wan, X. *et al.* Protein Architecture of the Human Kinetochore Microtubule Attachment Site. *Cell* 137, 672–684 (2009).

Wang, F. *et al.* Histone H3 Thr-3 phosphorylation by Haspin positions Aurora B at centromeres in mitosis. *Science* 330, 231–235 (2010).

Wang, F. *et al.* Haspin inhibitors reveal centromeric functions of Aurora B in chromosome segregation. *J Cell Biol* 199, 251–268 (2012).

Wang, J. *et al.* Crystal structures of the HslVU peptidase-ATPase complex reveal an ATP-dependent proteolysis mechanism. *Structure* 9, 177–184 (2001).

Warburton, P. E. *et al.* Immunolocalization of CENP-A suggests a distinct nucleosome structure at the inner kinetochore plate of active centromeres. *Current Biology* 7, 901–904 (1997).

Wei, R. R., Al-Bassam, J. & Harrison, S. C. The Ndc80/HEC1 complex is a contact point for kinetochore-microtubule attachment. *Nat Struct Mol Biol* 14, 54–59 (2007).

Wei, R. R. *et al.* Structure of a central component of the yeast kinetochore: the Spc24p/Spc25p globular domain. *Structure* 14, 1003–1009 (2006).

Weir, J. R. *et al.* Insights from biochemical reconstitution into the architecture of human kinetochores. *Nature* 537, 249–253 (2016).

Weiss, E. & Winey, M. The Saccharomyces cerevisiae spindle pole body duplication gene MPS1 is part of a mitotic checkpoint. *J Cell Biol* 132, 111–123 (1996).

Welburn, J. P. I. *et al.* Aurora B phosphorylates spatially distinct targets to differentially regulate the kinetochore-microtubule interface. *Mol Cell* 38, 383–392 (2010).

Westhorpe, F. G., Tighe, A., Lara-Gonzalez, P. & Taylor, S. S. p31comet-mediated extraction of Mad2 from the MCC promotes efficient mitotic exit. *J Cell Sci* 124, 3905–3916 (2011).

Whiteheart, S. W., Schraw, T. & Matveeva, E. A. N-ethylmaleimide sensitive factor (NSF) structure and function. *Int Rev Cytol* 207, 71–112 (2001).

Xia, G. *et al.* Conformation-specific binding of p31comet antagonizes the function of Mad2 in the spindle checkpoint. *EMBO J* 23, 3133–3143 (2004).

Xu, P., Raetz, E. A., Kitagawa, M., Virshup, D. M. & Lee, S. H. BUBR1 recruits PP2A via the B56 family of targeting subunits to promote chromosome congression. *Biol Open* 2, 479–486 (2013).

Yamagishi, Y., Yang, C.-H., Tanno, Y. & Watanabe, Y. MPS1/Mph1 phosphorylates the kinetochore protein KNL1/Spc7 to recruit SAC components. *Nature Cell Biology* 14, 746–752 (2012).

Yamaguchi, M. *et al.* Cryo EM of Mitotic Checkpoint Complex-bound APC/C reveals reciprocal and conformational regulation of ubiquitin ligation. *Mol Cell* 63, 593–607 (2016).

Yang, M. *et al.* Insights into Mad2 Regulation in the Spindle Checkpoint Revealed by the Crystal Structure of the Symmetric Mad2 Dimer. *PLOS Biology* 6, e50 (2008).

Yang, M. *et al.* p31comet blocks Mad2 activation through structural mimicry. *Cell* 131, 744–755 (2007).

Ye, Q. *et al.* The AAA+ ATPase TRIP13 remodels HORMA domains through N-terminal engagement and unfolding. *EMBO J* 36, 2419–2434 (2017).

Ye, Q. *et al.* TRIP13 is a protein-remodeling AAA+ ATPase that catalyzes MAD2 conformation switching. *eLife* 4, e07367 (2015).

Zhang, G., Lischetti, T. & Nilsson, J. A minimal number of MELT repeats supports all

the functions of KNL1 in chromosome segregation. *J Cell Sci* 127, 871–884 (2014).

Zhang, S. *et al.* Molecular mechanism of APC/C activation by mitotic phosphorylation. *Nature* 533, 260–264 (2016).

Acknowledgements

I would like to express my sincere gratitude to my supervisor Prof. Andrea Musacchio for the opportunity to do my PhD in his lab, for the continuous support throughout my PhD and for the numerous intriguing scientific discussions. I would also like to thank the members of my thesis advisory committee, Prof. Philippe Bastiaens and Dr. Peter Bieling for their valuable suggestions.

There are two people in the Musacchio lab that I am indebted to the most; Dr. Stefano Maffini and Dr. Valentina Piano. Both of them were always open for discussions, extremely patient with my trivial questions, willing to help in most of my experimental designs and offering constructive feedbacks on my scientific writing and presentations. I would like to thank Dr. Stefano Maffini, specially for all the mentoring in regard to FLIM and EP projects. I would like to thank Dr. Valentina Piano for teaching me how to purify proteins along with other biochemical methods, for the many brain-storming discussions and for the wonderful collaboration throughout my PhD. I wish to thank Patricia Stege for the help with cloning and purification of multiple protein constructs. I would like to thank Beate Voss and Ingrid Hoffmann for their great technical assistance. Furthermore, I would like to express my gratitude to Dr. Petra Janning and Franziska Müller for the help with MS analysis of samples. I like to thank Prof. Philipp Selenko and Marchel Stuiver for their great collaboration on Electroporation project. I would like to thank Sara Carmignani, Suruchi Sethi, Dr. Pim J. Huis in 't Veld, Dr. Kai Walstein, Dr. Giuseppe Ciossani, Dr. Marion Pesenti, Carolin Koerner and Sabine Wohlgemuth for all the help in the lab from time to time.

I consider it a privilege to have known and made friends with many wonderful people over the course of my PhD. I would like to thank Vivek, Arnaud, Hendrick, Richie, Marion, Sara, Suruchi, Devika, Justine, Satya, Siva, Akhilesh and Pragya for all the nice chats over coffee or beer.

My sincere thanks go to Antje Peukert and also to Christa Hornemann and Lucia Sironi from the IMPRS for their help with many administrative matters. I would also take this opportunity to express my gratitude to Dr. Bidisha Sinha who was my mentor for the Master's project.

I cherish the support and love of my family and friends. Big thanks to my parents and my sister for their continuous help and support. I would like to express special thanks to Maria for all the reassuring words at times when I was uncertain. Thanks for your support.

"The biography is not included in the online version for reasons of data protection

Max-Planck-Institut für molekulare Physiologie
Prof. Dr. Andrea Musacchio

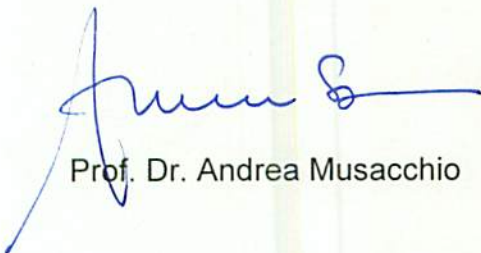MPI of Molecular Physiology Otto-Hahn-Str. 11 44227 Dortmund

Universität Duisburg-Essen
Fakultät für Biologie
Prof. Dr. Stefan Westermann
Promotionsausschuss
Schützenbahn 70

45127 Essen

Dortmund, 25.05.2021

Erklärung:

Hiermit erkläre ich, gem. § 6 Abs. (2) g) der Promotionsordnung der Fakultät für Biologie zur Erlangung der Dr. rer. nat., dass ich das Arbeitsgebiet, dem das Thema „Mechanistic insights into the mitotic checkpoint through biochemical characterisation and *in vivo* method development" zuzuordnen ist, in Forschung und Lehre vertrete und den Antrag von Herrn Amal Alex befürworte und die Betreuung auch im Falle eines Weggangs, wenn nicht wichtige Gründe dem entgegenstehen, weiterführen werde.

Prof. Dr. Andrea Musacchio

Postfach 50 02 47   Otto-Hahn-Str. 11   Telefon *49(0)231/133-2100
                                                  Telefax *49(0)231/133-2199
44202 Dortmund   44227 Dortmund   e-mail: andrea.musacchio@mpi-
dortmund.mpg.de

MAX-PLANCK-GESELLSCHAFT

Universität Duisburg-Essen
Fakultät für Biologie
Prof. Dr. Stefan Westermann
Promotionsausschuss
Schützenbahn 70

45127 Essen

Erklärung:

Hiermit erkläre ich, gem. § 7 Abs. (2) e) + g) der Promotionsordnung der Fakultät für Biologie zur Erlangung des Dr. rer. nat., dass ich keine anderen Promotionen bzw. Promotionsversuche in der Vergangenheit durchgeführt habe und dass diese Arbeit von keiner anderen Fakultät/Fachbereich abgelehnt worden ist.

Dortmund, 25. 05.2021

Amal Alex

Universität Duisburg-Essen
Fakultät für Biologie
Prof. Dr. Stefan Westermann
Promotionsausschuss
Schützenbahn 70

45127 Essen

Erklärung:

Hiermit erkläre ich, gem. § 7 Abs. (2) d) + f) der Promotionsordnung der Fakultät für Biologie zur Erlangung des Dr. rer. nat., dass ich die vorliegende Dissertation selbständig verfasst und mich keiner anderen als der angegebenen Hilfsmittel bedient, bei der Abfassung der Dissertation nur die angegeben Hilfsmittel benutzt und alle wörtlich oder inhaltlich übernommenen Stellen als solche gekennzeichnet habe.

Dortmund, 25.05.2021

Amal Alex